AD-A073 476 WRIGHT AIR DEVELOPMENT CENTER WRIGHT-PATTERSON AFB OH F/G 15/6
OPERATION UPSHOT-KNOTHOLE NEVADA PROVING GROUNDS, MARCH-JUNE 19--ETC(U)
OCT 55 E SEVIN

UNCLASSIFIED WADC-TR-55-421 DASA-WT-723 NL

| OF |
AD A073476

END
DATE FILMED
10-79
DDC

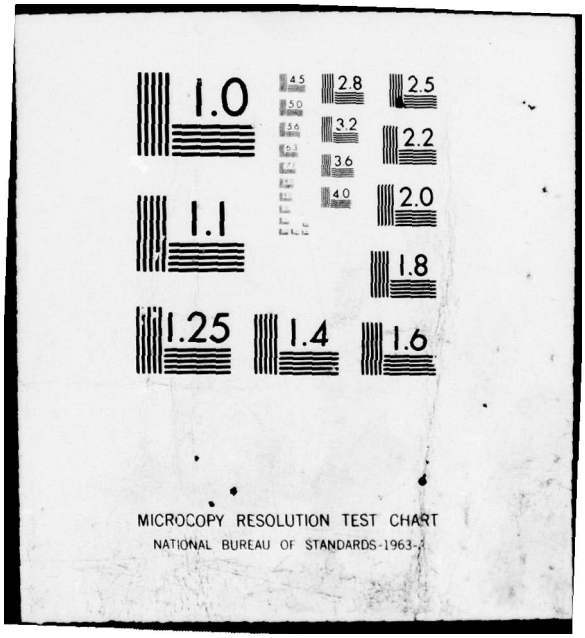
1.0
1.1
1.25
1.4
1.6
1.8
2.0
2.2
2.5
2.8
3.2
3.6
4.0
4.5
5.0
5.6
6.3
MICROCOPY RESOLUTION TEST CHART
NATIONAL BUREAU OF STANDARDS-1963-

UNCLASSIFIED

WT-723

Copy No. 187 A

Operation UPSHOT-KNOTHOLE

NEVADA PROVING GROUNDS

March - June 1953

Project 3.4

TESTS ON THE LOADING OF TRUSS SYSTEMS COMMON TO OPEN-FRAMED STRUCTURES

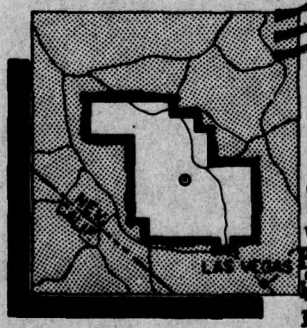

HEADQUARTERS FIELD COMMAND, ARMED FORCES SPECIAL WEAPONS PROJECT
SANDIA BASE, ALBUQUERQUE, NEW MEXICO

Statement A
Approved for public release;
Distribution unlimited.

UNCLASSIFIED

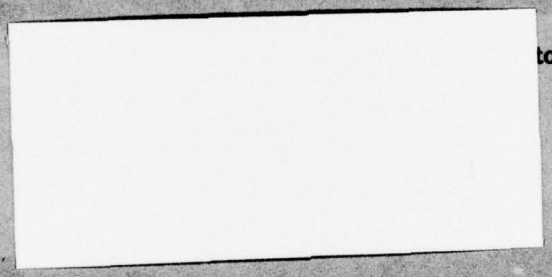

to

AD A073476

DDC ACCESSION NUMBER

II
LEVEL

DATA SHEET

PHOTOGRAPH

THIS SHEET

1
INVENTORY

WT-723
DOCUMENT IDENTIFICATION

DISTRIBUTION STATEMENT A
Approved for public release;
Distribution Unlimited

per telecon w/Betty Fox (DNA Tech Libr, Chief), the classified references contained herein may remain.

Lt. LaChance (DDA-2)
9-5-79

Accession For
NTIS GRA&I [X]
DDC TAB [ ]
Unannounced [ ]
Justification
per DDC
By
Distribution/
Availability Codes
Dist | Avail and/or special
A

DISTRIBUTION STAMP

DDC
RECEIVED
SEP 5 1979
E

DATE ACCESSIONED

79 08 21 050

DATE RECEIVED IN DDC

PHOTOGRAPH THIS COPY

WT-723

This document consists of 94 pages

No. 187 of 274 copies, Series A

OPERATION UPSHOT-KNOTHOLE

Project 3.4

TESTS ON THE LOADING OF TRUSS SYSTEMS COMMON TO OPEN-FRAMED STRUCTURES

REPORT TO THE TEST DIRECTOR

by

Eugene Sevin

October 1955

WADC TR 55-421
Air Materiel Command
Wright-Patterson Air Force Base
Dayton, Ohio

ABSTRACT

This report deals with pre- and post-test work on the Air Force Structures Test, Project 3.4, "Tests on the Loading of Truss Systems Common to Open Frame Structures." The over-all objective of the test was to determine the blast loading on open-framed structures, and to compare these loads with the results of steady-state wind-tunnel tests on model structures where possible. The items tested were a section of a plate girder bridge, a center section of a truss bridge, the upper chord and lower chord of this bridge, and a typical isolated structural member as represented by an I-beam. All items were at 2000 ft (intended) from ground zero in both Shots 9 and 10. Thus, they were in the regular reflection region in Shot 9 and in the precursor region in Shot 10. Instrumentation consisted of strain gage measurements taken on the supporting foundation of the structures.

Thirteen of eighteen strain gages provided usable records in Shot 9, and no usable records were obtained in Shot 10; even those records classified as usable appeared to have significant baseline shifts. For the most part, the strain data did not yield any interpretable results, and therefore none of the stated test objectives has been achieved. In view of the limited and uncertain nature of the strain data obtained, it is very doubtful if the test objectives could have been realized in any event. However, the anticipated methods of analysis were unsuccessful for the data obtained, and it is clear that additional work remains to be done with regard to the data-reduction problems associated with net force measurement systems such as employed on the present test.

The major conclusion of the program resulted from consideration of the response of the truss bridge section which sustained a slight permanent set on Shot 9 and was overturned on Shot 10. It was found that a simplified dynamic response analysis, incorporating the (pretest) predicted loading in the regular reflection region for Shot 9 and a tentative load prediction scheme applicable to the precursor region for Shot 10, provided an adequate estimate of the damage sustained by the bridge in these two shots. Thus, confidence in the utilization of existing methods for damage prediction estimates of open-framed structures is certainly increased as a result of this test, even though a precise determination of the blast loading was not achieved.

FOREWORD

This report is one of the reports presenting the results of the 78 projects participating in the Military Effects Tests Program of Operation UPSHOT-KNOTHOLE, which included 11 test detonations. For readers interested in other pertinent test information, reference is made to WT-782, Summary Report of the Technical Director, Military Effects Program. This summary report includes the following information of possible general interest.

a. An over-all description of each detonation, including yield, height of burst, ground zero location, time of detonation, ambient atmospheric conditions at detonation, etc., for the 11 shots.

b. Compilation and correlation of all project results on the basic measurements of blast and shock, thermal radiation, and nuclear radiation.

c. Compilation and correlation of the various project results on weapons effects.

d. A summary of each project, including objectives and results.

e. A complete listing of all reports covering the Military Effects Tests Program.

PREFACE

In a letter dated 12 March 1952, the Air Materiel Command was requested by Air Research and Development Command to submit for testing in Operation UPSHOT-KNOTHOLE existing requirements for a structures program which would be based on the needs of the Air Force for target analysis and indirect bomb damage assessment information. Within the Air Materiel Command, the responsibility for designing and executing such a program was delegated to the Special Studies Office, Engineering Branch of the Installations Division. The requirements which were submitted and approved became part of Program 3 of the operation and were designated as Projects 3.1, 3.3, 3.4, 3.5, 3.6 and 3.26.1. Mr. B. J. O'Brien of the Special Studies Office was appointed Project Officer and, as such, coordinated and successfully directed the planning and operational phases of five of the six projects. Due to the similarity in test objectives involving railroad equipment, the projects proposed by the Transportation Corps, U. S. Army, and the U. S. Air Force were combined into Project 3.6 with Lt. Colonel Donald G. Dow, TC, USA, as Project Officer and Mr. O'Brien as Assistant Project Officer.

Armour Research Foundation (ARF) of the Illinois Institute of Technology was awarded a contract to assist the Special Studies Office in planning and designing the experiments, and in analysis and reporting of test results. During the period of planning, close liaison was maintained with other interested Air Force agencies, particularly the Physical Vulnerability Division, Directorate of Intelligence, Headquarters, USAF. Many valuable suggestions were contributed by Colonel John Weltman, USAF, Lt. Colonel John Ault, USAF, Messrs. R. G. Grassy and S. White, Dr. F. Genevese and others of that Division, and by Mr. Louis A. Nees, Chief of the Engineering Branch, Installations Division, AMC.

Personnel of the Special Studies Section who were intimately connected with the program were Mr. Eric H. Wang, Chief, Special Studies Office, who was the technical and scientific monitor for the Air Force Program, Mr. Arthur Stansel, and Mrs. Maisie G. Ridgeway, secretary to Mr. Wang. Other members of the Office who were associated with the program were Messrs. R. R. Birukoff, P. A. Cooley, J. C. Noble, and Lts. T. M. Murray and G. A. Rockwell, USAF.

Most of the introduction section of this report was taken from the preface of the Preliminary Report, Operation UPSHOT-KNOTHOLE, Project (3.1) authored by Eric H. Wang and Bernard J. O'Brien.

The responsibility within the Air Force for execution of the six projects was transferred from the Special Studies Office, Installations Division, Air Materiel Command to Blast Effects Research, Mechanics Branch, Aeronautical Research Laboratory, Wright Air Development Center, on 15 November 1954.

ACKNOWLEDGMENTS

This report covers the activities of the Armour Research Foundation in connection with the Air Force Structures Program, Project 3.4, of Operation UPSHOT-KNOTHOLE. The work reported herein was technically monitored by the Special Studies Office of the Air Installations Division of the Air Materiel Command, Wright-Patterson Air Force Base, Ohio, under the terms of Air Force Contract AF33(038)-30029. It was sponsored by Wright Air Development Center, Wright-Patterson Air Force Base, Ohio.

ARF personnel who have contributed to this report include: R. Calvin, S. J. Fraenkel, K. Gandy, A. Hawkes, R. L. Janes, J. J. Kaganove, E. McDowell, R. W. Sauer, A. Sherman, T. Schiffman, L. A. Schmidt, E. Sevin, A. Wiedermann, and T. Zaker.

CONTENTS

ABSTRACT 3

FOREWORD 5

PREFACE 7

ACKNOWLEDGMENTS 8

ILLUSTRATIONS 11

TABLES 12

CHAPTER 1 INTRODUCTION 13

1.1 Purpose of Air Force Test Programs 13
1.2 Specific Objectives 14
1.3 Responsibilities 15

CHAPTER 2 GENERAL DESCRIPTION OF TEST 17

2.1 Test Items 17
2.2 Instrumentation 17
2.2.1 General 17
2.2.2 Strain Measurements 18
2.2.3 Instrument Records 18
2.3 Location of Test Structures 23

CHAPTER 3 PRETEST CONSIDERATIONS 24

3.1 Selection of Test Items 24
3.2 Load Predictions 24
3.2.1 Loading in the Mach Region 25
3.2.2 Loading in the Regular Reflection Region . . 27
3.3 Net Force Measurements 30
3.3.1 Sensor Design 30
3.3.2 Interpretation of Strain Measurements . . . 33
3.3.3 Relationship Between Strain and Forces . . 34

CHAPTER 4 EXPERIMENTAL RESULTS 39

4.1 Field Conditions 39
4.2 Physical Damage to Test Structures 39
4.3 Strain Gage Data 41

CHAPTER 5 POST-TEST CONSIDERATIONS 49

5.1 Interpretation of the Strain Data 49
5.1.1 Introduction 49
5.1.2 Application of Transient Analysis 49
5.1.3 Graphical Analysis 52
5.1.4 Analog Computer Method 55
5.2 Response of the Truss Bridge Section, 3.4a 56
5.2.1 Introduction 56
5.2.2 Effective Mass and Resistance of Bridge . . 57
5.2.3 Response Computations, Shot 9 58
5.2.4 Response Computations, Shot 10 60

CHAPTER 6 CONCLUSIONS AND RECOMMENDATIONS 74

6.1 Conclusions 74
6.2 Recommendations 75

APPENDIX A TRANSIENT ANALYSIS 76

A.1 Introduction 76
A.2 Derivation of the Basic Equation 76
A.3 Solution of the Basic Equation 79
A.4 Curve-Fitting 81
A.5 Discussion of Application of Transient Analysis (Method B) 84

BIBLIOGRAPHY 90

ILLUSTRATIONS

2.1	Preshot, Truss Bridge Section, 3.4a (End View)	19
2.2	Preshot, Top Chord, 3.4b (End View)	19
2.3	Preshot, Bottom Chord, 3.4c (Front View)	20
2.4	Preshot, Beam, 3.4e (Front View)	20
2.5	Preshot, Plate-Girder Bridge Section, 3.4f (Front View)	21
2.6	Typical Sensor Bar Showing Strain Gages (3.4f)	21
2.7	Location of Structures at Test Site	22
3.1	Average Loading on First Truss, Mach Reflection Region	36
3.2	Average Loading on Second Truss, Mach Reflection Region	36
3.3	Average Loading on Front of First Truss, Regular Reflection Region	37
3.4	Average Loading on Rear of First Truss, Regular Reflection Region	37
3.5	Free-Body Diagram of Typical Test Structure and Sensor Assembly	38
4.1	Postshot, Failure of Truss Section; 3.4a	43
4.2	Postshot, Plastic Bending of Front Diagonal, Truss Section; 3.4a	43
4.3	Postshot, Truss Section; 3.4a	44
4.4	Postshot, Bending of Gusset Plate, Bottom Chord, 3.4c	44
4.5	Typical Strain Gage Records	45
4.6	Tracings of Records 3.4aS1, 3.4aS2, and 3.4bS2	46
4.7	Strain Calibration Curves for Record 3.4aS1, Shot 9	47
5.1	Results of Transient Analysis, Strain Record 3.4aS2, Shot 9	63
5.2	Comparison of Experimental Strain Record 3.4aS1, Shot 9, with Calculated Strain Record	64
5.3	Results of Graphical Analysis, Strain Record 3.4aS1, Shot 9	65
5.4	Results of Graphical Analysis, Strain Record 3.4aS2, Shot 9	65
5.5	Results of Graphical Analysis, Strain Record 3.4aS3, Shot 9	66
5.6	Results of Graphical Analysis, Strain Record 3.4aS4, Shot 9	66

5.7 Comparison of Numerical and Graphical Data Reduction Schemes, Strain Record 3.4aS1, Shot 9 67
5.8 Horizontal Force on Truss Bridge Section 3.4a, Shot 9 (Based on Strain Records S1 and S2) 68
5.9 Horizontal Force on Truss Bridge Section 3.4a, Shot 9 (Based on Strain Records S3 and S4) 68
5.10 Assumed Elastic-Plastic Resistance Function for 3.4a Truss Bridge Section 69
5.11 Generalized Resistance Function for Newmark-Brooks Solution 69
5.12 Predicted Horizontal Loading on 3.4a Truss Bridge Section, Shot 9 70
5.13 Maximum Bridge Displacement Versus Resistance for Constant Period (Based on Predicted Loading for Shot 9) . . 71
5.14 Variation in Maximum Bridge Displacement with "Drag Coefficient" for Range of Resistance (Based on Predicted Loading for Shot 9) 71
5.15 Approximate Horizontal Precursor Loading, 3.4a Truss Bridge Section, Shot 10 72
5.16 Bridge Displacement Versus Peak Load (Based on Predicted Loading for Shot 10) 73

TABLES

3.1 Loading on the Front Surface of First Truss, Regular Reflection Region 31
3.2 Loading on Rear Surface of First Truss, Regular Reflection Region 32

4.1 Summary of Field Conditions 40
4.2 Summary of Strain Gage Data, Shot 9 42

5.1 Results of Transient Analysis 62

CHAPTER 1

INTRODUCTION

1.1 PURPOSE OF AIR FORCE TEST PROGRAMS

The series of tests conducted by the Air Force in Operation UPSHOT-KNOTHOLE is part of a continuing Air Force program designated as "Determination of Blast Effects on Buildings and Structures." The United States Air Force is mainly interested in the offensive aspects of such research.

The UPSHOT-KNOTHOLE projects sponsored by the Air Force and their specific objectives cannot be fully understood without some knowledge of the general objectives of the over-all program. The research results emanating from these studies and experiments conducted by the Air Force are used by a number of government agencies to improve their own systems of determining blast effects, or to further their own research.

One of these agencies is the Directorate of Intelligence, Headquarters, USAF, which feeds results as they are obtained into its own system of vulnerability classes, thereby making it possible to analyze prospective enemy targets with greater accuracy, and to recommend the desired ground zero. Another principal user of the research results is the Strategic Air Command, which applies them toward improvement of an existing indirect bomb damage assessment system. The purpose of this system is to make it possible to dispense with the usual reconnaissance after a strike, using instead information on the actual ground zero, height of burst, and yield of the weapon which is brought back to the operational base by the strike aircraft to determine the damage inflicted.

The task of determining the effect of blast on various types of building structures and tactical equipment is a rather formidable one. However, its difficulty is somewhat relieved by the fact that, for the offensive purposes in which the Air Force is interested, it is not necessary to determine the effect of transient loads on these items with the same accuracy as would normally be employed for static design purposes. In fact, even if it were possible to solve the dynamic problems satisfactorily, Intelligence information would be far too sketchy to furnish the information necessary to justify the use of an accurate analysis for items located in prospective enemy countries. From the experience that is so far available it is expected that it will be

possible within the foreseeable future to determine blast damage within broad limits with sufficient accuracy for planning as well as for operational purposes.

In view of the complex phenomena attending shock waves emanating from various types of atomic blasts and the uncertainties inherent in determining significant parameters, an investigator's first idea would be to obtain solutions through a long series of very elaborate and properly designed full-scale tests. However, neither funds nor time will allow such an approach. It has therefore been the objective of the agencies involved to obtain sufficiently accurate results by judicious use of theoretical analyses, laboratory tests, high-explosive field tests, and a small number of full-scale atomic tests.

Three of these research projects have involved full-scale atomic testing. The first was GREENHOUSE, the second was JANGLE (the first underground burst of an atomic weapon to which an Air Force structures program was subjected) and the third the present UPSHOT-KNOTHOLE program.

From previous analysis, laboratory tests, and full-scale tests (the latter especially as conducted in GREENHOUSE), methods of damage prediction have been developed by Armour Research Foundation (ARF) and others. These prediction methods have attempted to describe the character of the blast loads acting on a variety of items. Response computations based on the predicted loadings permit, in turn, an estimate of physical damage. However, the relation between the deflection or movement of a body and significant military damage has never been clearly established except for extreme cases, e.g., total destruction or no destruction. Another aim of these tests is, therefore, to establish the relationship between deflection and functional damage. A full-scale test also affords an excellent opportunity to determine scaling check points for laboratory tests.

In addition to the scientific aspects of the tests, most of the results of the Air Force projects can be used by other government agencies such as the Directorate of Intelligence to furnish "rough-and-ready" experimental answers to the behavior of various kinds of structures under blast. In many cases there is a statistically significant number of items involved which, added to previous experimental data such as those gathered at Hiroshima and Nagasaki, will help round out the present vulnerability picture. In other cases, mathematical analysis may have to rely on ad hoc information to furnish parameters which cannot be obtained in any other way.

The foregoing remarks are designed to furnish the background necessary for a full understanding of the objectives of this and other of the Air Force projects. The full significance and value of the results of each test will be realized only when they are correlated with results of past, current, and future analyses, laboratory tests, high-explosive field tests, and full-scale atomic investigations.

1.2 SPECIFIC OBJECTIVES

Many existing items of military importance are referred to as "drag-type structures." This nomenclature covers those structures having a

relatively small area as compared to the total volume they encompass. Some, like truss bridges, are constructed of small-dimensioned components. Others, such as buildings whose walls and roofs are quickly destroyed by the blast, consist of a structural frame of relatively small area. Evidence exists to show that for such structures most of the blast damage is due to forces acting after the initial diffraction period of the blast loading.

Present load prediction methods on drag-type structures are adaptations of steady-state concepts; that is, the net loads are taken to be proportional to the wind pressures behind the shock multiplied by the drag coefficient of the structural shape as determined from steady-state measurements. It is not known whether the laws developed for steady-state drag are applicable in this case, or whether the drag coefficients for various shapes determined under steady flow conditions apply. It has not yet been possible to produce transient flow in wind tunnels which adequately reproduce field conditions, and until either this or extended large shock tube experiments in this field are possible, the collection of full-scale check data becomes almost mandatory.

The specific objectives of this test were:

1. To determine the differences between drag loads due to an atomic blast and those of an apparently similar nature produced in wind tunnels under steady-state flow conditions.

2. To determine the ratio of diffraction impulse to drag impulse in drag-type structures.

3. To find the relationship between drag coefficients for the same body when subjected to transient as compared to steady-state flow conditions.

4. To find the effects on drag loading due to shielding of component parts.

5. To determine the relationship between the loadings on drag-type structures which are scale models.

The over-all objective of this test was to obtain sufficient information as to the loading on drag-type structures so that damage estimates can be made by means of analytical techniques.

1.3 RESPONSIBILITIES

Armour Research Foundation (ARF) was retained by the Air Materiel Command (AMC) of the United States Air Force to carry out the following specific objectives of the program:

1. Consultation on the selection of the test items.
2. Design of the test items.
3. Specification of instrumentation requirements.

4. Location of the structures at the test site.
5. Supervision of construction of the test items.
6. Theoretical analyses concerning pretest predictions of blast loading and response of the test items where required.
7. Analysis of the test results.
8. Submission of reports accounting for the ARF activities pursuant to the objectives of the program.

Detailed statements of the duties and obligations of the contracting parties can be found under the "Statement of Work" in Air Force Contract AF33(038)-30029.

Preparation of the construction drawings for most of the test items was subcontracted by ARF to the firm of Holabird and Root and Burgee. A member of this organization supervised the actual construction under the general direction of ARF. As-built drawings of all the test items were prepared by the Silas Mason Company.

All instrumentation was installed and operated by the Ballistic Research Laboratories (BRL) under UPSHOT-KNOTHOLE Project 3.28.1 ("Structures Instrumentation," WT-738).1/

1/ Complete reference concerning publications mentioned in parentheses may be found in the Bibliography at the end of this report.

CHAPTER 2

GENERAL DESCRIPTION OF TEST

2.1 TEST ITEMS

A series of five open-framed structures was included in both Shots 9 and 10. The structures were located in pressure regions where large deformations were not anticipated. The basic open-framed structure was a duplicate of the center section of a through-type, open-deck, single-track, truss bridge (designated as test item 3.4a). Duplicates of the top chord assembly (3.4b), the bottom chord assembly (3.4c), and a single I-beam from the latter section (3.4e) were tested. The fifth test item was a section of an Atchison, Topeka and Santa Fe Railroad Class D plate girder, through-type, open-deck bridge (3.4f).

Each item was mounted on specially designed supports, or sensor bars, which measured the reactions induced by the blast loading. The sensor bars were welded to the test structures at one end and bolted to reinforced concrete piers at the other end. The design of the piers was such as to prevent any gross motion of the test structures. Guy cables anchored to dead-men were fastened at each of the four corners, just above the sensor bars, on the four larger assemblies tested. Each cable was pre-tensioned to about 5000 lb, and the ends were secured with cable clamps. In addition, cross-bracing cables were added to each end of the 3.4a truss bridge section in lieu of end portals. Preshot photographs of the test items are shown in Figs. 2.1 through 2.5. As-built construction drawings are available upon request from AFSWP.[1/]

2.2 INSTRUMENTATION

2.2.1 General

The instrumentation was designed to measure the net blast forces acting on the test items. In view of the complex geometry involved (i.e., many members of relatively small dimension), it was impractical to obtain direct pressure measurements from which the desired net forces could be determined. The system employed consisted of mounting the items on specially designed supports (see Fig. 2.6). Time-dependent reactions

1/ Write to: Field Command, Armed Forces Special Weapons Project, Sandia Base, Albuquerque, New Mexico, Attention: WETD.

transmitted by the structures to the supports, or sensors, were measured by means of resistance strain gages. The strain gages were mounted on the front and back of each sensor support and connected in series electrically to cancel bending strains. Corresponding sensor bars on opposite sides of the structures were averaged so that a total of four instrumentation channels per structure was used for strain measurements, with the exception of the beam (3.4e) which used only two channels. The gages were numbered consecutively in the downstream direction, i.e., strain gage S1 was on the upstream sensor and strain gage S4 was on the furthest downstream sensor.

The strain data represent the output of a so-called net force measurement system. It should be recognized, however, that the strain data as such do not give a direct measure of the applied blast loading, but rather the response of the structure-sensor system to this loading. In effect, the test structures are being utilized as dynamometers, and a suitable analysis of the strain data is required in order to determine the desired information.

2.2.2 Strain Measurements

Standard SR4 strain gages were used in a four active arm bridge configuration to measure axial strain. The output of each bridge was fed into a Webster-Chicago recording system through a coupling unit and recorded on magnetic tape.

The calibration of the strain gages was accomplished electrically by shunting the proper arm of each gage installation with an accurately known resistance to simulate actual strain.

Complete details of the strain gage installations are contained in the final report of UPSHOT-KNOTHOLE Project 3.28.1 ("Structures Instrumentation," WT-738).

2.2.3 Instrument Records

The Ballistic Research Laboratories (BRL) handled all of the instrumentation on the program. The output of the strain gages was recorded initially on magnetic tape and later played back onto oscillographic paper. The records in this form exhibit characteristics which made them undesirable for purposes of interpretation and comparison (e.g., the ordinate scale is non-linear). For that reason, all of the records were converted into linear form.

BRL reduced, calibrated, and plotted to linear scales all of the strain records. The records as presented to ARF were in the form of plots made up of the points at which the records were read. ARF was responsible for fairing curves through these points. BRL also submitted tabulated listings of the points, as well as copies of the original playbacks.

The numerical data-reduction scheme employed on the strain records (see Section 5.1.1) required that the data be given in equal time intervals. Accordingly, BRL made a separate linearization of selected strain records at equal time intervals of about 4 ms, and supplied these results on IBM punched cards.

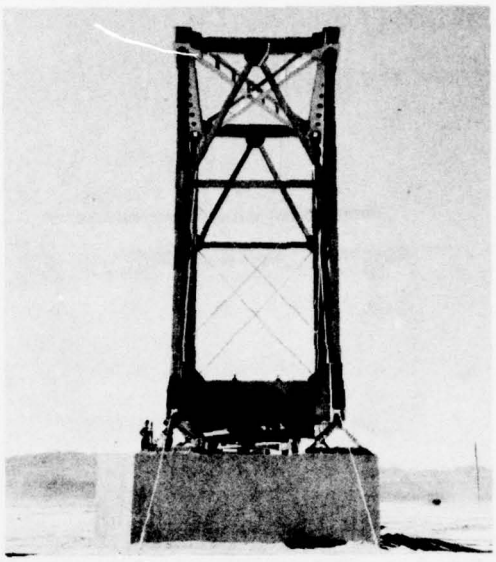

Fig. 2.1 Preshot, Truss Bridge Section, 3.4a (End View)

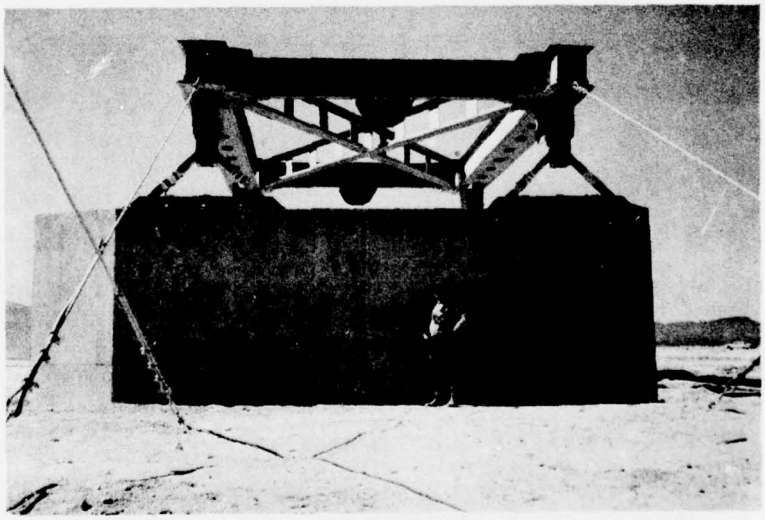

Fig. 2.2 Preshot, Top Chord, 3.4b (End View)

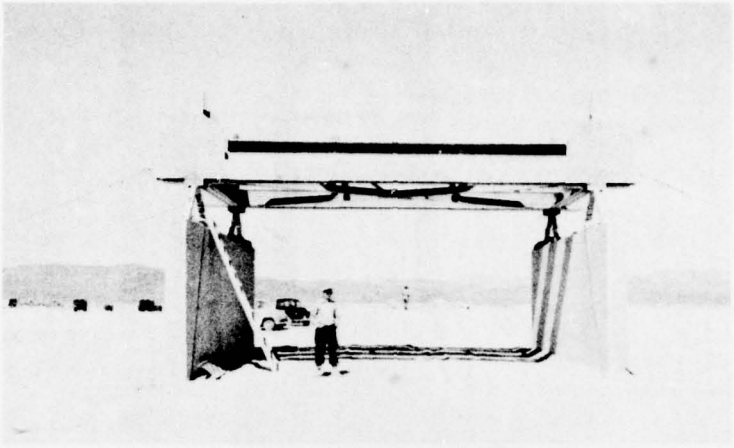

Fig. 2.3 Preshot, Bottom Chord, 3.4c (Front View)

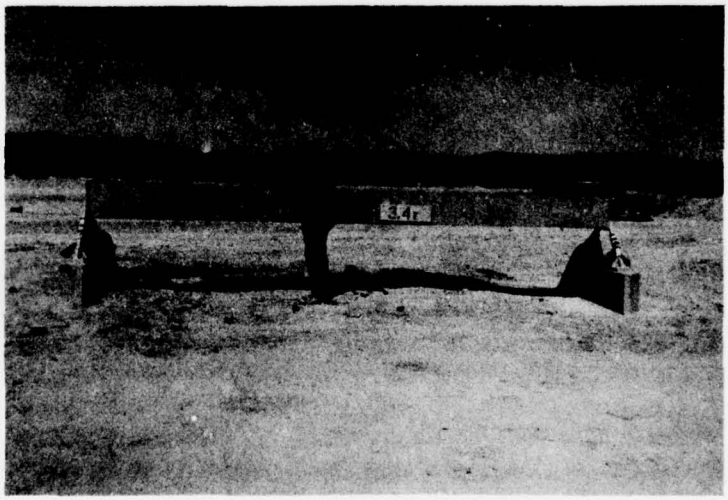

Fig. 2.4 Preshot, Beam, 3.4e (Front View)

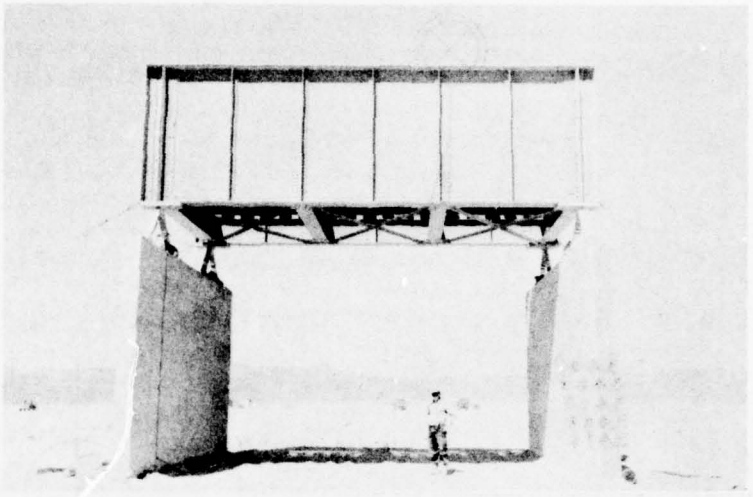

Fig. 2.5 Preshot, Plate-Girder Bridge Section, 3.4f (Front View)

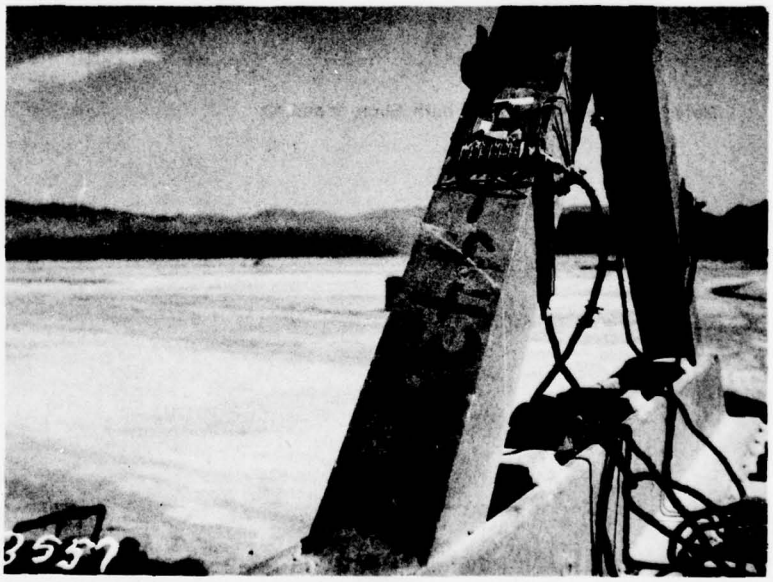

Fig. 2.6 Typical Sensor Bar Showing Strain Gages (3.4f)

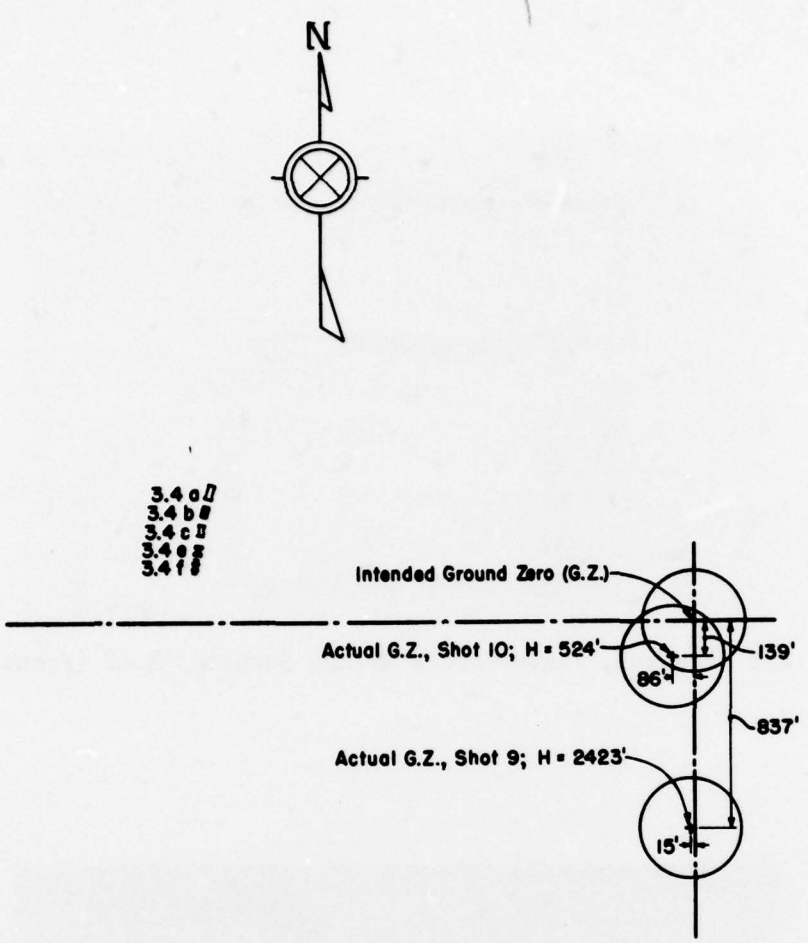

Fig. 2.7 Location of Structures at Test Site

2.3 LOCATION OF TEST STRUCTURES

The location of the structures at the test site is shown in Fig. 2.7. A summary of the field conditions including ground range from intended and actual ground zero and measured overpressure levels is given in Table 4.1. The maximum misorientation resulting from the bombing error was about 22 degrees in Shot 9 and about 5 degrees in Shot 10.

CHAPTER 3

PRETEST CONSIDERATIONS

3.1 SELECTION OF TEST ITEMS

The pretest work on this program is contained in the Planning Program for Air Force Structures Tests, Final Pretest Report (Part VIII, "Tests on Open-Grid Structures").

After consultation with the Air Force, the full-scale bridge sections (3.4a and 3.4f) were selected. The specific designs were chosen primarily because construction drawings were readily available.

The number and disposition of the test structures was chosen in order to achieve the stated objectives with the fewest items possible. It was felt that the objectives dealing with transient versus steady-state drag effects could be attained from the loading data on all five of the test items. The effects of shielding should be apparent from a comparison of the drag forces on the component sections with the forces on the entire bridge section.

It was planned to compare the test data with the results of laboratory tests whenever possible. With respect to shielding effects it was hoped that the test would serve to either confirm or suggest modifications of standard engineering approaches to this problem. For example, it is common practice to assume that the drag forces due to winds acting on the front or upstream truss of bridges are twice those acting on the rear truss. Steady-state wind-tunnel tests conducted at Massachusetts Institute of Technology ("Criteria for Collapse Damage To Structures in Relation to Weapon Yield, Height of Burst and Distance") have dealt with this type of shielding as a function of the distance between trusses.

3.2 LOAD PREDICTIONS

The Planning Program Final Pretest Report (Part VIII, "Tests on Open-Grid Structures") contains a detailed study of the anticipated blast loading on truss systems situated in the Mach and regular reflection regions. This work is based on steady-state drag concepts and does not account for shielding effects of multiple truss systems. A summary of the pertinent results is presented in this section.

3.2.1 Loading in the Mach Region

A number of relationships must be considered with reference to shock phenomena in the Mach reflection region. The shock strength, ξ is defined as the ratio of absolute pressures across the incident shock front, and is given by

$$\xi = 1 + (p_\sigma / P_0) \tag{3.1}$$

where p_σ is the initial overpressure (i.e., pressure in excess of atmospheric) and P_0 is the ambient atmospheric pressure.

The overpressure-time variation of the blast wave is approximated by the relation,

$$p_\sigma(t) = p_\sigma(0) e^{-ct/t_0} (1 - t/t_0) \tag{3.2}$$

where t_0 is the duration of the positive phase of the blast wave, and the empirical factor c is usually taken as unity.[1] The nominal drag pressure, $p_d(t)$, is given approximately by,

$$p_d(t) = p_d(0) e^{-2ct/t_0} (1 - t/t_0)^2 \tag{3.3}$$

where

$$p_d(0) = \frac{2.5 p_\sigma^{\,2}(0)}{7P_0 + p_\sigma(0)} \tag{3.4}$$

The shock front velocity, U, is given by

$$U = \frac{c_0}{\sqrt{7}} \sqrt{1 + 6\xi} = 422 \sqrt{1 + 6\xi} \text{ , ft/sec} \tag{3.5}$$

where c_0 is atmospheric sound velocity, evaluated above for standard atmospheric conditions.

When a plane shock front reflects from a rigid plane surface, the pressure behind the reflected wave, p_r, is given by

$$p_r = p_\sigma(0) \left[\frac{8\xi + 6}{\xi + 6} \right]. \tag{3.6}$$

---

[1] The factor c is known to depend on scaled height-of-burst and ground range. For test conditions, $c = 1.3$ represents a slightly better approximation to the free-stream pressure wave form for both Shots 9 and 10 than does $c = 1$. Plots of c as a function of height-of-burst and ground range are included in the final report on UPSHOT-KNOTHOLE Project 3.1 ("Tests on the Loading of Building and Equipment Shapes," WT-721).

The loading scheme for open-grid systems is an outgrowth of methods originally presented in the Operation GREENHOUSE Final Report, Project 3.3 which, in turn, were developed from shock tube and wind-tunnel data (Princeton University Technical Reports and wind-tunnel studies by Chien, Feng, Wang, and Siao and Eiffel) on simple geometric shapes. The loading on these structures consists of two phases: the initial diffraction phase, which depends primarily on characteristic dimensions of the structure, and the subsequent drag phase which depends on the geometry of the structure as well as on the blast wave.

For a single truss element (e.g., an isolated beam) the characteristic dimension or clearing distance, $\bar{h}$, refers to the half-width of the member. For a composite of such members, the situation is complicated. It is believed that an equivalent clearing distance for the entire assembly, $\bar{h}$, can be taken as a weighted average of the clearing times for individual members (see Operation GREENHOUSE, final report), that is,

$$\bar{h} = \frac{\sum_{i=1}^{n} A_i \bar{h}_i}{\sum_{i=1}^{n} A_i} \qquad (3.7)$$

where $\bar{h}_i$ is the clearing distance for the ith member and A_i is the frontal area of that member. The denominator of Equation 3.7 represents the total frontal area of the truss.

The force per unit frontal area of the first (i.e., upstream) truss in a structure similar to 3.4a is shown symbolically in Fig. 3.1. The diffraction loading pattern is modeled after the loading on the two-dimensional Princeton 1:2 block (Air Force Planning Program, Final Pretest Report, Part VIII, "Tests on Open-Grid Structures"). The average pressure on the front surfaces rises instantaneously to the reflected pressure, p_r, and then drops to side-on plus drag pressure, $p_\sigma(t) + C_{df}p_d(t)$, in an additional $7h/U$ time units. A combined drag coefficient, C_d, of 2 is selected. This leads to a value of the drag coefficient of the front surface of $C_{df} = 1$, which is the maximum value that can be obtained under steady-state conditions. The drag coefficient for the back surface is taken to be $C_{db} = -1$. Therefore, the net drag force on the truss is $2p_d(t)$.

The loading pattern on the second (i.e., downstream) truss is similar to the above, with minor exceptions introduced by the choice of drag coefficients. The value of C_d is taken to be 1 (i.e., half that of the first truss) in order to account for shielding effects. This choice, although arbitrary, is not in contradiction with experimental data ("Wind-Tunnel Studies of Pressure Distribution on Elementary Building Forms," State University of Iowa). To arrive at this value of C_d, the front and rear surface coefficients are chosen to be $C_{df} = 0$ and $C_{db} = -1$.

On order to compute the net loading on the combined trusses, it is necessary to introduce a time delay of L/U in the loading of the second truss (where L is the distance between trusses). This is the length of time relative to the first truss required for the shock to

reach the second truss. Figure 3.2 shows the loading (i.e., force per unit frontal area) on the second truss. The net loading on the structure can be found by superposing (graphically) the component loadings on each truss.

3.2.2 Loading in the Regular Reflection Region

The general methods for computing loading on solid structures in the regular reflection region has been described in the Final Pretest Report, Part V ("Regular Reflection on Cubical Structures"). Since open-grid structures in general do not obstruct the shock wave with solid boundaries of large cross-sectional area, and since there are no re-entrant corners in this type of structure, the diffraction phase will last for only a comparatively short time and the average loading will not build-up to as high a value as in the Mach region. This is one of the prime differences in the loading of solid and open-grid structures in the regular reflection region.

There exist certain similarities and differences between the loading on structural components located in the regular reflection and Mach regions. Among the similarities is the fact that the loading is probably two-dimensional in character, and hence, the concept of an average $\bar{h}$, (Equation 3.7) can be retained. The drag coefficients are also assumed to be the same for both cases. In addition, the ground reflected pressure, $p_{re}(t)$, is taken to have the same time-dependence in the regular reflection region as does the side-on pressure, $p_\sigma(t)$, in the Mach region.

Among the major differences in the loading is the manner of reaching pseudo-steady-state (drag phase) in regular reflection. Here the structure is struck by two separate shocks, the incident and ground reflected shock, and the load builds up in two distinct time intervals. This phase delay is a function of the height of the structure above ground a, the angle of incidence of the blast, α , and the shock front velocity U. In addition to this difference, the shock waves do not envelope the structure immediately, but rather an additional phase delay is encountered due to the inclination of the shock fronts. This inclination results in a finite time for the shock wave to sweep the total height, H, of the structure.

In considering the diffraction loading on the front surface, it is convenient to consider first the limiting cases of head-on reflection ($\alpha = \pi/2$) and glancing incidence ($\alpha = 0$). The peak pressure resulting from the incident shock occurs at the time when the shock has covered the entire height, H, of the truss; namely, at $t = H \cos\alpha/U$; this reduces to zero and H/U, respectively, for the two limiting cases mentioned above. For head-on reflection with the truss, the peak average pressure at this time is

$$p = \frac{6 + 8\xi}{6 + \xi} p_\sigma(0) = \beta(\xi)\, p_\sigma(0) \text{ at } t = \frac{H \cos\alpha}{U} = 0 \quad (3.8)$$

while for glancing incidence it is

$$p = p_\sigma(0) \text{ at, } t = \frac{H \cos \alpha}{U} = \frac{H}{U} \quad . \tag{3.9}$$

For an arbitrary incident angle, α, the reflected pressure must be a function of α, the shock strength of the free-stream incident wave, ξ, and the ratio of the height of truss, H, to the relief distance, $3\bar{h}$. By dividing the truss into infinitely small segments and summing the average pressure on each segment at the time $t = H \cos \alpha/U$, one obtains for the average pressure above side-on

$$p_1 = \frac{p_\sigma(0)(C - 1)}{2(2 - \eta)} \tag{3.10}$$

for

$$\eta = \frac{H \cos \alpha}{3\bar{h}} \leq 1$$

and

$$p_1 = \frac{p_\sigma(0)(C - 1)}{2\eta} \tag{3.11}$$

when

$$\eta = \frac{H \cos \alpha}{3\bar{h}} > 1.$$

In both instances the factor C is referred to as the modified oblique reflection coefficient. According to Equations 3.8 and 3.9, the reflection coefficient, C, is equal to $\beta(\xi)$ for $\alpha = \pi/2$ and equal to unity for $\alpha = 0$. If the average pressure behind the shock front in oblique reflection is plotted against the angle of incidence, the resulting curve is approximately a straight line. On this basis an empirical relationship for the reflection coefficient as a function of the incidence angle is taken to be,

$$C = \frac{2\alpha}{\pi} \left[\beta(\xi) - 1\right] + 1 \tag{3.12}$$

When $\eta \geq 5$, the average pressure rises very rapidly to the value given by Equation 3.11. This rise time can reasonably be neglected, in which case the average pressure at $t = 0$ is taken to be

$$p(0) = p_1 = \frac{p_\sigma(0)(C - 1)}{2\eta} \qquad \text{for } \eta \geq 5 \ .$$

The average pressure then rises linearly from this value to $p_1 + p_\sigma(0)$ at $t = H \cos \alpha/U$. Now for $\eta \leq 1$, the average pressure rises linearly from zero at $t = 0$ to $p_1 + p_\sigma(0)$ at $t = H \cos \alpha/U$, where here p_1 is given by Equation 3.10. For $1 < \eta < 5$, the average pressure at $t = 0$ is obtained by interpolating linearly for η between the values for $\eta = 1$ and $\eta = 5$.

The pressure build-up, p_2, due to reflection when the ground-reflected wave covers the truss, can be expressed in a similar fashion where now, however, p_σ must be replaced by the ground reflected pressure p_{re}. The pressure p_2 initiates at a phase delay of $2a \cos \alpha / U$ time units (a is the distance from ground to the bottom of the truss, see Fig. 3.3) to allow for the reflected shock to reach the structure. The pseudo-steady-state pressures on the front surfaces are taken to be $p_\sigma(0) + C_{df} p_{dl}(0) \sin \alpha$ for the incident wave, and $p_{re}(0) + C_{df} p_{dr}(0)$ for the reflected wave. The zero times are again used, since the time interval during which this load acts is very short and, hence, the loads have approximately their initial value.

Expressions for the reflected pressure, $p_{re}(t)$, and the nominal drag pressures, $p_{dl}(t)$, and $p_{dr}(t)$, were derived in the pretest report. They are as follows:[2/]

$$p_{re}(t) = p_{re}(0) e^{-t/t_o} (1 - t/t_o) \tag{3.13}$$

and,

$$p_{dr}(t) = \left[1 + \frac{p_\sigma(0)}{10\, P_o} \right] p_{dr}(0) e^{-2t/t_o} (1 - t/t_o)^2 \tag{3.14}$$

where

$$p_{dr}(0) = \frac{10 p_\sigma{}^2(0) \left[6 p_\sigma(0) + 7P_o \right]}{\left[7P_o + p_\sigma(0) \right]^2} \sin^2 \alpha \tag{3.15}$$

is the drag pressure behind the ground-reflected shock front parallel to the ground. Also

$$p_{dl}(0) = \frac{2.5\, p_\sigma{}^2(0)}{7P_o + p_\sigma(0)} \qquad \text{(cf. Eq. 3.4)} \tag{3.16}$$

where $p_{dl}(0)$ is nominal drag pressure behind the incident shock front normal to the incident shock front. Hence, the component normal to the structure is given by $p_{dl}(0) \sin \alpha$.

The diffraction loading on the front of the second truss is assumed to be identical to the loading on the front of the first truss if the proper time delay for the shock to reach the rear truss is taken into account, i.e., a time delay of $t = L \sin \alpha / U$. The drag coefficients for the front surfaces are taken the same as in Mach reflection, i.e., $C_{df} = 1$ on the front surface of the first truss, and $C_{df} = 0$ on front surface of the second truss.

2/ The empirical exponent c which determines the wave form of the pressure is chosen as unity throughout this section, see footnote on page 25.

The loading on the downstream surfaces also build up in two steps since two waves are involved. The build up time for each wave is given by

$$t = \frac{H \cos \alpha}{U} + \frac{\bar{h}}{U_m} \frac{\alpha}{\alpha_{ext}} + \frac{\ell \sin \alpha}{U} \qquad (3.17)$$

where

α_{ext} = limiting angle for regular reflection ($\alpha \leq \alpha_{ext}$, i.e., Mach reflection occurs whenever α_{ext} is exceeded)

U_m = the equivalent Mach shock front velocity

$= 422 \sqrt{1 + 6\xi^2}$

ℓ = depth of the truss in the direction of flow.

The term $\ell \sin \alpha/U$ is the time required for the wave to reach the back surface of a truss. The time between the two buildups (incident and reflected waves) is given by $2a \cos \alpha/U$, which is the time required for the ground-reflected shock to reach the back surface. Again the pseudo-steady state values are given by $p_{\sigma}(0) + C_{db} p_{dl}(0) \sin \alpha$ for the incident wave and $p_{re}(0) + C_{db} p_{dr}(0)$ for the reflected wave. The drag coefficients are taken the same as for Mach reflection, namely $C_{db} = -1$ for the back surfaces of both the first and second trusses.

Loading on front and rear surfaces of the first truss is shown symbolically in Figs. 3.3 and 3.4 and Tables 3.1 and 3.2. The loadings on the rear truss are similar to those on the front truss. The time details of the diffraction phase are the same but initiate at a time $L \sin \alpha/U$ later than on the front truss, where L is the distance between trusses. The pseudo-steady-state pressure on the front of the second truss is $p_{re}(t)$, rather than $p_{re}(t) + C_{df} p_{dr}(t)$, while on the rear of both trusses it is $p_{re}(t) - p_{dr}(t)$. Hence, the total drag on the front truss is $2p_{dr}(t)$, while on the rear truss it is $p_{dr}(t)$, which accounts for the shielding effect of the front truss.

3.3 NET FORCE MEASUREMENTS

3.3.1 Sensor Design

An important part of the planning phase of this program was the development of a method for direct measurement of the net blast forces acting on the test structures. Ideally, a direct measurement system would be one whose output is either proportional to the net blast loading over the entire structure, or one whose output can be converted to net loads in a straightforward fashion. This requirement for a net force measurement system is meant to exclude pressure gage instrumentation, at least in the present case.

Table 3.1 - Loading on Front Surface of First* Truss, Regular Reflection Region

Time, t (sec)	Average Pressure, p (psi)
0	0 for $\eta = \frac{H \cos \alpha}{3\bar{h}} \leq 1$ $p_1 = \frac{p_\sigma(0)(C-1)}{2\eta}$ for $\eta \geq 5$ Interpolate linearly between 0 and p_1 for $1 < \eta < 5$ (See Equation 3.12 for C)
$t_1 = \frac{H \cos \alpha}{U}$	$p_1 + p_\sigma(0) = \frac{p_\sigma(0)(C-1)}{2(2-\eta)} + p_\sigma(0)$ for $\eta \leq 1$ $p_1 + p_\sigma(0) = \frac{p_\sigma(0)(C-1)}{2\eta} + p_\sigma(0)$ for $\eta > 1$
$t_2 = t_1 + \frac{3\bar{h} \cos \alpha}{U}$	$p_\sigma(0) + C_{df} p_{dl}(0) \sin \alpha$ $(\ldots C_{df} = 1)$
$t_3 = t_1 + \frac{2a \cos \alpha}{U}$	$p_\sigma(0) + C_{df} p_{dl}(0) \sin \alpha$
t_3	$p_2 + p_\sigma(0) + C_{df} p_{dl}(0) \sin \alpha$ where $p_2 = \frac{p_{re}(0)(C-1)}{2(2-\eta)}$ for $\eta \leq 1$ $p_2 = \frac{p_{re}(0)(C-1)}{2\eta}$ for $\eta > 1$
$t_4 = t_1 + t_3$	$p_2 + p_{re}(0)$
$t_5 = t_2 + t_4$ $= \leq t \leq t_o$	$p_{re}(t) + C_{df} p_{dr}(t)$
$> t_o$	0

*For the front surface of the second truss all times are increased by $L \sin \alpha / U$, and $C_{df} = 0$.

Table 3.2 - Loading on Rear Surface of First* Truss,
Regular Reflection Region

Time, t (sec)	Average Pressure, p (psi)
0	0
$t_6 = \frac{\ell \sin \alpha}{U}$	0
$t_7 = t_6 + t_1 + \frac{7\bar{h}\ \alpha}{\bar{U}_m\ \alpha_{ext}}$	$p_\sigma(0) + C_{db}p_{dl}(0) \sin \alpha$ $(\ldots C_{db} = -1)$
$t_8 = t_6 + t_3$	$p_\sigma(0) + C_{db}p_{dl}(0) \sin \alpha$
$t_9 = t_7 + t_3 \leq t \leq t_o$	$p_{re}(t) + C_{db}p_{dr}(t)$
$>t_o$	0

* For the back surface of the second truss all times are increased by $L \sin \alpha / U$, and $C_{db} = -1$.

While there are certain types of structures for which net forces over the entire structure can be adequately determined by means of combining and averaging individual pressure gage data, there are many structures where such averaging is either subject to considerable uncertainty or is totally impractical. There are also cases where the presence of pressure gages may sufficiently alter the flow conditions around the test items so as to rule out this means of force measurement. In the present case both of these objections can be raised to the use of pressure gage instrumentation. Thus, an alternate force measurement system had to be devised.

In the present setup, each test structure was utilized in the sense of a dynamometer. That is, the structure and the sensor arrangement as a whole constituted the gaging device. The output of the strain gage system (i.e., the strain in the sensor bars) was thus dependent upon the dynamic characteristics of the structure-sensor system as well as upon the applied blast force.

In order for the strain data to be utilized as a direct measure of the applied blast loadings, it is necessary that the frequency response of the test items be considerably greater than that of the sensor supports alone and, in turn, that the fundamental period of the

system as a whole be sufficiently less than the significant time details of the applied blast loading. In this case, the response is that of a single-degree-of-freedom system (i.e., a rigid structure on flexible supports), and, with suitable damping, the strain data could be interpreted much as is pressure data - simply by inspection. Unfortunately, it was not possible to satisfy these conditions for any of structures tested. The frequency response of the sensor bars was also limited by the requirement that a sufficiently great strain be produced to yield a reliably measurable signal from the strain gages throughout most of the loading period. Also, the sensor arrangement was designed on the basis of there being no provision for pretest field calibration of the entire setup (and there was none). This necessitated a longer sensor bar than might otherwise have been utilized, since it was imperative that the measured surface strain be an adequate measure of the actual force in the bar.[3] This, in turn, further reduced the frequency response of the setup.

Details of the sensor bar construction are shown in Fig. 2.6, and in the as-built construction drawings. Briefly, the end support consisted of a rigid right-angle frame of welded construction attached at the four corners of the bridge sections, and at the two ends of the beam. On the bridge sections the sensor bars were 4-1/4 in. square and approximately 3 ft long between welds (i.e., the unsupported sensor bar length); on the beam (3.4e) the bars were 1-1/2 in. square and approximately 15 in. long. High-strength steel was used for all sensor bars. The geometry of the supports was such that each sensor bar could be considered as a two-force member. This would, of course, be true if the frame were ideally pin-connected,[4] but a rigid frame was more desirable from a construction viewpoint.

3.3.2 Interpretation of Strain Measurements

The final sensor design was such that the measured forces in the sensor supports would most likely be influenced by the dynamic characteristics of the entire test structure and, thus, would not be a direct measure of the applied blast force. This situation necessitated a data-reduction system that was capable of taking this effect into account and providing the desired net applied forces. In essence the problem here is the inverse of the conventional dynamic response problem. That is, the usual problem is "given the dynamic system and the input, find the output"; here the problem is "given the dynamic system and the output, find the input."

3/ That is, the sensor bar had to be sufficiently long so that the stress distribution at the cross section being gaged was essentially uniform.

4/ An analysis of the maximum error introduced by the assumption of pin ends was carried out in the final pretest report("Planning Program for Air Force Structures Test,"Part VIII,"Tests on Open-Grid Structures"). The error in the magnitude of the force was found to be less than 6 per cent, and about 1.5 degrees in direction relative to the centerline of the bars.

The solution to the inverse problem is generally the more complicated but in principle can be achieved, at least for linear dynamic systems, provided the response of the system to a given input is known. However, the present problem is made more difficult by the fact that the characteristics of the dynamic system itself are not known with any certainty. That is, the system is sufficiently complicated that the response (i.e., the force in the sensor bars) to a known input cannot be computed with sufficient accuracy to justify a solution to the inverse problem by standard methods. (The beam (3.4e) may be an exception to this statement.)

A numerical data-reduction scheme referred to as "transient analysis" was developed during the course of the pretest work and was believed to be adequate for the needs of this program. In principle, the method of transient analysis is applicable to the determination of the time variation of the input function (the magnitude of the input can only be determined to within an arbitrary scale factor) from a known output function, even when the equations of motion of the system are not known in detail. The method is restricted to dynamic systems characterized by linear second-order differential equations with constant coefficients, and input functions which can adequately be represented by finite sums of exponential functions (i.e., "e" functions) all of whose coefficients and exponents are real numbers. In effect, this last requirement limits the input functions to those having no harmonic components, which seemed a reasonable enough assumption in the case of blast loading functions. A further restriction is that the forcing function components associated with the various modes of the system are either zero or timewise proportional (see Appendix A).

The restrictive assumptions which permit the valid use of transient analysis as a technique for data reduction in the present application were considered to be satisfied during the pretest planning period. As discussed in Chapter 5, the initial application of transient analysis to the strain data was largely unsuccessful. However, a brief second application gave more encouraging results. The development and critical discussion of transient analysis is presented in Appendix A of this report.

3.3.3 Relationship Between Strain and Forces

The relationship between strain and total force in each sensor bar is given by,

$$S = A_s E \epsilon \tag{3.18}$$

where

S = force in sensor bar, lb

ϵ = measured strain in sensor bar, in./in.

E = Young's modulus for the sensor bar material, psi

A_s = cross-sectional area of sensor bar, $in.^2$

Figure 3.5 shows a free-body diagram of a typical test structure and sensor assembly applicable to all items with the exception of the 3.4e beam which was supported on only one sensor assembly per end. With reference to Fig. 3.5, the incident blast loading is assumed to be spanwise symmetrical, and is represented by horizontal, F_h, and vertical F_v, time-dependent force components. The sensor bar forces represent the total force in corresponding sensors on opposite ends of the test structure and, as such, are assumed to be numerically equal to twice the measured force in a single bar as given by Equation 3.18; hence the factor 2 indicated in Fig. 3.5. The length M is the distance from the vertex of the sensor assembly to the center of pressure of the test structure; the length N is the distance between the sensor assemblies in the direction of flow.

If the bottom chord members are assumed to be effectively rigid and transmit one-half the applied horizontal load to each sensor assembly, and, further, if the sensor assembly is assumed to be pin-connected (see Section 3.3.1) the determination of the forces in the individual sensor bars becomes a statically determinate problem. From a static point of view, the horizontal and vertical components of the blast loading are then given in terms of the sensor bar forces at each instant of time by,

$$\left.\begin{aligned} F_h &= 2\sqrt{2}\ (S_1 - S_2) = 2\sqrt{2}\ (S_3 - S_4),\ \text{lb} \\ F_v &= -2\sqrt{2}\ (S_2 + S_3) = -2\sqrt{2}\ (S_1 + S_4),\ \text{lb} \end{aligned}\right\} \qquad (3.19)$$

where the sensor bar forces, $S_1 \ldots S_4$, are assumed positive in tension as shown in Fig. 3.5; F_h is positive directed downstream and F_v is positive directed downward.

Note that, on the basis of this being a statically determinate problem, the applied loading can be determined from the measurements taken at any one sensor assembly.

The 3.4e beam is supported by only one sensor assembly per end, and the distance M is approximately zero. Thus, for this case the horizontal and vertical force components are given by,

$$\left.\begin{aligned} F_h &= \sqrt{2}\ (S_1 - S_2),\ \text{lb} \\ F_v &= \sqrt{2}\ (S_1 + S_2),\ \text{lb} \end{aligned}\right\} \qquad (3.20)$$

The applied forces can be expressed in terms of the measured strains by means of the above equations. That is, for structures 3.4a, b, c and f

$$\left.\begin{aligned} F_h &= 1532\ (\epsilon_1 - \epsilon_2) = 1532\ (\epsilon_3 - \epsilon_4),\ \text{lb} \\ F_v &= 1532\ (\epsilon_2 + \epsilon_3) = 1532\ (\epsilon_1 + \epsilon_4),\ \text{lb} \end{aligned}\right\} \qquad (3.21a)$$

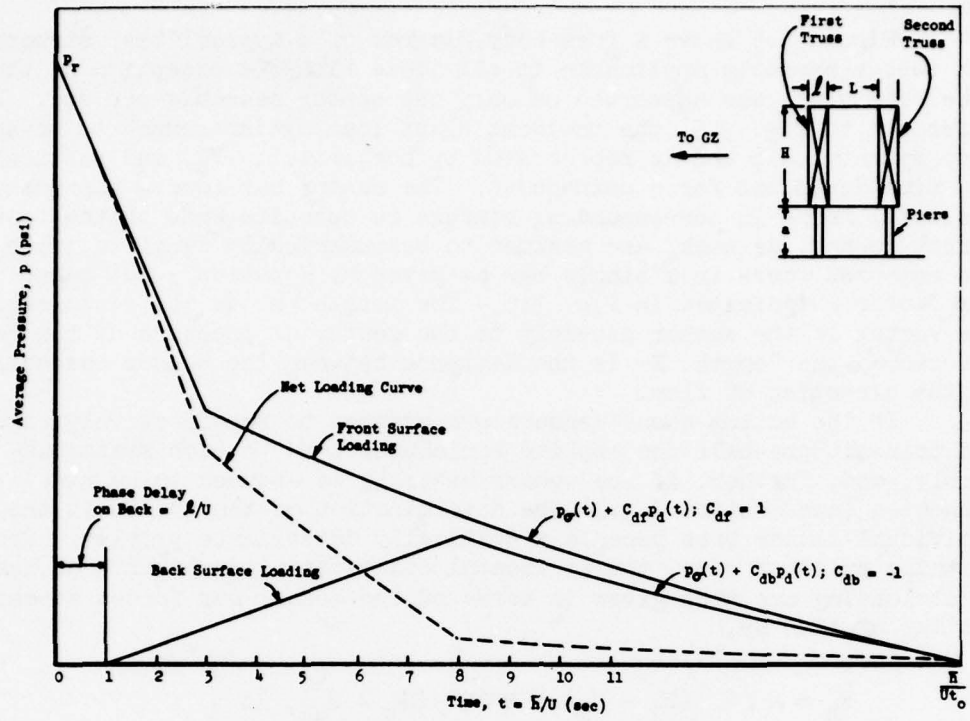

Fig. 3.1 Average Loading on First Truss, Mach Reflection Region

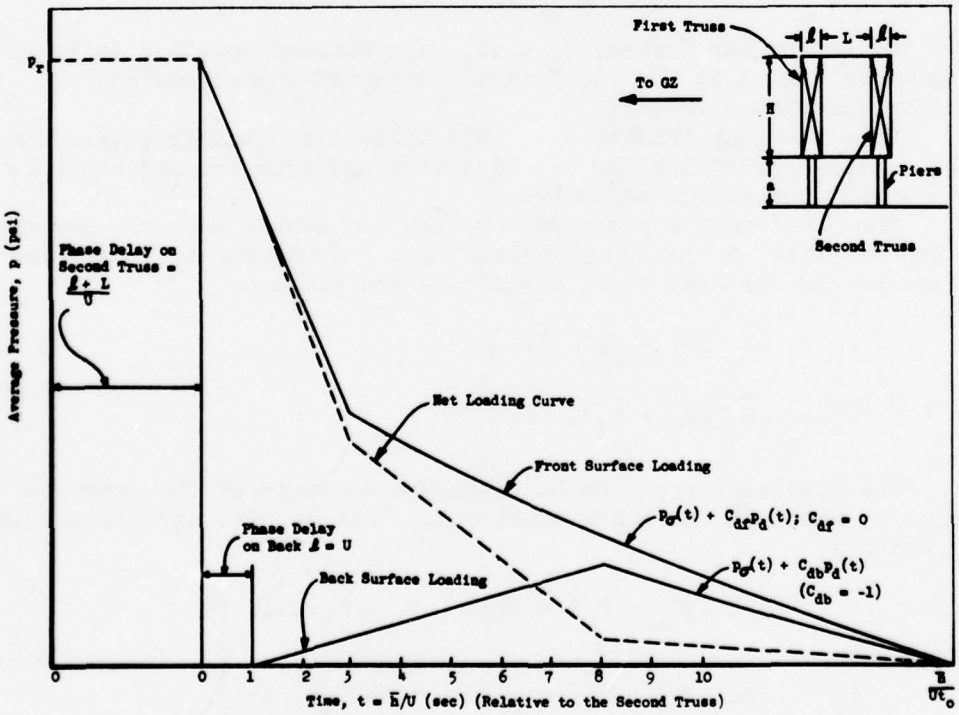

Fig. 3.2 Average Loading on Second Truss, Mach Reflection Region

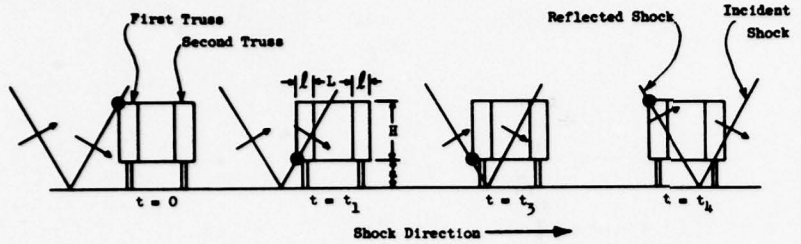

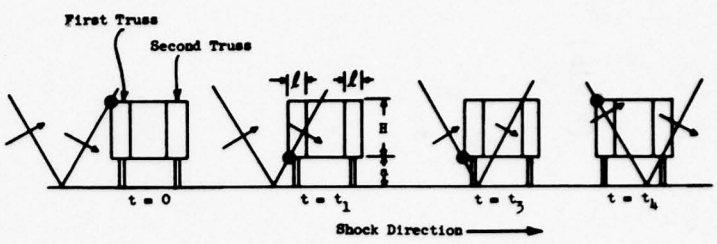

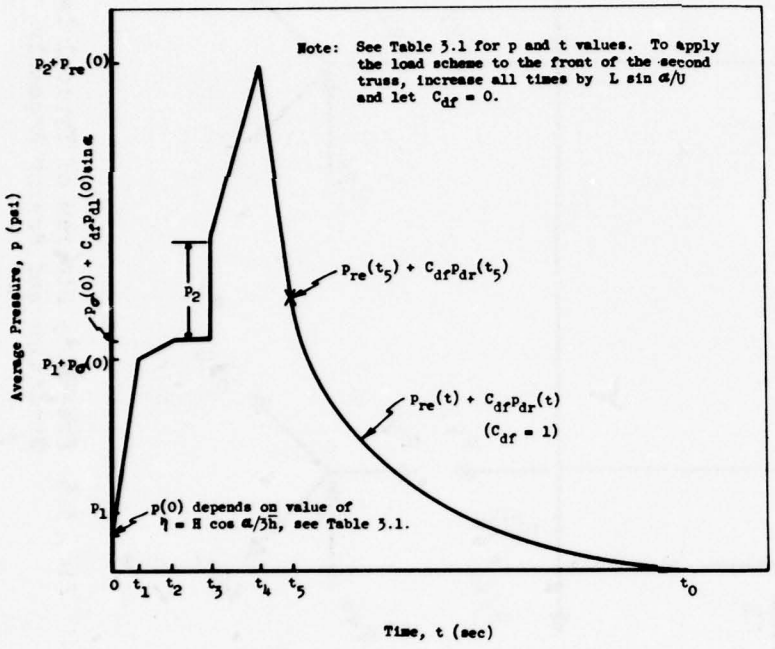

Fig. 3.3 Average Loading on Front of First Truss, Regular Reflection Region

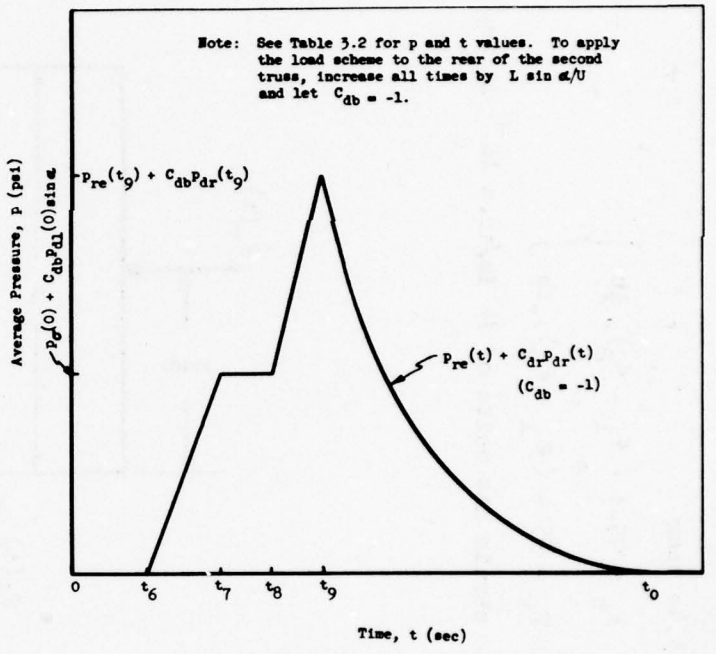

Fig. 3.4 Average Loading on Rear of First Truss, Regular Reflection Region

For the 3.4e beam

$$\left.\begin{aligned} F_h &= 95.4\ (\epsilon_1 - \epsilon_2),\ \text{lb} \\ F_v &= 95.4\ (\epsilon_1 + \epsilon_2),\ \text{lb} \end{aligned}\right\} \qquad (3.21b)$$

where the strain has units of μ in/in. = 10^{-6} in/in.

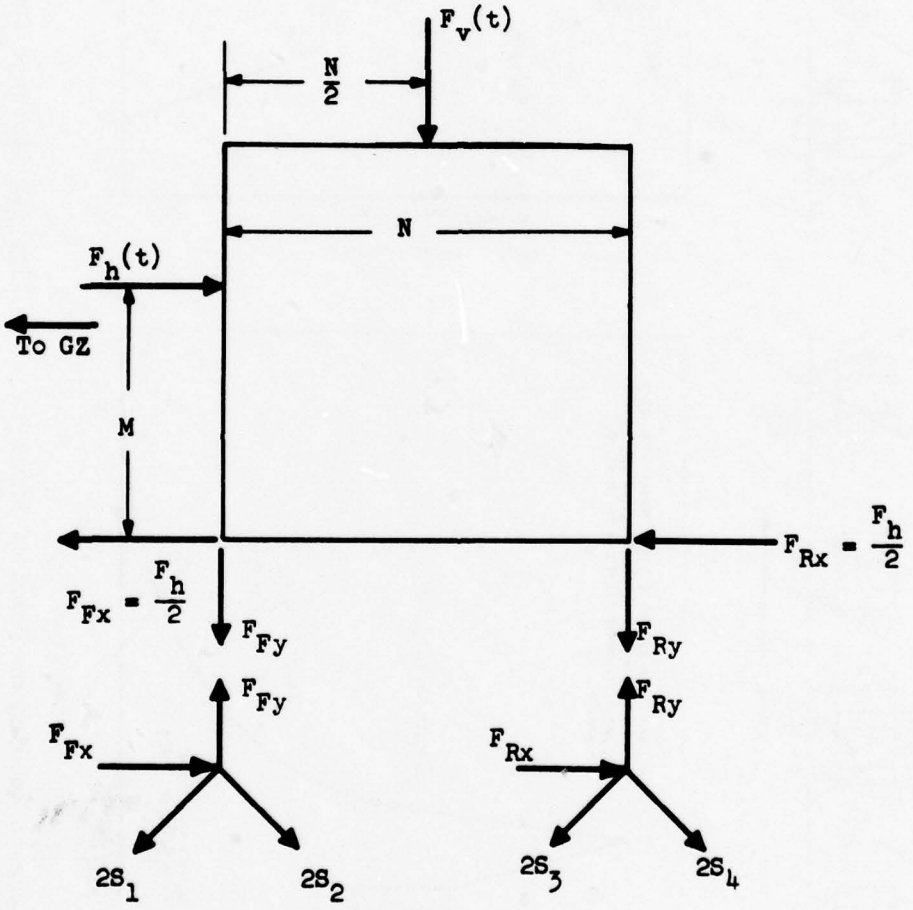

Fig. 3.5 Free Body Diagram of Typical Test Structure and Sensor Assembly

CHAPTER 4

EXPERIMENTAL RESULTS

4.1 FIELD CONDITIONS

All of the test structures were located in the regular reflection region of Shot 9, and within the precursor region of Shot 10. The field conditions are summarized in Table 4.1. As indicated in the table, the bombing error in Shot 9 resulted in misorientations up to 22 degrees.

4.2 PHYSICAL DAMAGE TO TEST STRUCTURES

The blast caused little damage to the test items in Shot 9. The damage that did occur consisted of a small permanent set of approximately 3 in. at the top of the truss bridge section (3.4a) and the cracking of two sensor bars at the weld of the plate girder bridge section (3.4f). In addition, guy cables became loose - apparently due to the cable clamp slipping. All cables were tightened and cracks welded before Shot 10. Two additional clamps were installed on each cable, making five at each end. The permanent deformation of structure 3.4a could not be corrected before Shot 10; however, this damage was not considered serious.

The damage to the test items on Shot 10 was considerably more severe than had been anticipated.[1/] The upper part of the truss section (3.4a) failed and overturned. The overturning began when the vertical posts and diagonals on the ground zero side pulled loose from the gusset plates. The entire upper section then rotated about the rear posts, which eventually failed. The rear diagonals remained intact even after the upper section reached the ground. This condition is shown in Figs. 4.1 through 4.3.

A small permanent set was observed on the top chord component 3.4b. The majority of the guy cables again failed. The bottom chord of structure 3.4a, including ties and rails, was undamaged. The bottom chord (3.4c) appeared to have sustained damage from flying debris. Damage was confined to bending of the gusset plates (see Fig. 4.4).

1/ The test was not originally intended for Shot 10 precursor conditions. When it was known that the test structures were to be located in the precursor region of Shot 10, rough response computations indicated that some damage to the truss section might occur, but not to the degree actually sustained.

Table 4.1 - Summary of Field Conditions

Test Structure	Shot No.	Ground Range (ft)		Orientation (Degrees from Normal)	Over-Pressure (psi)	Duration* (sec)
		Intended	Actual			
3.4a	9	2000	2330	20	11.4	0.78
	10		1930	4.6	9.0	0.57
3.4b	9	2000	2300	21	11.5	0.78
	10		1925	4.5	9.0	0.57
3.4c	9	2000	2275	21	11.6	0.78
	10		1920	4.5	9.0	0.57
3.4e	9	2000	2230	21	11.7	0.77
	10		1915	4.4	9.0	0.57
3.4f	9	2000	2200	22	11.8	0.77
	10		1910	4.3	9.0	0.57

Ambient Preshot conditions: Shot 9 air pressure P_o = 13.2 psi;
air temperature = 16.7° C
Shot 10 air pressure P_o = 13.2 psi;
air temperature = 14.8° C

* Duration of the positive phase of the blast wave
Data obtained from, Summary Report of the Technical Director, WT-782.

4.3 STRAIN GAGE DATA

All of the strain gages provided records of some sort on both Shots 9 and 10. However, five records on Shot 9 and all eighteen records on Shot 10 are considered to be unusable. Comments on the strain gage data for Shot 9 are shown in Table 4.2 and discussed below. Typical records are shown in Fig. 4.5. All records on Shot 10 consisted entirely of what might be termed high-frequency hash; many of these show predominant zero shifts and off-scale readings. It is believed that electromagnetic effects associated with the detonation of the bomb were responsible for the erratic gage behavior in Shot 10. This behavior is considered in the UPSHOT-KNOTHOLE Project 3.28.1, Final Report ("Structures Instrumentation," WT-738).

The records were played back by BRL at two speeds; a slow speed which gave information during and, in most cases, well beyond the positive loading period, and a fast speed which indicated greater detail of the response during the first 300 ms or so after shock arrival. Linearizations were made of both playbacks. The entries in Table 4.2 labeled EC_1 and EC_2 refer to electrical calibration marks; EC_1 is a field calibration taken just prior to shot time, and EC_2 is an earlier calibration taken some time before the tests. No postshot calibrations were made. As is seen, these marks are generally only approximately equal, and in those cases marked "not equal," the difference is of the order of the strain calibration jumps. The linearizations were based on BRL's best estimate of the proper calibration; where EC_1 differed appreciably from EC_2, the possible error involved was not estimated by BRL.

Inspection of the Shot 9 records points out the strong possibility that at least three significant baseline shifts occurred in all records between about 40 and 100 ms after shock arrival. All of the strain channels utilized the same recorder unit. Tracings of the original fast playbacks from structures 3.4a and b are shown in Fig. 4.6. What appear to be three baseline shifts are seen to occur at the same absolute time (i.e., time measured from the bomb detonation). The approximate time increment between these shifts for the Shot 9 records are listed in Table 4.2. The average time between jumps is about 10 and 55 ms; the uncertainty in establishing these times from inspection of the records is of the order of variation in the values listed in Table 4.2.

On the average these jumps occur at 1786, 1796, and 1851 ms after bomb detonation. As indicated in the table, of the apparently usable records only record $3.4eS_2$ does not show three jumps, but this record is suspect because of the extremely low signal level. On some records (e.g., $3.4aS_1$) it is not at first obvious that the jumps occurring at the above times are indeed baseline shifts; only when all records are viewed in this light does this conclusion seem inescapable, see Fig. 4.6.

The magnitude of the first baseline jump is, on the average, about +80 per cent of the maximum recorded strain; for the second jump it is about -40 per cent of the maximum strain; and for the third jump it is also about -40 per cent. The fact that, on the average, these jumps

Table 4.2 - Summary of Strain Gage Data, Shot 9

Strain Record	Remarks	Time Increment Between Probable Baseline Shifts (ms)
$3.4aS_1$	$EC_1 \neq EC_2$	10, 55
$3.4aS_2$	$EC_1 \neq EC_2$	10, 56
$3.4aS_3$	$EC_1 \simeq EC_2$	10, 53
$3.4aS_4$	$EC_1 = EC_2$	10, 55
$3.4bS_1$	$EC_1 \simeq EC_2$	11, 55
$3.4bS_2$	$EC_1 \neq EC_2$	10, 55
$3.4bS_3$	Extremely hashy baseline; signal off scale, not usable	
$3.4bS_4$	$EC_1 \simeq EC_2$	12, 54
$3.4cS_1$	$EC_1 \simeq EC_2$	11, 54
$3.4cS_2$	Zero shift; no recognizable signal	
$3.4cS_3$	$EC_1 \simeq EC_2$	11, 54
$3.4cS_4$	$EC_1 \simeq EC_2$	10, 54
$3.4eS_1$	High frequency hash, not usable	
$3.4eS_2$	$EC_1 = EC_2$, Extremely low signal level	
$3.4fS_1$	High frequency hash, not usable	
$3.4fS_2$	Zero shift; no recognizable signal	
$3.4fS_3$	$EC_1 \simeq EC_2$	11, 57
$3.4fS_4$	$EC_1 \simeq EC_2$	10, 52

Notes - See Fig. 2.7 for explanation of strain gage code
EC_1, EC_2 refers to pretest electrical calibration (see Text).

Fig. 4.1 Postshot, Failure of Truss Section; 3.4a

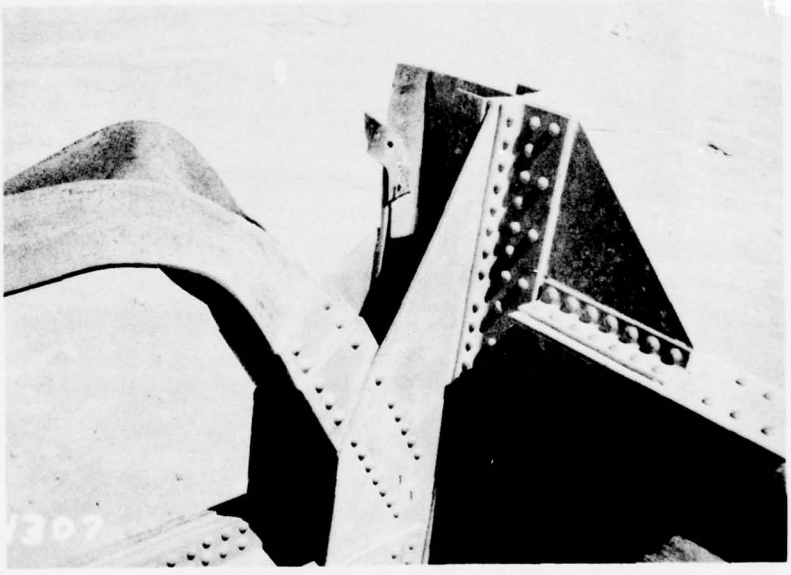

Fig. 4.2 Postshot Plastic Bending of Front Diagonal, Truss Section, 3.4a

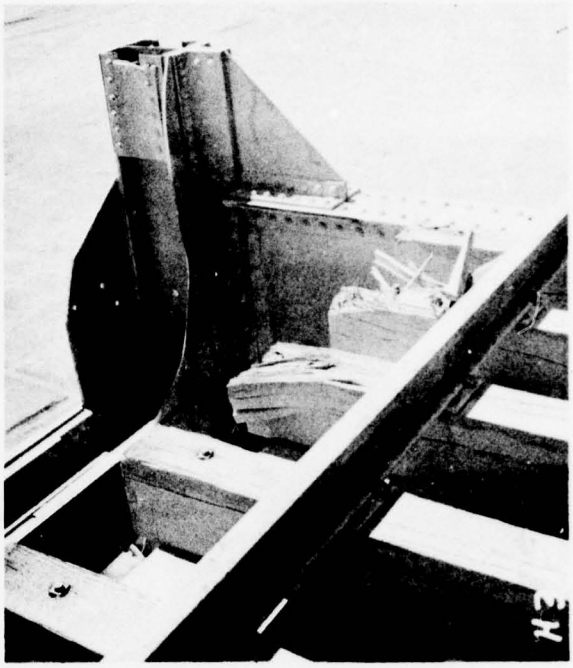

Fig. 4.3 Postshot, Truss Section, 3.4a

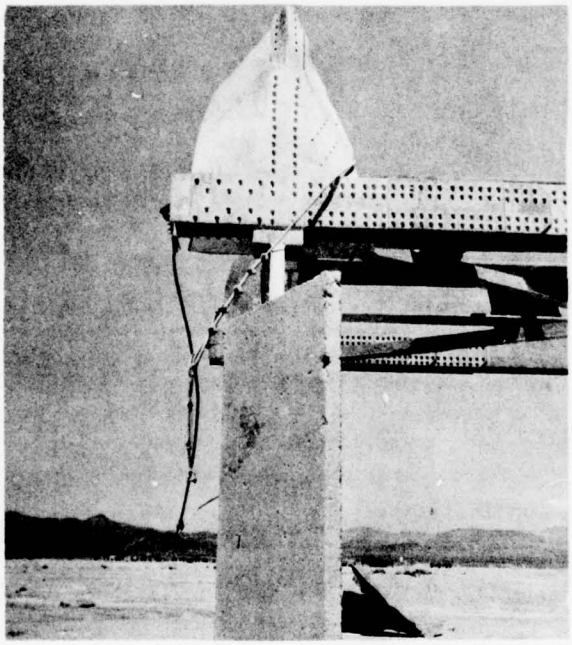

Fig. 4.4 Postshot, Bending of Gusset Plate, Bottom Chord, 3.4c

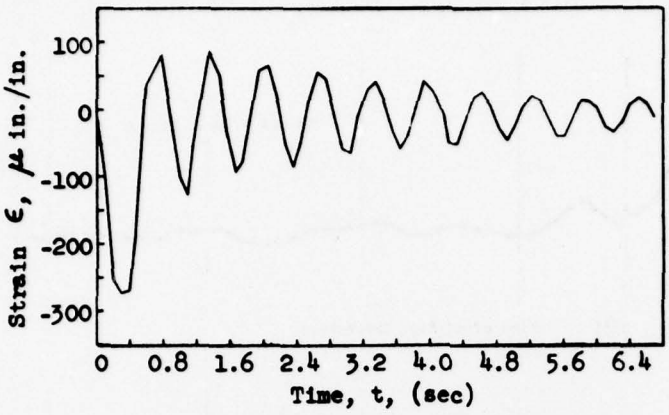

a. 3.4aS1, Shot 9 (Slow Playback)

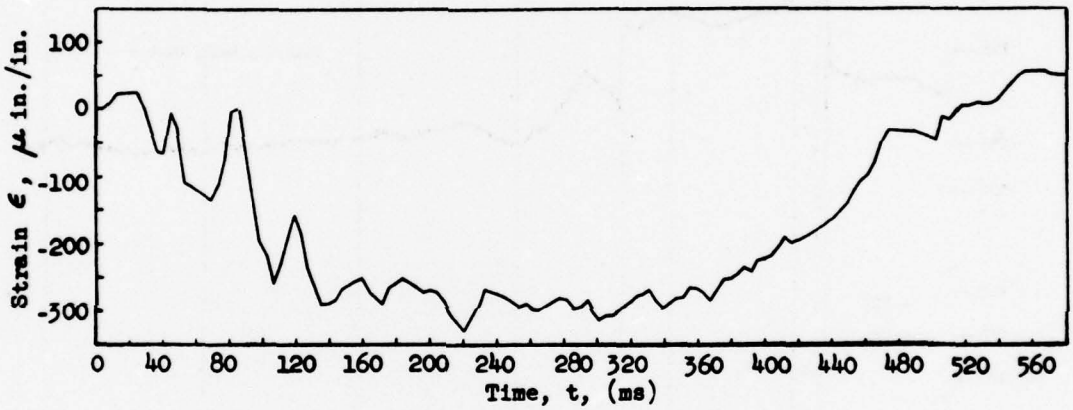

b. 3.4aS1, Shot 9 (Fast Playback)

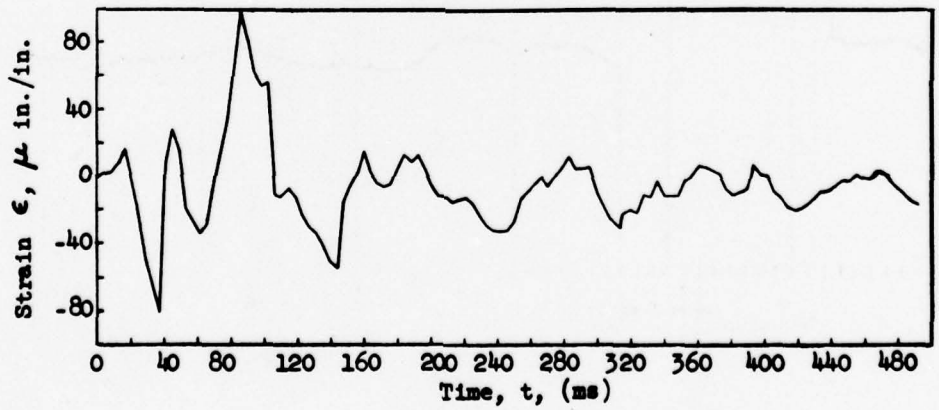

c. 3.4bS1, Shot 9 (Fast Playback)

Fig. 4.5 Typical Strain Gage Records

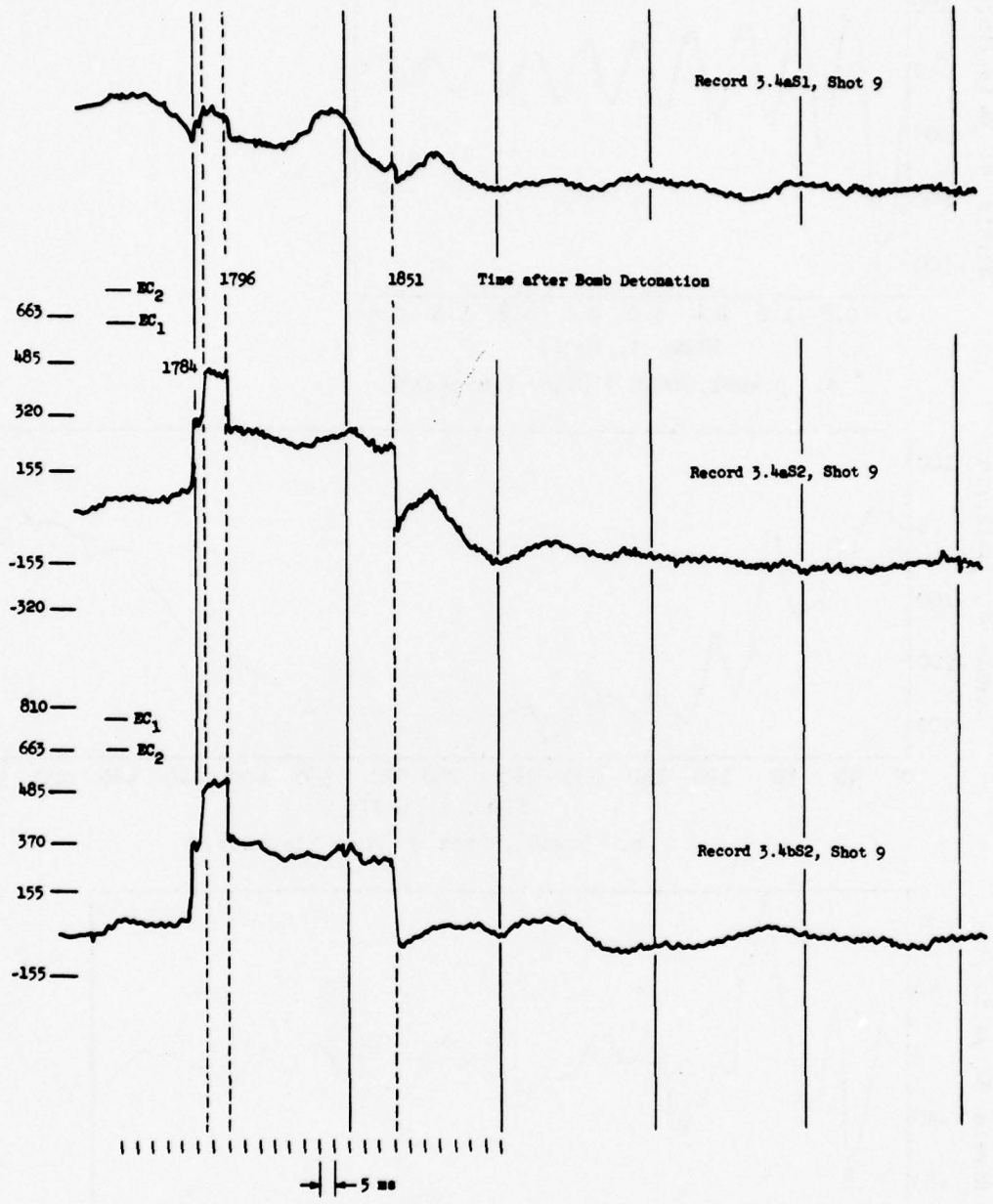

Fig. 4.6 Tracings of Records 3.4aS1, 3.4aS2, and 3.4bS2

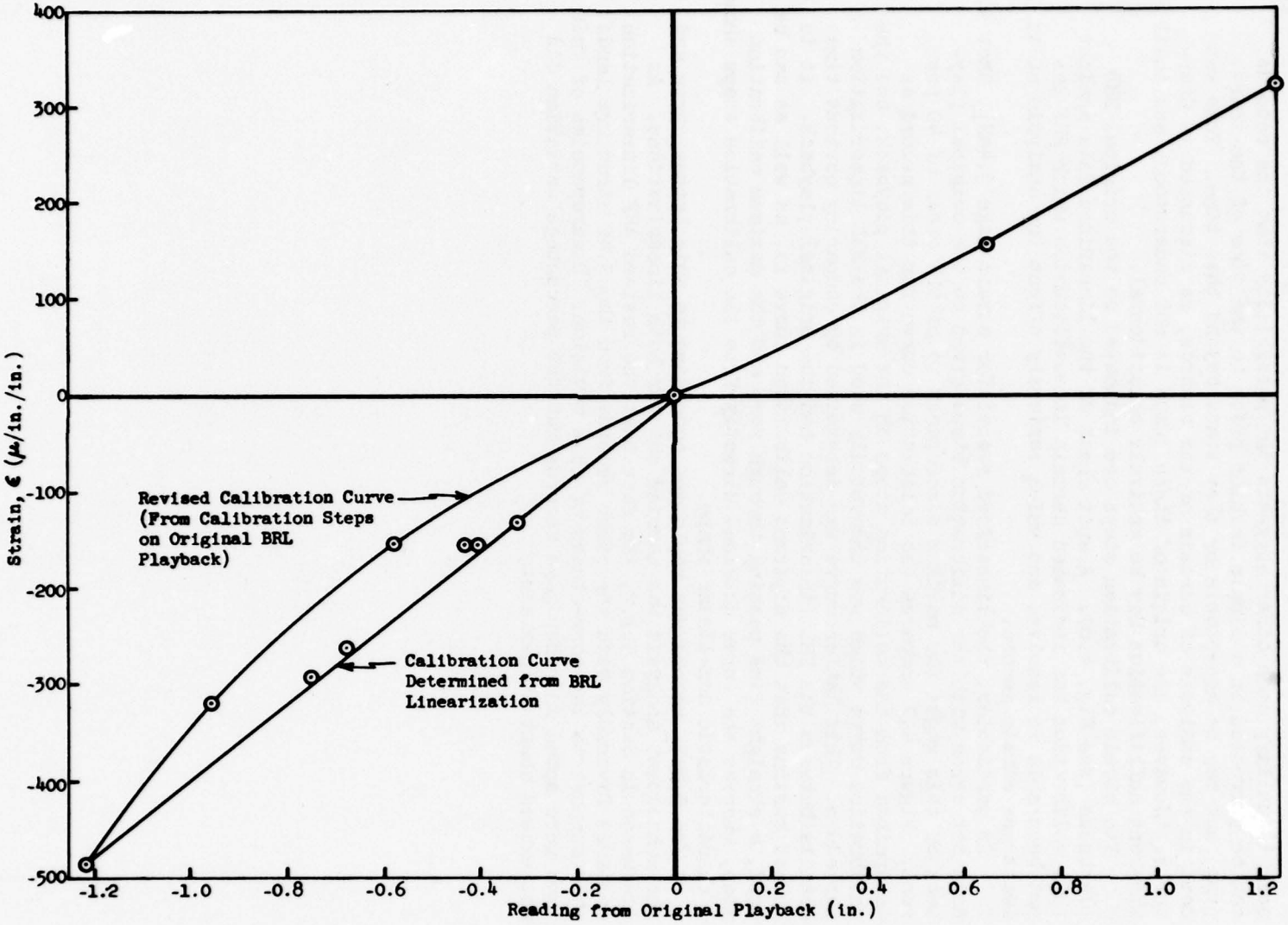

Fig. 4.7 Strain Calibration Curves for Record 3.4aS1, Shot 9

seem to nullify each other suggests the possibility that the records can be corrected in a simple fashion prior to the time of the third jump, and may be acceptable or they stand beyond this time. This was done in the analysis of certain of the records, as discussed in Chapter 5. However, the origin of these jumps is not understood, and their apparent nullification may be entirely coincidental.

The strain calibration steps are indicated on the original BRL playbacks (see Fig. 4.6). A spot check of the linearized data against this calibration has indicated certain inconsistencies which ARF has not been able to resolve, and which seriously affect the analysis of at least one strain record.

In particular, the linearized record for strain gage $3.4aS_1$, Shot 9, does not agree with the calibration steps given on the original playback of this gage; the maximum discrepancy is of the order of 40 per cent. Figure 4.7 compares the calibration curve for this record as determined from the calibration steps on the original playback, and the calibration curve which was undoubtedly used in the BRL linearization procedure. This latter curve was determined by comparing obvious time details between the BRL linearization and the original playback. It is indeed curious that the apparent calibration curve is, as well as can be told, a straight line passing through zero and the maximum calibration step, whereas the curve obtained directly from the calibration steps shows a characteristic non-linear shape.

The $3.4aS_1$ record was replotted according to this latter curve and the subsequent analysis was carried out for both linearizations. As discussed in Section 5.1.2, the fact that the revised ARF linearization compares favorably with the other records from the 3.4a structure lends some support to the correctness of this revision. Discrepancies of this type were noted in other gage records but the percentage deviation did not exceed about 15 per cent.

CHAPTER 5

POST-TEST CONSIDERATIONS

5.1 INTERPRETATION OF THE STRAIN DATA

5.1.1 Introduction

Visual inspection of the strain data did not yield any obvious information as to the nature of the applied blast forces. As discussed in Section 3.3.2, this was not unanticipated and the numerical data reduction scheme referred to as transient analysis was applied to all usable strain records. This work is discussed in Section 5.1.2.

Due to the relatively unsuccessful application of transient analysis, another approach to the data reduction problem was employed in an attempt to get additional useful information from the data. This method, referred to as graphical analysis, is presented in Section 5.1.3.

UPSHOT-KNOTHOLE Project 3.3 ("Tests on the Loading of Horizontal Cylindrical Shapes," WT-722) was concerned with exactly the same data reduction problems as in the present program. Toward the end of the post-test phase of Project 3.3, work was initiated on a rapid trial-and-error procedure of curve fitting utilizing an analog computer. While this technique was not applied to the present Project 3.4 strain data, a brief description of the method is contained in Section 5.1.4.

5.1.2 Application of Transient Analysis

It was originally felt that, due to the relatively complicated response of the dynamic systems involved, the magnitude and time details of the incident blast loading probably could not be determined adequately from inspection of the strain records alone. Furthermore, it did not appear feasible to determine the response of most of the test items to even a known input by analytical procedures. Thus, the analysis of the data could not proceed by ordinary means. This situation was realized during the pretest planning phase of the program and a numerical data-reduction scheme, referred to as "transient analysis," was developed which held the promise of determining the forcing function from a known response even when the transfer functions[1] of the system were not known.

[1] The transfer function refers to the response of the system in one mode due to a unit impulse applied in another mode (see Appendix A).

In general, the solution to this problem is not unique, even for a linear dynamic system; that is, a given response in a particular mode of the system may result from more than one combination of forcing functions in the various modes. At the outset it was believed that, in the present application, uniqueness stemmed from the fact that both the unknown forcing and transfer functions could be adequately represented by a particular class of analytic functions. Specifically, the forcing function was represented by a finite sum of exponential terms (i.e., "e" functions), all of whose exponents and coefficients were real; the transfer function was represented by a similar series all of whose exponents and coefficients occurred in complex conjugate pairs. (This is equivalent to assuming a forcing function which has no harmonic components, and transfer functions consisting of damped sinusoids.) Based on this particular representation, the method, in brief, consisted of curve-fitting the known response (i.e., strain data) to a similar exponential series and then identifying those coefficients and exponents belonging to the forcing function. In the process the transfer function is also determined. The detailed development of the method of transient analysis as well as a critical discussion of its general applicability is presented in Appendix A. The present section is concerned with the specific application of the method to the strain data.

The analysis was applied to all four records on structure 3.4a, records S_1, S_2 and S_4 on 3.4b, and records S_1, S_3 and S_4 on 3.4c - all on Shot 9.2/. These strain records were fit to a five-term exponential series as described in Appendix A. It was hoped that the fifth-order polynomial resulting from this fit would have three real roots and two complex conjugate roots. If so, the analysis would yield a forcing function consisting of three exponential terms and a transfer function containing a single frequency. However, in all but one case the analysis provided only a one term approximation to the forcing function and two frequencies. The results obtained are shown in Table 5.1 with only a relative scale being indicated for the magnitude of the forcing function since a true force scale cannot be determined from the analysis alone (See Appendix A.)

The one case in which a three-term approximation to the forcing function was obtained (i.e., for record 3.4aS_2) is plotted in Fig. 5.1. The shape of the drag curve from Fig. 5.12 (based on the pretest load prediction scheme) is shown for comparison. With reference to Table 5.1, the decay rate of the forcing functions determined from the 3.4a strain records appear to be reasonable in terms of what is known about the loading. Inspection of these strain records shows a frequency of about 29 cps and possibly one of about 50 cps, (see Fig. 4.5) which is of the order of magnitude found for the frequencies of the transfer function. That the analysis completely missed the principal frequency of about 1.5 cps,

2/ The analysis was applied to these records before the probable occurence of baseline shifts and calibration errors was appreciated (see Section 4.3). The possible error introduced in the analysis is considered later in this section.

however, is not surprising since the results are based on data for only the first 300 to 400 ms of the loading. The results for the other structures shown in Table 5.1 indicate that the proper frequencies may have been picked out, but most of the decay rates appear to be too large.

In general, the results indicated in Table 5.1 are not believed to be an adequate interpretation of the strain data and, as such, it must be concluded that this first application of transient analysis was unsatisfactory. In an attempt to understand just why the analysis failed, a rather detailed post-test reappraisal of the method was undertaken. Much of the critical discussion presented in Appendix A is a result of this additional study.

The first application of transient analysis was completed before the occurrence of probable baseline shifts and calibration errors in the strain data was fully appreciated (see Section 4.3). The fact that the strain scale of the records might be in error by a constant factor would not affect the reliability of the analysis, inasmuch as the forcing function can be determined only within an arbitrary scale factor. However, if the time details of the strain record are distorted due to non-linear scale errors or baseline shifts, the situation is different. Here the forcing function determined by transient analysis might not have physical meaning since it would be based on prime data that was in part arbitrary.

Thus, the uncertainty attributed to the strain data could account to some extent for the unsatisfactory results obtained, although present understanding of the transient analysis makes it impossible to determine the extent to which errors in the prime data can influence the final results. In the present instance, however, it is felt that the failure of this first application of transient analysis can be more readily explained in terms of the poor curve-fit obtained for the known response. Whether it was due to computational errors or simply an inadequate number of terms in the approximating series (most probably the latter), the fact remains that the determination of the forcing functions was based on analytical expressions which were not adequate representations of the measured strain time curves - even though these curves may themselves be in error.

As discussed in Appendix A, the valid application of transient analysis is limited to linear systems where the forcing functions associated with each mode are either zero or timewise proportional. When the forcing functions are not all timewise proportional, the results of the analysis probably cannot be given physical meaning. (This limitation of the method was not fully appreciated at the outset.) Now it is possible that in as complicated a structure as the truss bridge, the forcing functions associated with each mode are not timewise proportional. But this cannot be demonstrated one way or the other at the present time, and the applicability of the method is not sufficiently well-understood to decide definitely as to its validity.

A second application of the method of transient analysis based on a more realistic fit of the strain records was initiated, but this work could not be completed within the scope of the post-test phase of

the program. Only preliminary results with respect to one strain record were obtained, and while these appear encouraging no general conclusions can be drawn. The data considered was strain record $3.4aS_1$ on Shot 9. A comparison is made between the actual strain record[3] and the results of the curve-fitting in Fig. 5.2. This rerun of the analysis differed from the first computation in that the approximating series consisted of seven exponential terms rather than five, and the obvious frequency of about 1.5 cps was curve-fitted directly. The second frequency as determined by the analysis itself was 29 cps, which agrees very closely with an observable frequency in the data.

While the results of this curve-fitting appear to be realistic (see Fig. 5.2), they could no doubt be improved. The resulting forcing function is shown in Fig. 5.7 and is compared with certain results obtained in the following section. At present, the curve labeled "graphical analysis" in Fig. 5.7 may be accepted as representing an independent estimate of the forcing function component leading to the measured strain of gage $3.4aS_1$ (see Section 5.1.2). Inasmuch as the forcing function obtained from transient analysis has an arbitrary scale factor, the present results were fitted to the results of graphical analysis at about 100 ms.

With reference to Fig. 5.7, the forcing function determined by transient analysis shows the same broad time details as does the graphical approach. That is, the time of rise to maximum load and the rate of decay during the drag phase of the loading are in good agreement. However, the time details during the diffraction period are not adequately reproduced and, indeed, such detail could not be expected from a three-term exponential series.

On the basis of this comparison transient analysis appears to be a feasible method in the present application, provided that the analytical approximation to the strain data (i.e., curve-fitting) is itself realistic. But this is not a definite conclusion, and much additional work remains to be done in application of the method.

5.1.3 Graphical Analysis

In view of the rather unsuccessful results of the first application of transient analysis, it was necessary to follow another approach in an effort to obtain the desired information from the strain data. The method adopted was an attempt to remove the obvious harmonic components of the response by inspection and thereby yield at least the shape of the forcing function. For lack of a better name this technique was referred to as graphical analysis. The method was applied with greatest success to the 3.4a strain records, and only these results are considered in this section.

The probable baseline shifts in the 3.4a strain records (see Section 4.3) were eliminated prior to the application of the present analysis.

[3] The baseline shifts on this particular record were not appreciable and, hence, they were not compensated for (see Fig. 4.6).

The procedure consisted of determining both the time of occurrence and magnitude of the shifts by visual inspection of the linearized strain records, and replotting the records accordingly. Three baseline shifts were removed from each of the four 3.4a strain records in this fashion.

The strain records from the 3.4a truss bridge section show a well-defined frequency of about 1.5 to 1.6 cps (Fig. 4.5) which is undoubtedly due to vibration of the top chord members relative to the bottom chord (see Section 5.2). The period of this vibration is just slightly less than the duration of the positive phase of the blast wave.

It was possible to determine an analytical approximation to this principal harmonic component of the response by means of measurements taken from the strain records. The analytical approximation determined from each of the strain records is;

$$\left.\begin{array}{l} \text{for strain record } 3.4aS_1 \\ \quad 149e^{-0.31t}\cos(9.96t - 1.20) \\ \text{or} \\ \quad 97e^{-0.31t}\cos(9.96t - 1.20) \\ \text{for strain record } 3.4aS_2 \\ \quad 97e^{-0.31t}\cos(9.96t - 1.20) \\ \text{and for strain records } 3.4aS_3 \text{ and } 3.4aS_4 \\ \quad 97e^{-0.31t}\cos(9.96t + 2.29),\ t \text{ in sec.} \end{array}\right\} \quad (5.1)$$

The two amplitudes given for strain record $3.4aS_1$ are based on the BRL linearization (amp = 149) and the revised ARF linearization (amp = 97), as discussed in Section 4.3. The numerical values given above are all average values, the variation in each being about $\pm$ 15 per cent. The fact that the four records yield the same amplitude if the revised linearization is accepted, lends some support to this procedure.

The first step in the analysis was to subtract (at each instant of time) the harmonic component given by Equation 5.1 from the appropriate strain record. The results of this subtraction are referred to in Figs. 5.3 through 5.6 as the "first reduction." From these results a rather obvious median curve can be faired in, about which the record appears to be oscillating. This curve is referred to as the "second reduction" in Figs. 5.3 through 5.6 and represents, according to this approach, the shape of the forcing function contributing to the reaction in the individual sensor bar.

In the case of record $3.4aS_1$ a second frequency can be identified in both the BRL and ARF linearizations, which permits a somewnat more

rational approach to the second reduction. From Fig. 5.3 this frequency is seen to be about 29 cps and, as discussed in Section 5.2, is due apparently to the vibration of the entire structure on the sensor supports. The analytical approximation of this component of the response for the ARF linearization was determined to be[4]

$$132e^{-7.6t} \cos 182t$$

This component was subtracted from the first reduction and the resulting second reduction for this record is shown in Fig. 5.7 where the strain scale has been converted to force per unit frontal area of the upstream truss. The second reduction introduces a strong harmonic component during the first 50 ms of the loading and then becomes increasingly similar to the first reduction as the 29 cps frequency is damped out.

The predicted diffraction loading from Fig. 5.12, is compared with the result of the second reduction in Fig. 5.7. As can be seen, the two curves compare quite favorably when allowance is made for the uncertainty in zero times. Thus, these results tend to substantiate the load prediction scheme during the diffraction period, at least with respect to time details.

As discussed in the previous section, the rerun of transient analysis was carried out for strain record $3.4aS_1$, Shot 9. These results are compared with the results of the present method in Fig. 5.7. Inasmuch as the forcing function obtained from transient analysis has an arbitrary scale factor, the solid curve in Fig. 5.7 was fitted to the present results at about 100 ms. A discussion of this comparison is contained in the previous section.

The horizontal component of force transmitted to the sensor bars is proportional to the algebraic difference in strain as given by this equation. According to this equation, which results from treating the structure-sensor system as a statically determinate problem, the horizontal force may be obtained from either strain records S_1 and S_2 or records S_3 and S_4. The horizontal force per unit projected area of the first truss as determined from strain records S_1 and S_2 is shown in Fig. 5.8. Results are shown for both the BRL and ARF calibration of strain record S_1. The horizontal force, as determined from records S_3 and S_4, is shown in Fig. 5.9.

The horizontal force as determined from strain records S_1 and S_2 is compared with the predicted horizontal loading based on the measured blast parameters for Shot 9 (see Section 5.2) in Fig. 5.8. Allowing for uncertainties in the location of zero time, these results utilizing the ARF linearization of record S_1 are seen to compare remarkably well with pretest predictions; the results using the BRL calibration indicate the same time details, but show pressures about twice the predicted values

4/ The damping term is admittedly quite approximate, since only several cycles of the vibration can be identified in Fig. 5.4.

during the drag phase. The horizontal force computed from records S_3 and S_4 (see Fig. 5.9) shows different time details during the diffraction period and much larger drag forces. In this respect the drag forces are in agreement with the results of the BRL linearization of record S_1 shown in Fig. 5.8. The differences in horizontal force as determined from the front and rear sensor gages may be due in part to orientation effects. The predicted loading is, of course, based on head-on orientation; wheras the blast wave which struck the 3.4a bridge section was oriented about 20 degrees from the normal.

In view of the uncertainty attending both the pretest load prediction scheme and the strain data, the agreement between measurement and shock theory in Fig. 5.8 is indeed remarkable, and may in fact be coincidental. Considering the rather conflicting nature of other results obtained however, one is not justified in definitely concluding that the test data support the pretest load prediction method.

5.1.4 Analog Computer Method

UPSHOT-KNOTHOLE Project 3.3 ("Tests on the Loading of Horizontal Cylindrical Shapes," WT-722) was concerned with many of the same problems encountered here. That is, the test was designed to determine the loading on horizontal cylinders utilizing, in part, a net force measurement system with strain output identical to the one in the present test. In connection with Project 3.3, work was initiated on the use of the ARF analog computer to deduce the desired information from the strain records. While time would not allow this technique to be employed in the present program, this approach appears to be well suited to it and will be summarized briefly in this section.

The method of solution utilizing the analog computer consists of simulating a dynamic system on the computer which yields displacements similar to the strain record under consideration, and then adjusting the circuit parameters so that the two displacement-time curves are essentially the same. The system equations are taken to be a series of linear second-order differential equations with constant coefficients, an assumption which is also basic to the method of transient analysis. The forcing function may be represented by a variety of analytical or graphical functions on the computer but only decaying exponential terms were utilized in connection with the work on Project 3.3, again as in the method of transient analysis.

On first thought, this approach might seem rather hopeless in view of the large number of unknown quantities involved, i.e., the constants of the system equations and the parameters of the forcing function. However, in practice, the method appears to be quite feasible, and while not carried sufficiently far as to provide any conclusive results, gives indications of being an advantageous approach. The feasibility of the method in practice stems from the fact that the strain records to be matched can be plotted on graph paper and the displacement arising from the simulated system can be superposed automatically be means of an "x-y recorder." This allows a visual estimate of the accuracy of the matching, and permits much more judgment on the part of

the operator in carrying out the solution than is possible when using a numerical method. This advantage, together with the brief time required for varying parameters and obtaining solutions, permits the matching to be completed in a relatively short time.

Use of the analog computer technique as a means of data reduction is only in the very early preliminary stages. However, this work has indicated a reasonable expectation of ultimate success, and it is strongly recommended that this work be pursued further as a part of an over-all study into the data-reduction problems associated with net force measurement systems. One advantage of the analog computer approach which concerns the forcing function approximation should be emphasized. It is not necessary in the analog scheme to be restricted to an exponential approximation of the forcing function since it is possible to generate many other functions on the computer. For example, one form of representation which could be handled easily is a series of straightline sections during the initial loading period, followed by either a linear or exponential decay to zero. Existing load prediction schemes could be generated on the computer and the response of the simulated system compared with the actual response data.

5.2 RESPONSE OF THE TRUSS BRIDGE SECTION, 3.4a

5.2.1 Introduction

The truss bridge section (3.4a) suffered a small permanent set of about 3 in. on Shot 9 (no precise measurement of this deformation was taken), and was completely overturned as a result of Shot 10. An attempt is made in this section to correlate the predicted blast loading with the observed response of the bridge.

The truss bridge represents a rather complicated structure, and a precise determination of its response to even a known loading is not practical on the basis of present-day knowledge. However, circumstances are such that an approximate, though fairly realistic, estimate of the response can be made as a result of the test data obtained.

The strain records on Shot 9 indicate the bridge to be responding in two principal modes; one with a frequency of about 1.5 cps which is undoubtedly due to vibration of the top chord members relative to the bottom chord, and one with a frequency of about 29 cps which appears to be due to the total mass of the bridge vibrating on the flexible sensor supports. In the following discussion the higher frequency mode will be ignored and the bridge assumed to be a single-degree-of-freedom system possessing a frequency of 1.54 cps of a period of 0.65 spc.[5/] The measured frequency determines the ratio of effective stiffness to effective mass of the bridge section. These quantities are computed in the following section.

5/ This is an average value, the variation being about ± 0.02 sec cycle-to-cycle and record-to-record.

5.2.2 Effective Mass and Resistance of Bridge

Figure 4.1 is a postshot 10 photograph of the bridge showing the manner of failure. It is seen that the members above the lower sway brace strut remained essentially rigid and that plastic hinges formed at the ends of the vertical posts just below this strut. It seems reasonable, therefore, to take the effective mass of the bridge as being the total mass of the members above the lower sway brace strut plus 1/4 the mass[6] of the unsupported posts and main diagonals. This mass is found to be, $m = 142$ lb-sec^2/in. Using the following relationship for the period of a simple mass-spring system,

$$T = 2\pi \sqrt{m/k_1} = 0.65 \text{ spc}$$

The effective stiffness is computed to be $k_1 = 13.2 \times 10^3$ kips/in.

There is now the problem of determining the effective resistance of the bridge from this stiffness value. The major uncertainty concerns the effectiveness of the main diagonals which are the same section as the posts (14WF78) but of longer length, and oriented to bend in the strong direction. If the diagonals are discounted for the moment, and the posts assumed to act as cantilever beams with guided ends, the total stiffness (for four posts) is

$$k_1 = \frac{48EI}{\ell^3}$$

Using $I = 206$ in.^{4} for a 14WF78 section bending in the weak direction and $E = 30 \times 10^6$ psi, the effective length ℓ is found to be about 23.5 ft. This is close to the unsupported post length of about 21 ft.

In computing the response of the bridge, the resistance function is assumed to have an idealized elastic-plastic form as indicated in Fig. 5.10. The stiffness during the elastic portion is given by

$$k_1 = \frac{R_p}{X_p}$$

where R_p is the maximum (plastic) resistance and X_p is the limiting elastic displacement. Based on a yield stress of $\sigma_y = 45{,}000$ psi, the maximum (plastic) moment of a 14WF78 section oriented to bend in the weak direction is computed to be

$$M_p = \frac{3}{2} \sigma_y S = 2.4 \times 10^6, \text{ in.-lb per post.}$$

6/ This is the usual approximation in computing the fundamental frequency of a vibrating cantilever beam with a concentrated mass on the end wherein the effective mass of the system is taken as 1/4 (actually 0.23) of the mass of the beam plus the total end mass.

For a guided cantilever with end shear R, and end moment M,

$$R = (2/\ell)\, M$$

Using this relation and the effective post length computed above, the maximum resistance of the bridge, R_p, is computed to be

$$R_p = \frac{4 \times 2 \times 2.4 \times 10^6}{23.5 \times 12} = 68 \text{ kips}$$

The associated yield displacement is then

$$X_p = \frac{R_p}{k_1} = \frac{68 \times 10^3}{13.2 \times 10^3} = 5.2 \text{ in.}$$

The maximum plastic resistance determined above is felt to be a minimum value, inasmuch as the resistance of the diagonals has been neglected. The diagonals are also 14WF78 sections, but are longer (total length about 50 ft) and are oriented to bend in the strong direction. All things considered, the actual resistance is not believed to exceed the computed value by more than a factor of 2, and this range of resistance will be considered in the following response computations.

5.2.3 Response Computations, Shot 9

Brooks and Newmark ("Development of Procedures for Rapid Computation of Dynamic Structural Response") have determined the response of non-linear mass-spring systems to triangular-shaped loading functions which are typical of blast loadings based on current prediction methods. These solutions are given in graphical form and by empirical relationships determined from many numerical solutions. In particular, Brooks and Newmark have developed an empirical formula for determining the maximum displacement of a mass-spring system having an elastic-plastic resistance function which may include the deadweight overturning effect of the structure, see Fig. 5.10. The loading considered consists of an initial impulse plus an initially peaked triangular pulse. This relationship is,

$$\frac{F_m}{R_p} = \frac{T}{\pi t_2}\left[\sqrt{A} - \sqrt{D}\right] + \frac{A - D}{2\frac{X_m}{X_p}\left(1 + \frac{0.7T}{t_2}\right)} \qquad (5.2)$$

where

$$A = 2\frac{X_m}{X_p} - 1 + k\left(\frac{X_m}{X_p} - 1\right)^2$$

$$D = (2\pi I_o/R_p T)^2$$

and where

F_m = peak load of triangular pulse

R_p = maximum resistance

X_m = maximum displacement of mass

X_p = yield displacement

k_1 = slope of elastic portion of resistance function

k_2 = slope of plastic portion of resistance curve

$k = \frac{k_2}{k_1}$

M = effective mass of system

$T = 2\pi \sqrt{\frac{M}{k_1}}$ = natural period of system

t_2 = duration of triangular load

I_o = initial impulsive loading.

Equation 5.2 becomes exact in the limiting cases for both infinitely short and infinitely long duration pulses, i.e., for $t_2 > 0$ and $t_2 > \infty$. For loads of an intermediate duration, Brooks and Newmark state that Equation 5.2 is generally accurate to within 6 per cent. This is considered completely adequate for the present application.

The pretest load prediction scheme described in Chapter 3 was applied to the 3.4a bridge section using the measured blast wave parameters for Shot 9 (see Table 4.1). The net horizontal load is shown in Fig. 5.12. Inspection of this figure shows that it is not unreasonable to approximate the loading by an equivalent initial impulse followed by a triangular decay. The shaded area under the net load-time curve from zero to the duration of the diffraction loading (i.e., at t = 80 ms) is taken to be the initial impulse I_o 7/; I_o = 0.225 psi sec. The remaining portion of the loading (i.e., the drag loading) is approximated by a triangle whose initial peak (F_m) is taken to be the peak drag force and whose duration (t_1) is chosen so that the total drag impulse is preserved. The equivalent loading is shown in Fig. 5.12; F_m = 3.2 psi, t_2 = 0.32 sec.

Equation 5.2 was solved numerically for the maximum resistance, R_p, as a function of maximum displacement, X_m, based on a constant

7/ Brooks and Newmark state that a load applied over a finite time interval may be approximated by an equivalent impulse provided the interval is less than about 1/10 the period of the system. In the present case the duration of the diffraction loading is about 12 per cent of the period.

period, T, and the above load parameters. The results are plotted in Fig. 5.13. It was estimated that the bridge sustained a 3-in. permanent set in Shot 9, or a maximum displacement of $X_m = X_p + 3$ in. From Fig. 5.13, a displacement of this amount corresponds to a resistance about 50 per cent greater than the estimated minimum value. Since the maximum possible resistance is estimated at something less than twice the minimum value, this result is plausible. Based on the estimated minimum value for R_p, $X_m = 15.4$ in. $\cong X_p + 10$ in. For the estimated maximum value of R_p, $X_m = 9.7$ in. $= X_p$[8] $- 0.7$ in. (i.e., the bridge would have remained elastic).

A further computation was carried out in which displacement as a function of drag coefficient was determined for the range of interest in resistance. These results are shown in Fig. 5.14, where the drag coefficient is expressed as a percentage of the nominal value used in the pretest load prediction scheme. This nominal value is $C_d = 3 = C_d^o$, based on the horizontal projected area of the first truss only as discussed in Chapter 3. The value of C_d as determined from the condition that $X_m = X_p + 3$ in. is seen from Fig. 5.14 to vary between 0.6 and 1.3 for the range of resistance considered.

There is one important conclusion to be drawn from the above analysis; namely, that the pretest load prediction scheme for the 3.4a truss bridge in conjunction with a simplified response analysis leads to a valid estimate of the actual behavior of this structure under field conditions. That is not to say that the present result amount to a verification of the load prediction scheme or lead, say, to any revision in over-all drag coefficient. The present analysis is certainly too crude to permit this, although such was the intent of this test program. Rather, existing load and response prediction methods would, in the present case, lead one to conclude that the 3.4a bridge would not suffer excessive damage for Shot 9 conditions — whether the displacement turned out to be 5 in. or 15 in. — and this result was indeed borne out. In other respects it is felt that this analysis has no quantitative meaning.

5.2.4 Response Computations, Shot 10

The 3.4a bridge section was overturned as a result of the loading experienced in Shot 10. The bridge was well within the precursor region in this shot and its response was more violent than had been anticipated, although detailed pretest response computations had not been made for estimated Shot 10 conditions. One result of the UPSHOT-KNOTHOLE Project 3.1 ("Tests on the Loading of Building and Equipment Shapes," WT-721) was to propose, quite tentatively, a load prediction scheme applicable to items of simple geometry in the precursor region. The present section is concerned with response computations for the 3.4a bridge based on this load prediction scheme.

8/ In order to preserve the measured period of 0.65 spc, the yield displacement, X_p must vary directly with the maximum plastic resistance, R_p. For $R_{p_{max}} = 136$ kips, $X_p = 10.4$ in.

The loading method developed in WT-721 stemmed from pressure gage data obtained on a solid rectangular parallelepiped located in the precursor region of Shot 10 that rigidly withstood the effects of the blast. These data have led to an average force-time variation experienced by the structure as indicated in Fig. 5.15. The load rises linearly from zero to a maximum value in approximately 100 ms, a time which is felt to be independent of the geometry of the structure. The load then decays linearly to zero in a time equal to the positive phase duration of the blast wave. The maximum pressure attained is taken to be the peak drag pressure associated with the peak overpressure which would have occurred over an "ideal" surface in the absence of a precursor, multipled by some over-all drag coefficient for the structure. This loading is markedly different from what is generally felt to the case in the conventional Mach reflection region in the absence of a precursor. There is a finite rise time, no diffraction period, and a wave form during the drag phase which differs from the usually accepted wave form of the dynamic pressure curve.

There exists considerable doubt concerning the prediction of peak dynamic pressure in the precursor region. In UPSHOT-KNOTHOLE Project 1.1d ("Dynamic Pressure Versus Time and Supporting Air Blast Measurements," WT-714), dynamic pressure gages were located on the main blast line at a ground range of 1920 ft and elevations of 10, 25, and 40 ft in Shot 10. (The 3.4a structure was at a ground range of about 1930 ft and extended from 15 ft to about 65 ft above ground level.) These gages recorded maximum dynamic pressures of 10.9, 11.6 and 12.4 psi, in order of increasing elevation. However, the quantity measured by these gages is believed to be strongly influenced by the presence of suspended dust in the air and, in addition, there is some uncertainty associated with the calibration of these gages. Theoretical predictions for dynamic pressure over an ideal surface are contained in both WT-714 and WT-721, and indicate a peak pressure of about 9 psi for the 3.4a bridge. Using a nominal overall drag coefficient of 3 for the bridge, the peak force per unit frontal area of the first truss is believed to be in excess of 27 psi as indicated in Fig. 5.15.

Brooks and Newmark have obtained the response of an elastic-plastic mass-spring system to the triangular-shaped loading discussed above and shown in Fig. 5.15. Their results are presented in graphical form in "Development of Procedures for Rapid Computation of Dynamic Structural Response." Based on this solution, the response of the 3.4a truss bridge section has been computed as a function of the peak load to resistance ratio and is shown in Fig. 5.16. Brooks and Newmark have results for $k = -0.04$ and $k = 0$ (the factor k determines the relative shape of the resistance function, see Fig. 5.10 and Equation 5.2). In the present case, $k = -0.014$ and, as seen in Fig. 5.16, there is some uncertainty in interpolation at the large displacements.

A convenient failure or collapse criterion is the displacement beyond which the structure would overturn of its own weight. In terms of the present notation, this collapse displacement, X_c, is given by,

$$X_c/X_p = 1 - 1/k$$

$$= 1 + 1/0.014 = 72 \text{ for the 3.4a bridge section.}$$

From Fig. 5.16, collapse is thus assured for[2/]

$$F_m = C_d p_d(0) > 2.5R_p$$

For the range of resistance considered in the response computations for Shot 9, the collapse load will thus vary between about 6 and 12 psi. Inasmuch as the peak load for Shot 10 is estimated to exceed 27 psi (based on an over-all drag coefficient of 3), the result of the present analysis is entirely consistent with the actual behavior of the bridge. In fact, one would predict failure or large permanent set even if the over-all drag coefficient were taken as low as 1.

Table 5.1 - Results of Transient Analysis

$$f(t) = F_1 e^{\alpha_1 t} + F_2 e^{\alpha_2 t} + F_3 e^{\alpha_3 t} \quad (t \text{ in sec})$$

Strain Record	Numerical Constants of Forcing Function						Frequencies of Transfer Function	
	F_1	F_2	F_3	α_1 (1/sec)	α_2 (1/sec)	α_3 (1/sec)	ω_1 (cps)	ω_2 (cps)
$3.4aS_1$	1	-	-	- 1.13	-	-	45	150
$3.4aS_2$	1	0.423	-0.537	- 9.1	-0.290	-0.226	48	
$3.4aS_3$	1	-	-	- 2.67	-	-	27	37
$3.4aS_4$	1	-	-	- 1.03	-	-	32	120
$3.4bS_1$	1	-	-	-599	-	-	23	91
$3.4bS_2$	1	-	-	- 15.2	-	-	29	71
$3.4bS_4$	1	-	-	-157	-	-	18	62
$3.4cS_1$	1	-	-	-115	-	-	32	81
$3.4cS_3$	1	-	-	-397	-	-	13	66
$3.4cS_4$	1	-	-	- 8.51	-	-	35	39

2/ The bridge would actually be expected to fail at some lesser displacement than 72 yield displacements. However, in the region of collpase the displacement is an extremely sensitive function of peak load, and it is not unrealistic to base the collapse load on this value.

As in the response computations for Shot 9, the present results can be given no further meaning other than to state that the simplified loading and response schemes described above provide a realistic estimate as to the actual behavior of the 3.4a truss bridge in Shot 10. Whether this agreement is mostly coincidental or indeed reflects on the general validity of the load prediction scheme for the precursor region, cannot of course be known on the basis of one result.

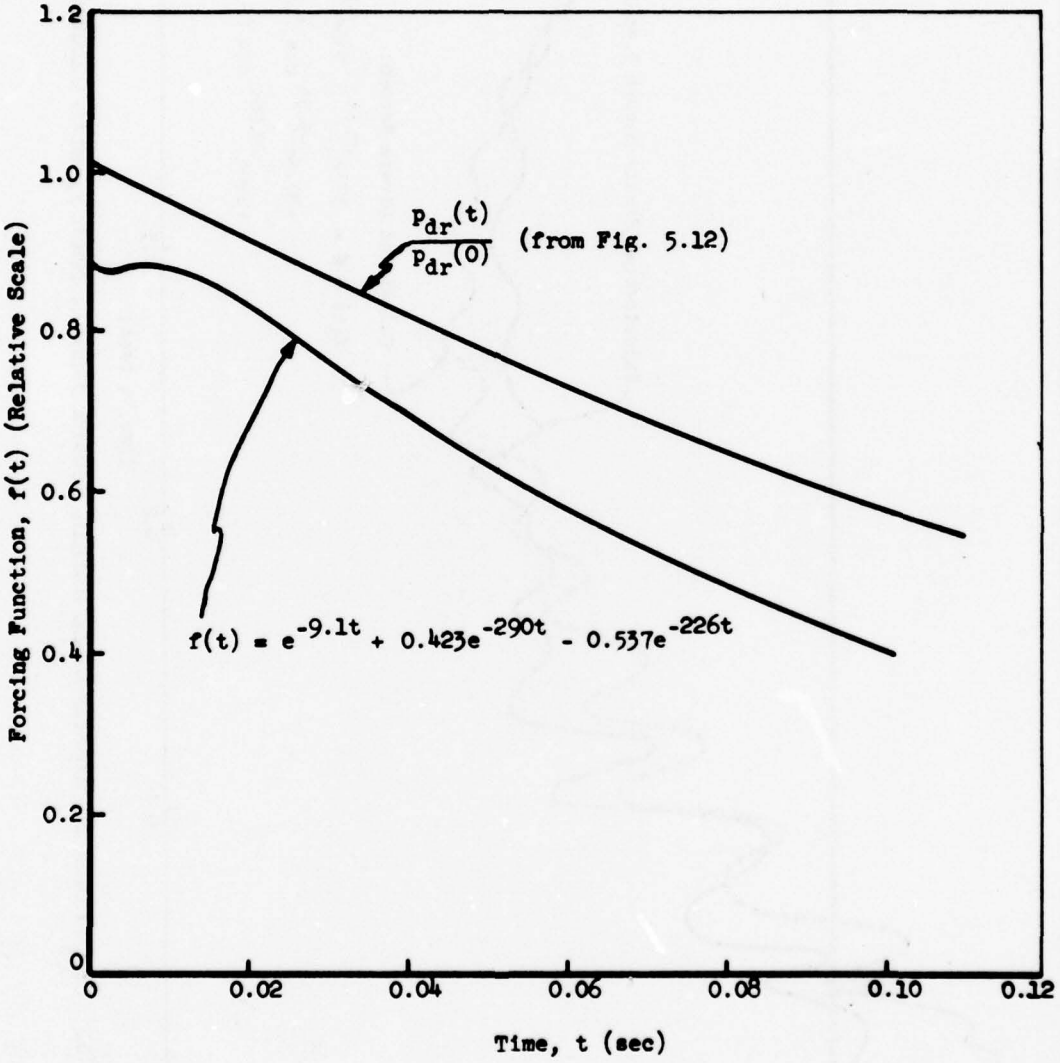

Fig. 5.1 Results of Transient Analysis, Strain Record 3.4aS2, Shot 9

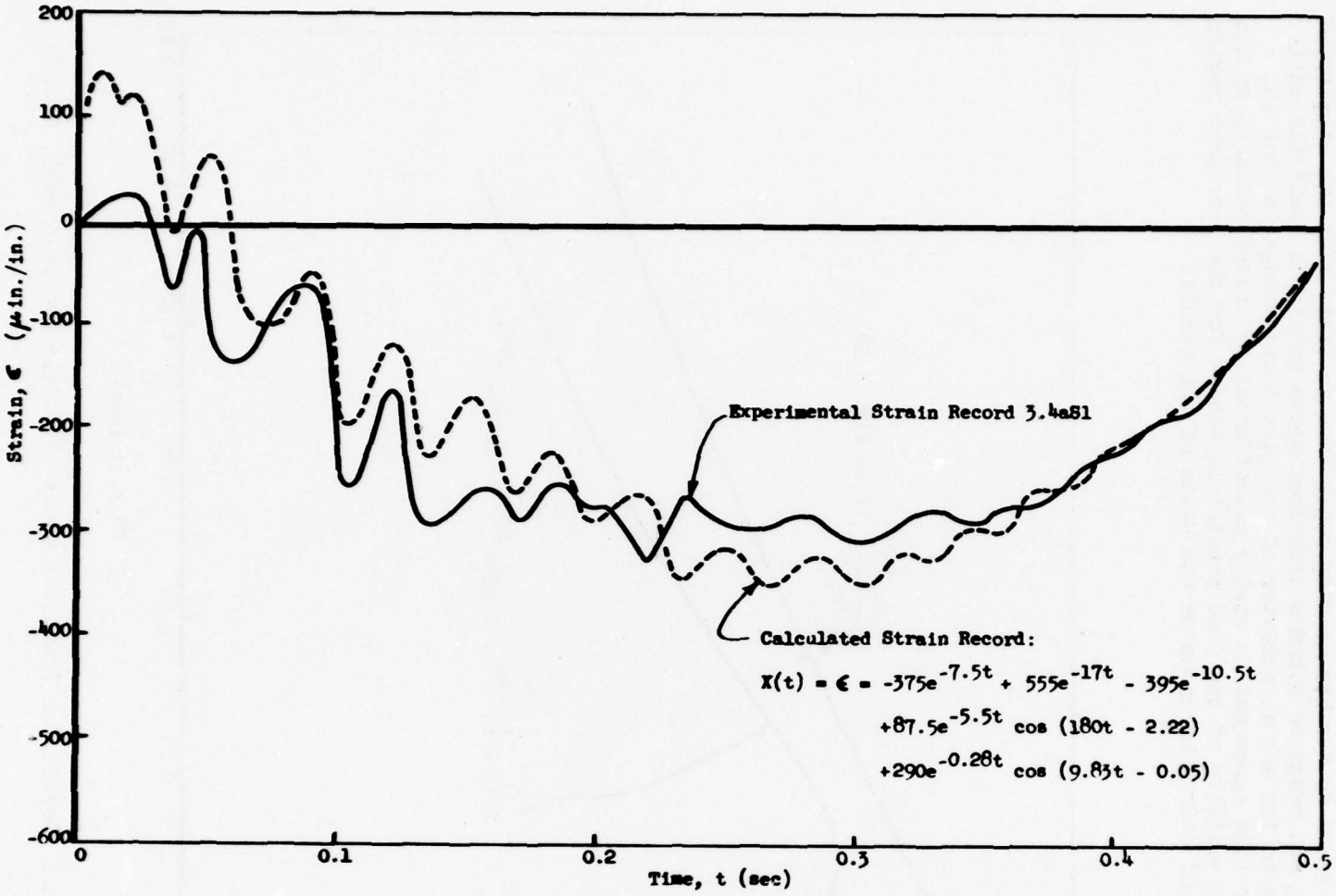

Fig. 5.2 Comparison of Experimental Strain Record 3.4aS1, Shot 9, with Calculated Strain Record

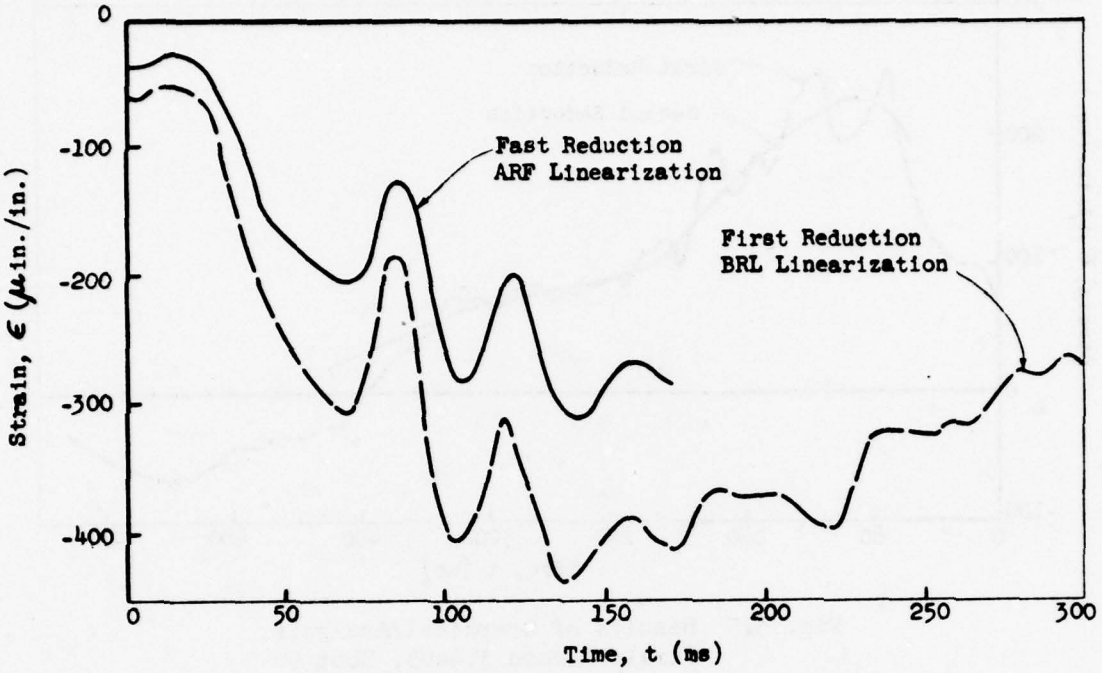

Fig. 5.3 Results of Graphical Analysis, Strain Record 3.4aS1, Shot 9

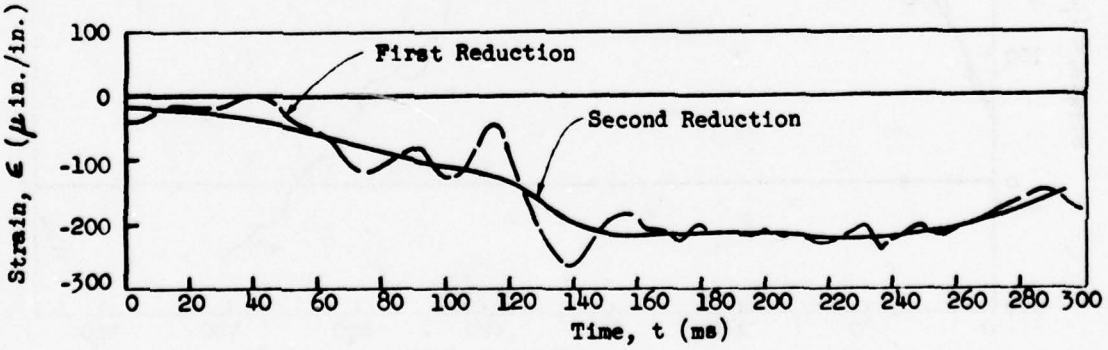

Fig. 5.4 Results of Graphical Analysis, Strain Record 3.4aS2, Shot 9

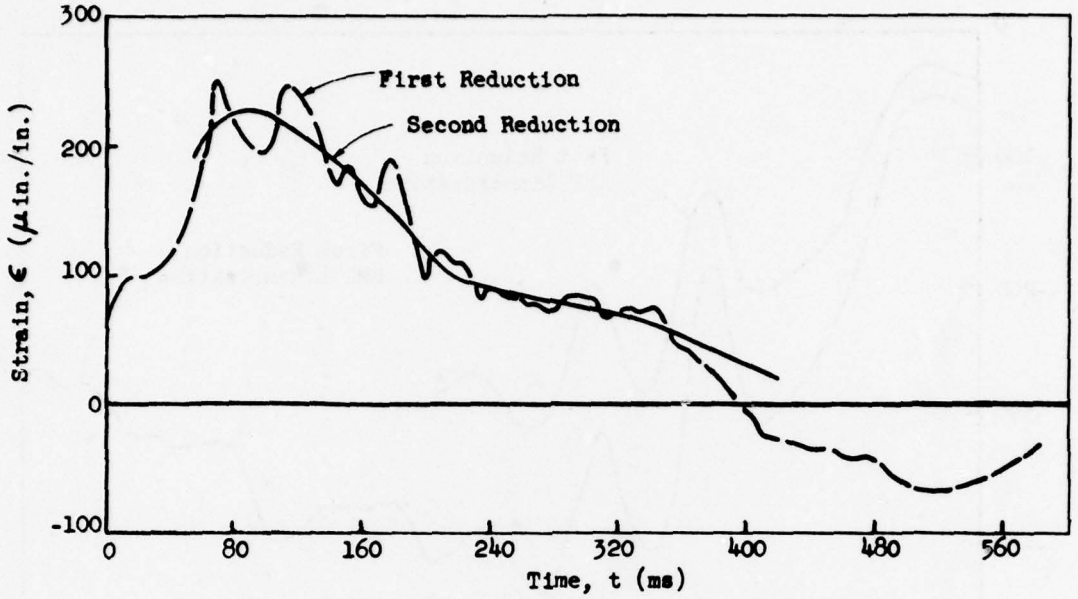

Fig. 5.5 Results of Graphical Analysis,
Strain Record 3.4aS3, Shot 9

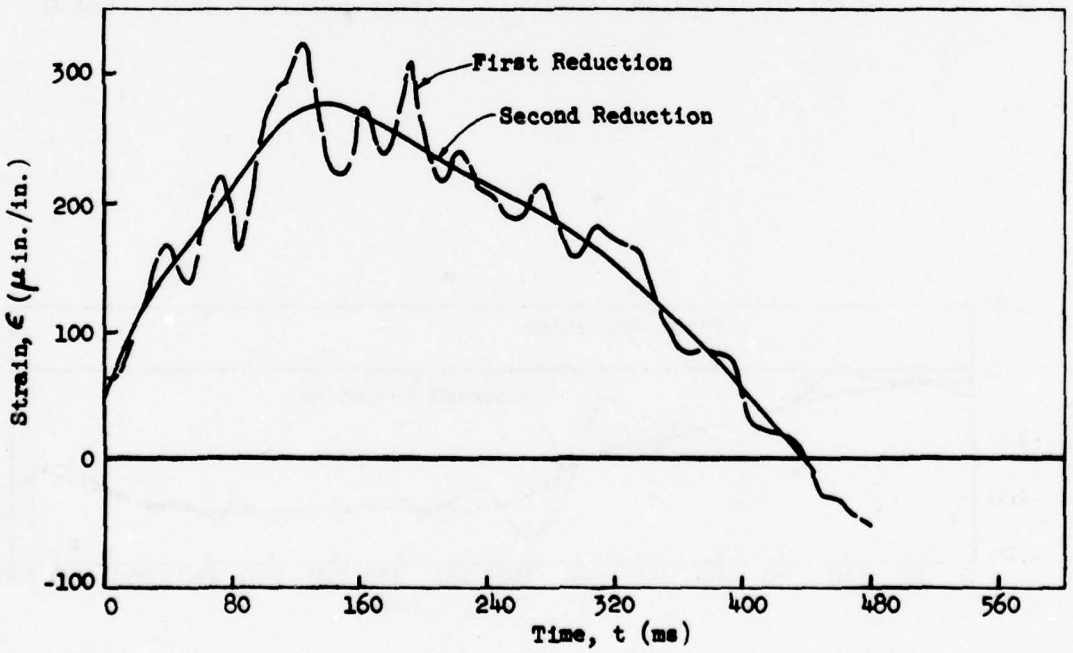

Fig. 5.6 Results of Graphical Analysis,
Strain Record 3.4aS4, Shot 9

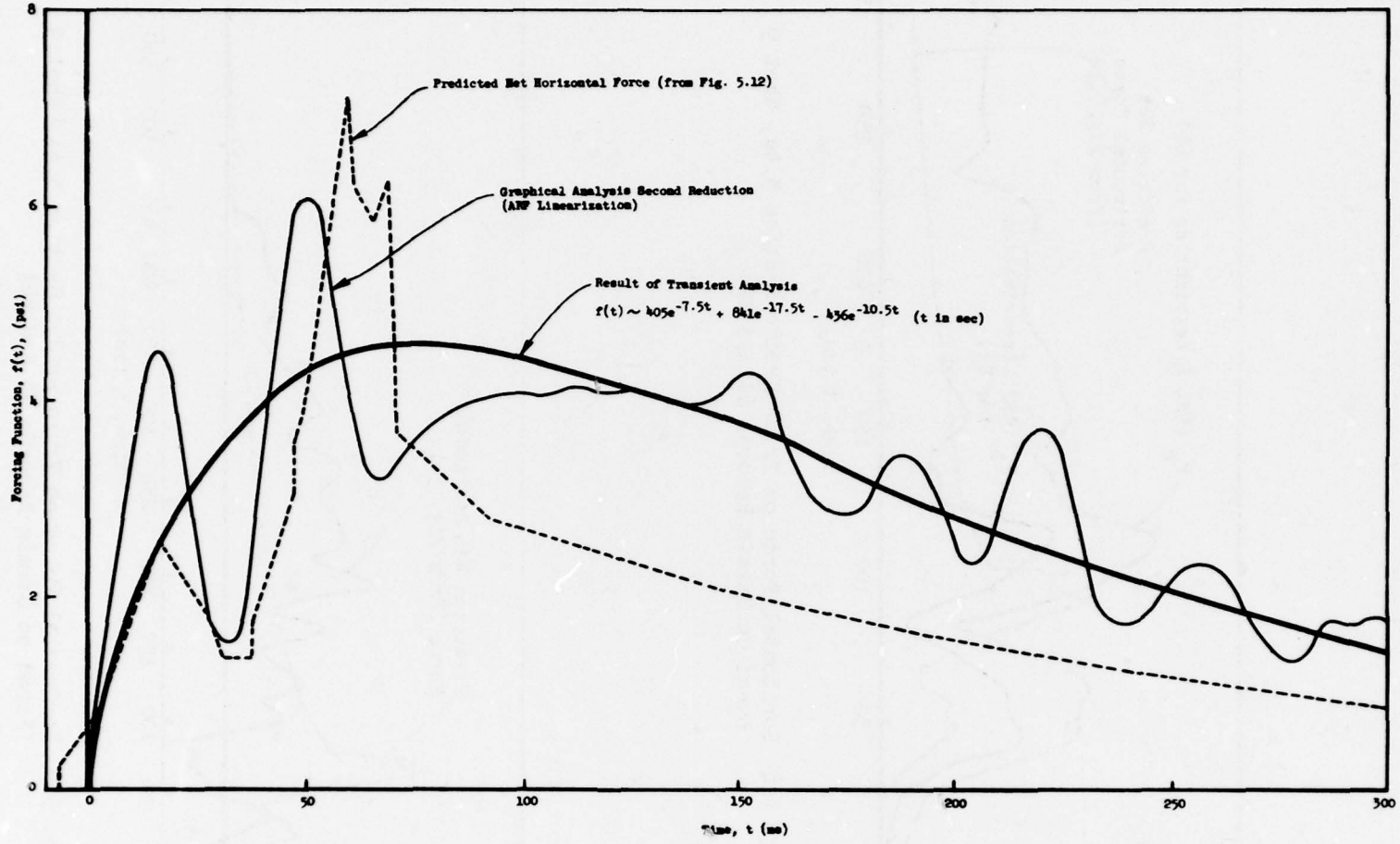

Fig. 5.7 Comparison of Numerical and Graphical Data Reduction Schemes, Strain Record 3.4aS1, Shot 9

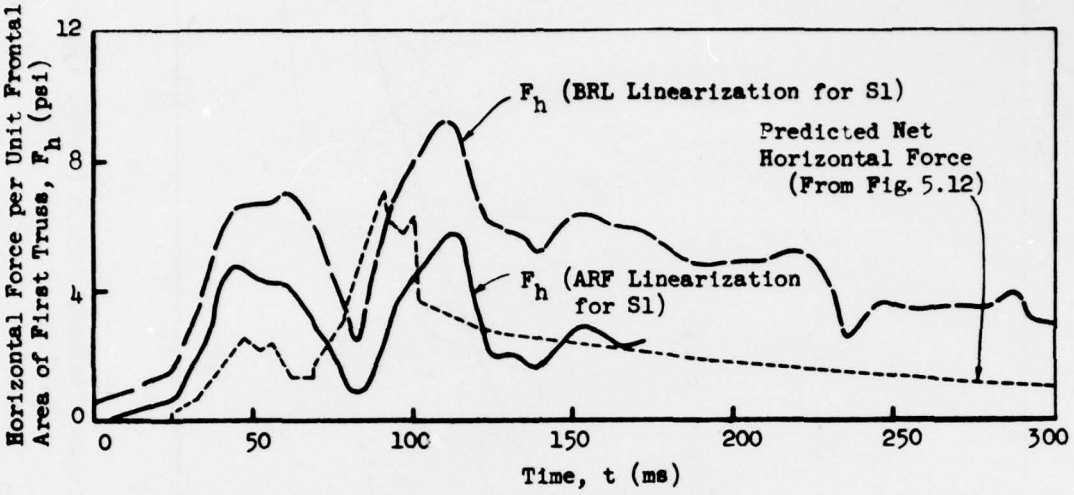

Fig. 5.8 Horizontal Force on Truss Bridge Section 3.4a, Shot 9 (Based on Strain Records S1 and S2)

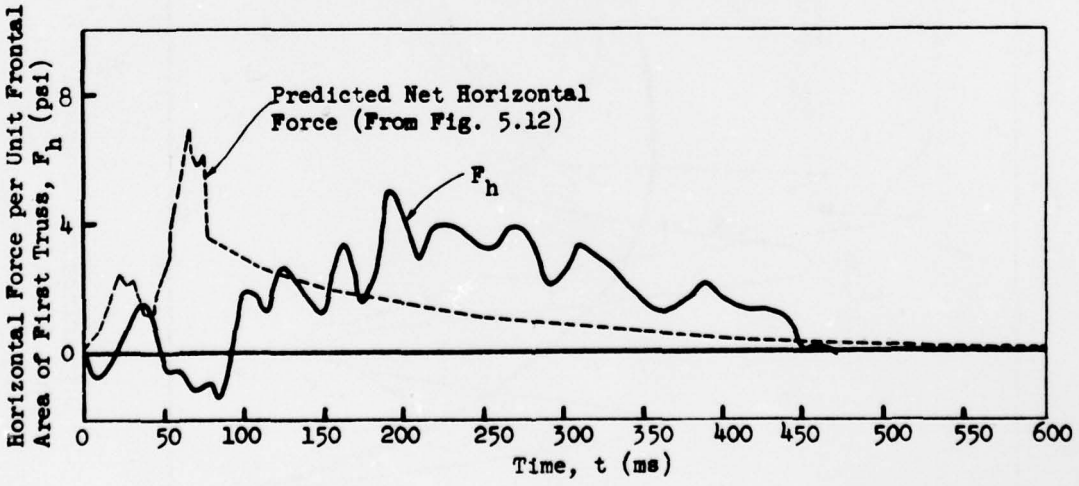

Fig. 5.9 Horizontal Force on Truss Bridge Section 3.4a, Shot 9 (Based on Strain Records S3 and S4)

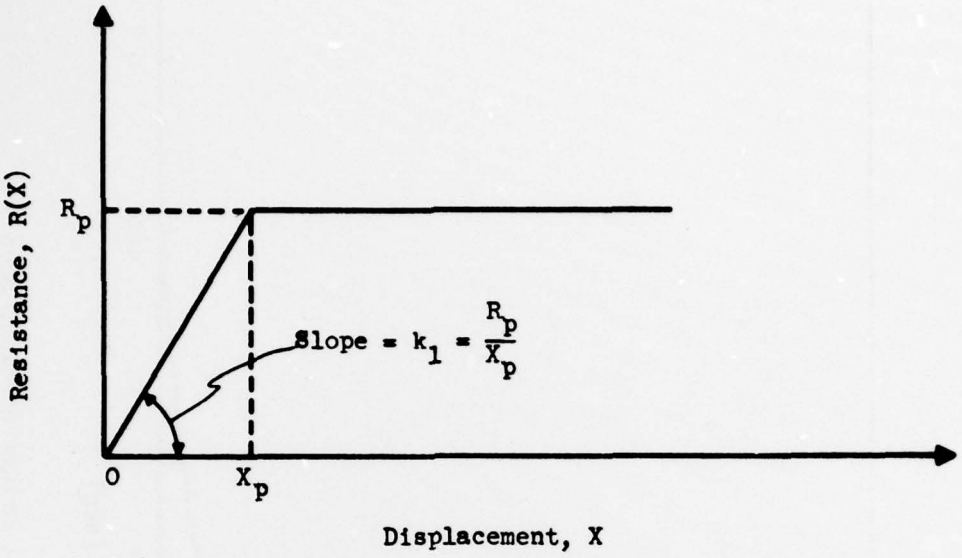

Fig. 5.10 Assumed Elastic-Plastic Resistance Function for 3.4a Truss Bridge Section

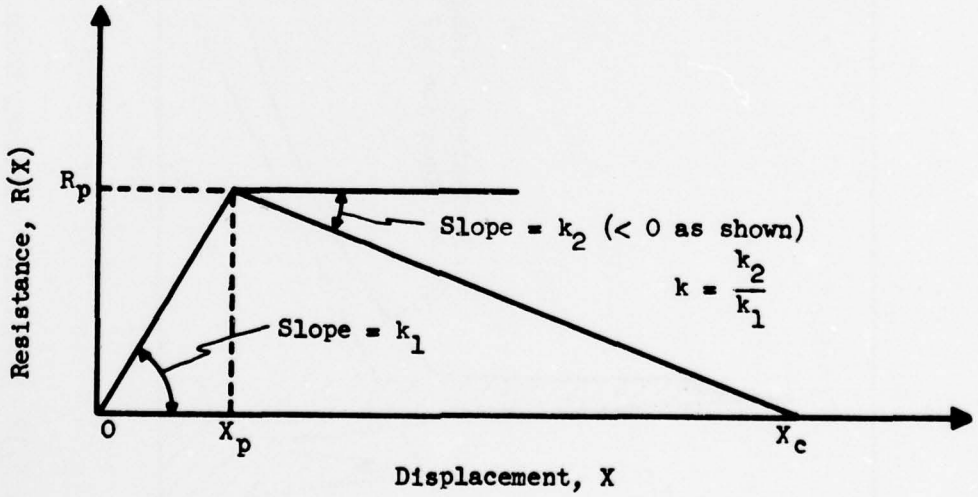

Fig. 5.11 Generalized Resistance Function for Newmark-Brooks Solution

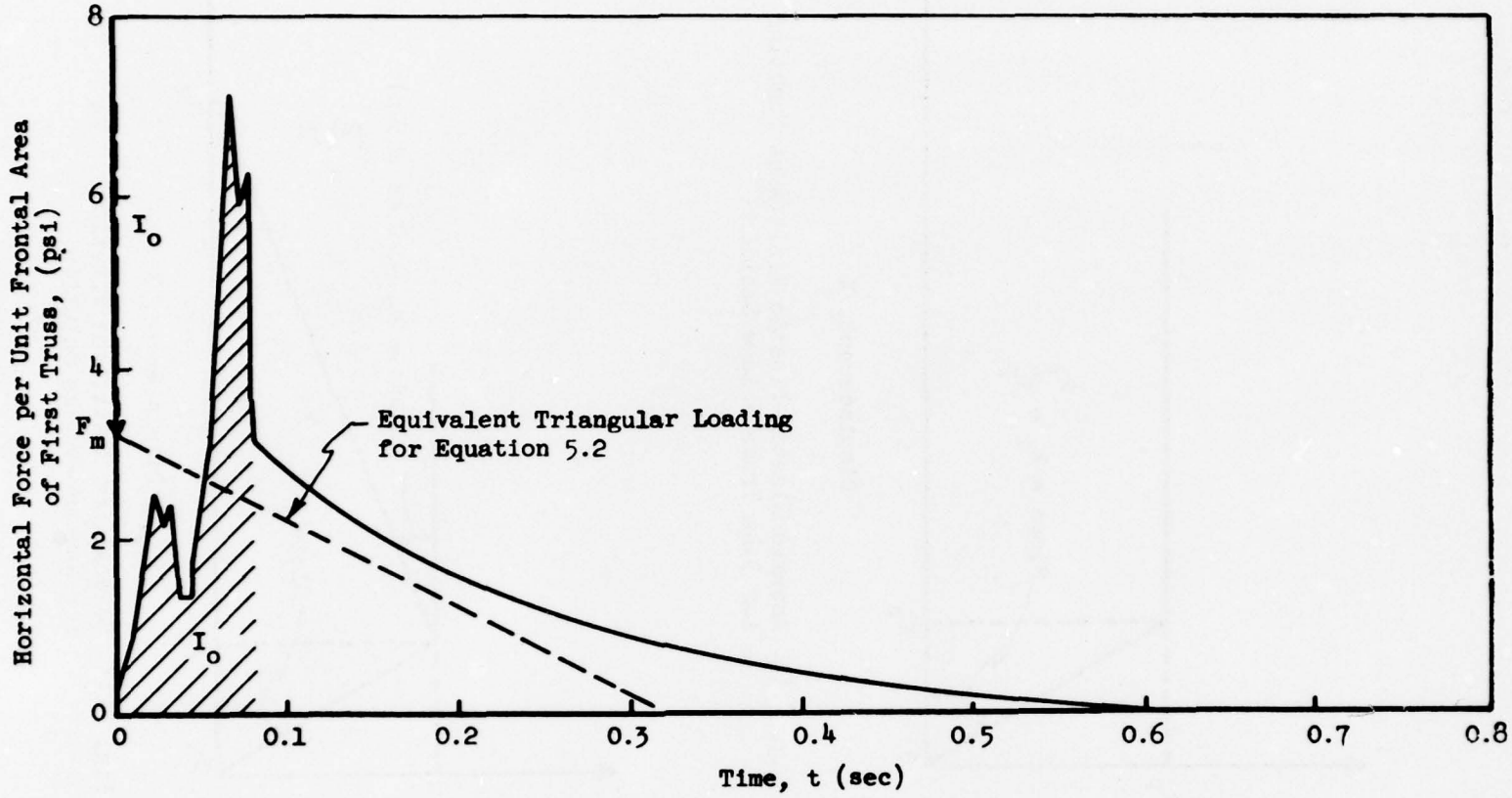

Fig. 5.12 Predicted Horizontal Loading on 3.4a Truss Bridge Section, Shot 9

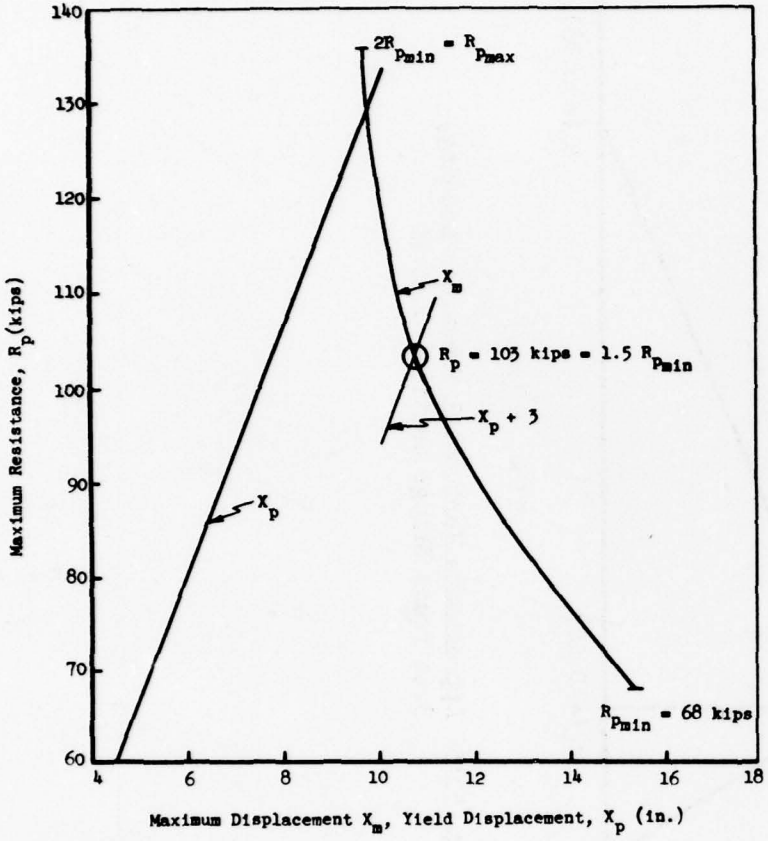

Fig. 5.13 Maximum Bridge Displacement Versus Resistance for Constant Period (Based on Predicted Loading for Shot 9)

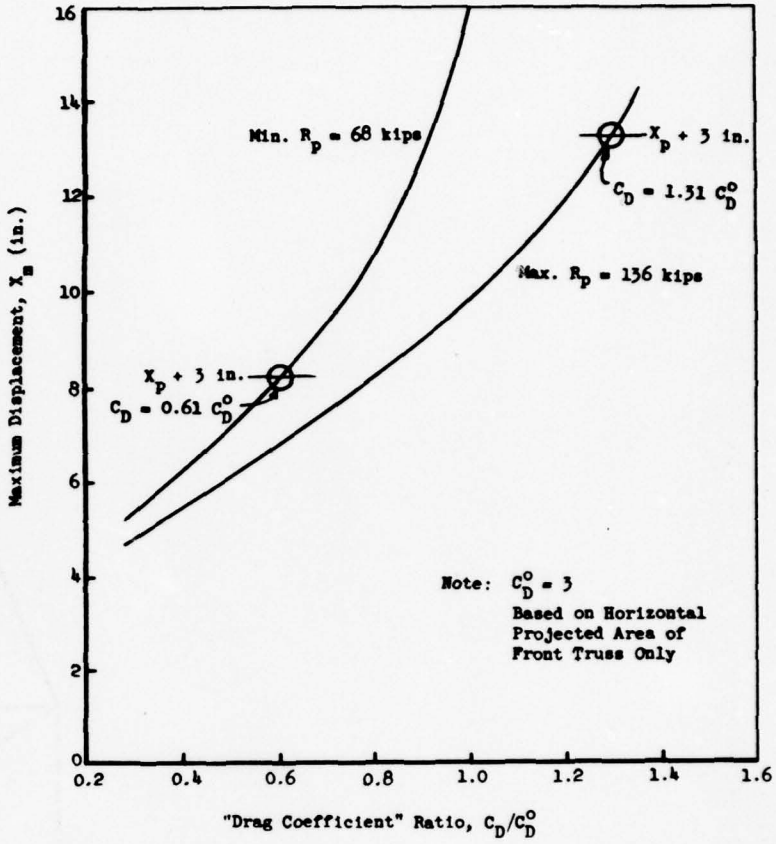

Fig. 5.14 Variation in Maximum Bridge Displacement with "Drag Coefficient" for Range of Resistance (Based on Predicted Loading for Shot 9)

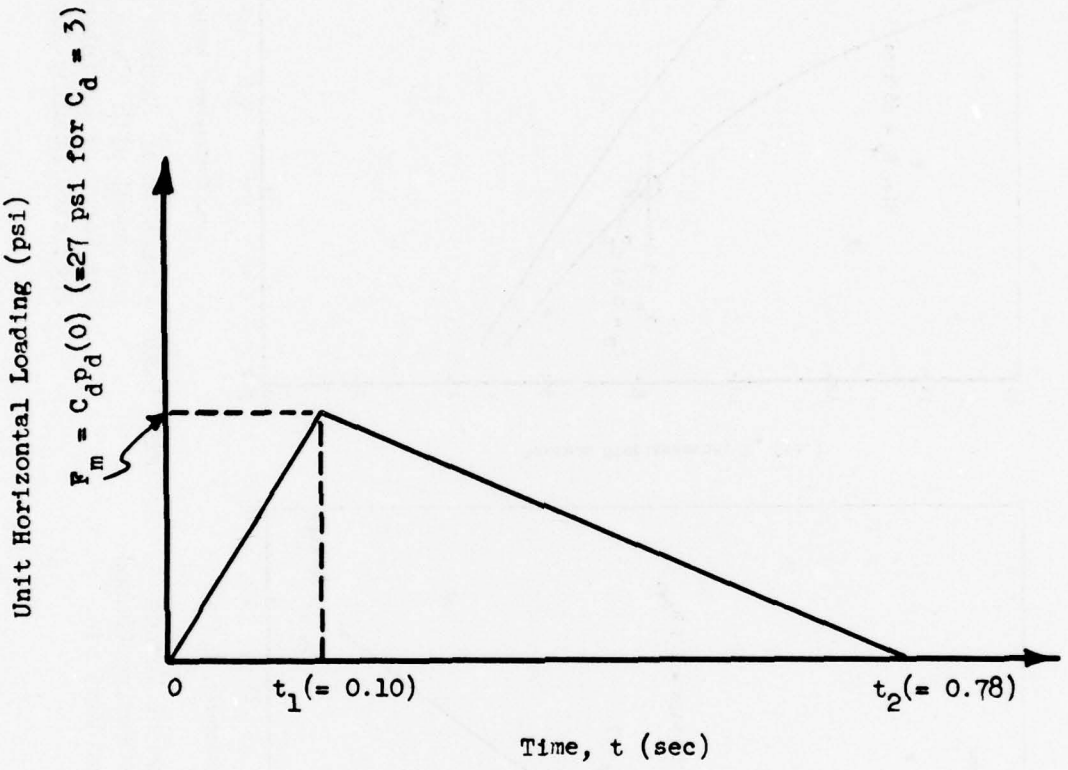

Fig. 5.15 Approximate Horizontal Precursor Loading, 3.4a Truss Bridge Section, Shot 10

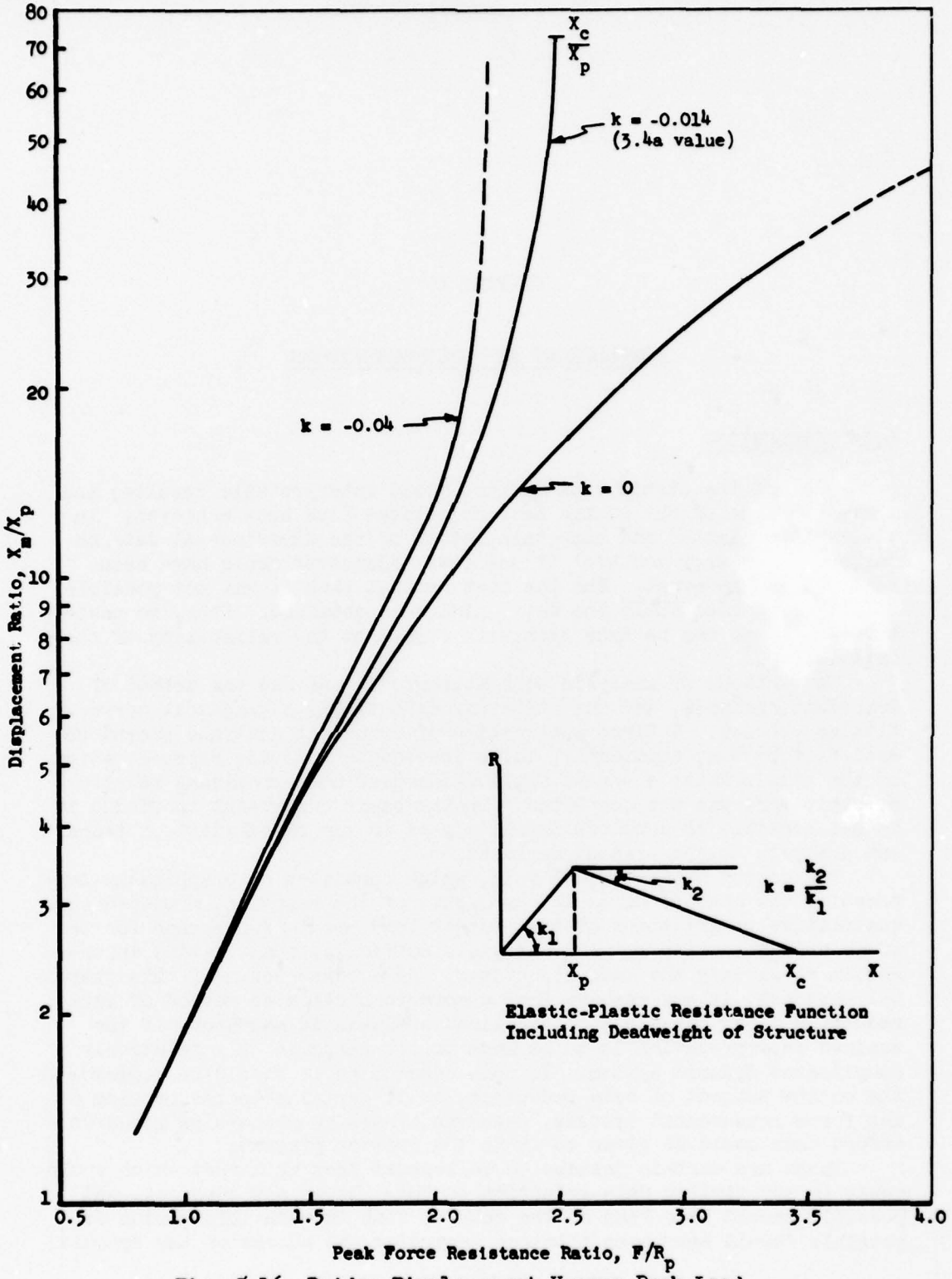

Fig. 5.16 Bridge Displacement Versus Peak Load
(Based on Predicted Loading for Shot 10)

CHAPTER 6

CONCLUSIONS AND RECOMMENDATIONS

6.1 CONCLUSIONS

Most of the strain data did not yield interpretable results, and therefore none of the stated test objectives have been achieved. In view of the limited and uncertain nature of the experimental data obtained, it is very doubtful if the test objectives could have been realized in any event. But the fact remains that it was not possible to interpret adequately the data which were obtained. Thus, no positive statement can be made even with regard to the reliability of the data itself.

Two methods of analysis were attempted: one was the method of transient analysis, and the other was essentially a graphical curve-fitting process. A first application of transient analysis proved unsatisfactory due, apparently, to an inadequate analytic representation of the strain data; a second application gave more promising results but this work was not completed. On the basis of present knowledge it is not possible to conclude definitely as to the feasibility of transient analysis in the present application.

The second method of analysis, which consisted of graphically suppressing the obvious harmonic components of the response, provided some qualitative verification of the pretest load prediction method for the truss bridge section but did not yield sufficient quantitative information to satisfy the test objectives. As a consequence of this graphical approach, it now appears that a more sophisticated method of data reduction along the lines of transient analysis is mandatory if the desired interpretation is to be made of the response of a relatively complicated dynamic system. In this connection it should be emphasized the entire subject of data reduction, as it pertains to the problem of net force measurement systems, deserves a more comprehensive research effort than could be given to it in the present program.

There are certain lessons to be learned from this test which would apply to any similar data-reduction scheme. It is now apparent, and possibly should have been at the outset, that as much information as possible should have been obtained regarding the nature of the dynamic

systems being tested. That is, pre- and post-test static calibration tests should have been conducted for all of the test items. This would serve to determine certain elastic properties of the test items as well as to provide a check on the strain gage system. In addition, it would have been most desirable to conduct suitable dynamic tests in order to determine the principal frequencies and damping of the test items. Information of this type would have undoubtedly aided in the study and interpretation of the strain data.

Perhaps the most important result of the test program has come about through consideration of the damage sustained by the 3.4a truss bridge section. It was found that a simplified dynamic response analysis, incorporating the (pretest) predicted loading in the regular reflection region for Shot 9 and a tentative load prediction scheme applicable to the precursor region for Shot 10 provided an adequate estimate of the damage sustained by the bridge in both instances. While the assumptions of the response analysis are sufficiently uncertain to invalidate this agreement as a check on the essential accuracy of the load prediction methods, confidence in the utilization of existency methods for damage prediction estimates of open-framed structures is certainly increased as a result of this test.

6.2 RECOMMENDATIONS

While the present test has been rather unsuccessful, it is believed that the original objectives are still valid ones, and can be fully satisfied only by means of full-scale testing. The experience of this test indicates that much additional work needs to be done with respect to net force measurement systems, both as to physical design and interpretation of data before such tests can be successfully carried out. Despite the present unsuccessful utilization of the test structures as dynamometers with strain output, this approach has obvious advantages. It is recommended, therefore, that a comprehensive study be initiated on the data-reduction problems associated with net force measurement systems. The objectives of this study would be to (a) devise methods of analysis, (b) specify the class of physical systems whose response will successfully permit the inverse solution, and (c) to determine the type and quality of the necessary data to permit such solutions. It is felt that particular consideration should be given to the analog computer technique of data analysis presented briefly in this report.

APPENDIX A

TRANSIENT ANALYSIS

A.1 INTRODUCTION

In the present application, the prime data (i.e., measured strains) do not represent in a direct sense the desired information (i.e., net forces). In fact, the data obtained represent the response of a rather complicated dynamic system to an input which is itself the desired information. The dynamic system consists of aerodynamic, elastic, plastic, electronic, thermal and possibly stochastic components coupled in many and varied fashions. The problem at hand is to remove from the prime data the influence or contributions of these various components and of the system itself, leaving the desired information. Since it is difficult (probably impossible) to assess the exact contribution or influence that the dynamic system contributes to the prime data, a rational approach to the problem is to attempt to assess the contribution or influence of those components which could be expected to have the most pronounced effects. Due to lack of sufficient knowledge of the test conditions and the reliability and characteristics of the various recording and data-reduction instruments, the magnitude of the contributions of some of the above components cannot even be estimated. Nonetheless, it has been assumed that the major influence on the prime data stems from an elastic response of the cylinder-support system.

The following analysis, referred to as "transient analysis," is designed to remove the influence of the elastic components in the prime data, which is undoubtedly strongest regardless of other effects. The analysis as applied here, represents the function or input required to produce the prime data as the response of an elastic model.

A.2 DERIVATION OF THE BASIC EQUATION

For the present application, the elastic model is assumed to be linear and possess several (but a finite number of) degrees of freedom. Its motion is then determined by a system of linear differential equations with constant coefficients. One such equation for each degree of freedom occurs. Some of the possible degrees of freedom which might

be effective are the rigid-body translation and rotation of the foundation, rigid-body motions of the cylinder, bending and axial vibrations of the cylinder supports, bending of the cylinder, torsional deflections of the cylinder, or vibrations of the cylinder as a shell. Regardless of the number of degrees of freedom present, the equations of elastic motion may be written in the form:

$$m_j \ddot{X}_j(t) + \sum_{i=1}^{N} a_{ij} \dot{X}_i(t) + \sum_{i=1}^{N} b_{ij} X_i(t) = f_j(t) \qquad (A.1)$$

$$j = 1, 2, \ldots N$$

where the a_{ij}, b_{ij}, and m_j are real constants, and $f_j(t)$ is the forcing term for the jth degree of freedom. $X_j(t)$ is the response of the jth degree of freedom represented by the jth mass, m_j. Equation A.1 is the most general system of equations for N degrees of freedom without inertial coupling. The constants a_{ij} and b_{ij} are the damping and elastic coupling coefficients, respectively, some of which may be zero.

For the present application, the forcing terms $f_j(t)$ arise primarily from the pressure acting on the cylinder. It is reasonable to assume that motion of the foundation, if it occurs, can result only from coupling with the cylinder motion. Thus, only those of Equation A.1 corresponding to masses m_j associated with motion of the cylinder are non-homogeneous (i.e., $f_j(t) \neq 0$).

The masses m_j associated with the motion of the cylinder are of two types; namely, total mass corresponding to rigid-body motions, or generalized modal masses for the bending or shell vibrations. The forcing terms for each of these result from either the integrated pressure over the cylinder alone or the integrated pressure times a modal deflection curve over the cylinder. If the pressure is assumed to be nearly constant in the axial direction along the cylinder, these forcing terms will be essentially proportional to one another at each instant of time so that their time histories will be similar. In effect, Equation A.1 will contain the same righthand members up to a constant factor, which may be zero.

In this case, Equation A.1 becomes,

$$m_j \ddot{X}_j(t) + \sum_{i=1}^{N} a_{ij} \dot{X}_i(t) + \sum_{i=1}^{N} b_{ij} X_i(t) = c_j f(t) \qquad (A.2)$$

$$i = 1, 2, \ldots N$$

It is well-known (see S. Timoshenko, Vibration Problems in Engineering) that the response, $X_j(t)$, Equation A.1, subject to homogeneous initial conditions, can be given by a sum of Duhamel-type integrals as:

$$X_j(t) = \sum_{k=1}^{N} \int_0^t f_k(\tau) h_{kj}(t - \tau)\, d\tau \qquad (A.3)$$

where the h_{kj} are referred to as transfer functions and, for a fixed (k,j), represent the impulsive response in the jth degree of freedom to a unit impulse applied in the kth degree. In other words, $h_{kj}(t)$ is the solution, $X_j(t)$, of the corresponding homogeneous system of equations

$$m_j \ddot{X}_j(t) + \sum_{i=1}^{N} a_{ij} \dot{X}_i(t) + \sum_{i=1}^{N} b_{ij} X_i(t) = 0 \qquad (A.4)$$

$$j = 1, 2, \ldots N$$

subjected to the inhomogeneous initial conditions

$$X_j(0) = \dot{X}_j(0) = 0$$

$$X_k(0) = 0, \quad \dot{X}_k(0) = 1, \qquad j \neq k$$

Such a solution $X_j(t) = h_{kj}(t)$ is known to be a linear combination of exponential functions (in general, complex)[1] of the form (see S. Timoshenko, Vibration Problems in Engineering).

$$h_{kj}(t) = \sum_{n=-N}^{N} \alpha_n^{kj} e^{\lambda_n t} \qquad (A.5)$$

where λ_n, $(n = 0, \pm 1, \ldots \pm N)$ are the 2N roots of the characteristic equation (system of equations)

$$m_j \lambda^2 + \sum_{i=1}^{N} a_{ij} \lambda + \sum_{i=1}^{N} b_{ij} = 0$$

$$j = 1, 2, \ldots N$$

If Equation A.5 is substituted in Equation A.3, there results:

$$X_j(t) = \sum_{k=1}^{N} \int_0^t f_k(\tau) \sum_{n=-N}^{N} \alpha_n^{kj} e^{\lambda_n (t - \tau)}\, d\tau \qquad (A.6)$$

If, in addition, the $f_k(t)$ are timewise proportional so that

$$f_k(t) = c_k f(t) \qquad (A.6a)$$

as in Equation A.2, then Equation A.6 may be written,

[1] It is assumed here that the 2N characteristic roots are distinct.

$$X_j(t) = \int_0^t f(\tau) \sum_{k=1}^{N} \sum_{n=-N}^{N} c_k \alpha_n^{kj} e^{\lambda_n(t-\tau)} d\tau$$

$$X_j(t) = \int_0^t f(\tau) \sum_{n=-N}^{N} \beta_n^j e^{\lambda_n(t-\tau)} d\tau$$

$$X_j(t) = \int_0^t f(\tau)\, h_j(t-\tau)\, d\tau \qquad \text{(A.7)}$$

where:

$$\left.\begin{aligned} \beta_n^j &= \sum_{k=1}^{N} c_k \alpha_n^{kj} \\ h_j(t) &= \sum_{n=-N}^{N} \beta_n^j e^{\lambda_n t} \end{aligned}\right\} \qquad \text{(A.7a)}$$

It is seen that the quantity $h_j(t-\tau)$ in Equation A.7 is precisely the form of the transfer functions $h_{kj}(t)$ in Equation A.3 (independent of k, however) and is a linear combination of exponential functions involving only the characteristic roots of the system. Equation A.7 is the desired basic equation and may be used to obtain the unknown forcing function $f(t)$ from a known response $X_j(t)$. The quantity $f(t)$ actually represents only the shape of the forcing function, since it is defined up to the constant factors c_j of Equation A.2.

The problem of uniqueness and the effect of "errors" in the response curve $X_j(t)$ as they affect the solution for $f(t)$ obtained, will be discussed at the appropriate steps in the subsequent analysis. It will be seen that the uniqueness problem essentially reduces to a problem in curve-fitting and may be treated in several ways.

A.3 SOLUTION OF THE BASIC EQUATION

Equation A.7 can be solved by a variety of methods, none of which, however, leads to a unique solution for the forcing function $f(t)$. For the present application it is assumed that $f(t)$ can be represented by exponential functions in the form:

$$f(t) = F_1 e^{\alpha_1 t} + \ldots F_k e^{\alpha_k t} = \sum_{i=1}^{K} F_i e^{\alpha_i t} \qquad (A.8)$$

where the F_i and α_i are constants. The number (K) of terms in Equation A.8 will be determined by the complexity of the actual forcing function or, at least, the complexity required of $f(t)$ in order to produce the known response $X(t)$. It should be mentioned that the form of Equation A.8 in no way restricts the generality of application.

If Equation A.8 is substituted into Equation A.7, and Equation A.7a is used, there results upon integration:

$$X_j(t) = \sum_{i=1}^{K} a_i e^{\alpha_i t} - \sum_{n=-N}^{N} B_n e^{\lambda_n t} \qquad (A.9)$$

where,

$$\left.\begin{aligned} a_i &= \left[\sum_{n=-N}^{N} \frac{\beta_n^j}{\alpha_i - \lambda_n} \right] F_i \\ B_n &= \left[\sum_{i=1}^{K} \frac{F_i}{\alpha_i - \lambda_n} \right] \beta_n^j \end{aligned}\right\} \qquad (A.10)$$

It is assumed here that $\alpha_i \neq \lambda_n$ for each i and n, since otherwise a resonance condition would result, which certainly does not happen in the physical case considered here. Equation A.9 gives $X_j(t)$ as a sum of exponential functions, and the present problem reduces to that of fitting such a sum to the prime data representing $X_j(t)$ for a discrete set of times, t.

A curve-fitting scheme results in the constants, A_i, α_i, B_n, and λ_n (real and complex, in general) which, in turn, may be used to compute the desired F_i through Equation A.10. Actually, Equation A.10 will also yield the β_n^j which, however, are not of direct concern in the present application. With the α_i, A_i, B_n, and λ_n known, Equation A.10 constitutes a system of $2N + K$ equations in the $2N + K$ unknowns, β_n^j and F_i. With the α_i and F_i determined, the desired forcing function is then given by Equation A.8. Actually, a little more information is assumed here; namely, that not only the constants α_i, A_i, B_n, and λ_n are obtained from the curve-fitting, but that the sets of A_i's and α_i's can be distinguished from the set of B_n's and λ_n's. Otherwise, the structure of Equation A.10 would not be determined so that a unique forcing function could not be constructed through Equation A.8. In the present application, the distinction between the two classes of terms in Equation A.9 can be made through the exponents α_i and λ_n themselves. Since Equation A.1 can be assumed to be stable, none of the characteristic roots λ_n can be pure real. On the other

hand, it is assumed that the forcing function, f(t), contains no harmonic components so that a realistic curve-fitting scheme should yield only real exponentials α_i for f(t) in Equation A.8. In brief, the non-real exponents obtained from curve-fitting are associated with the transfer function

$$h_j(t) = \sum_{n=-N}^{N} \beta_n^j e^{\lambda_n t}$$

and give the α_n, while any real exponents obtained are associated with the forcing function

$$f(t) = \sum_{i=1}^{K} F_i e^{\alpha_i t} .$$

The appropriateness of this choice of association can be asserted only after some study is made of the effect of errors, etc., of the prime data on the computed exponentials. It would be desirable, of course, to obtain the natural frequencies of the system either analytically or experimentally independent of the above analysis, since then they could be identified in Equation A.9, and f(t) could then contain harmonics without affecting the above solution.

A.4 CURVE-FITTING

Equation A.9 may be written in the form:

$$X(t) = \sum_{k=1}^{M} c_k e^{\gamma_k t} \qquad (A.11)$$

where the c_k and γ_k are in general complex numbers, and where the subscript j has been dropped, since the only concern is with the response of but one component of the system. Curve-fitting consists of finding those values for c_k and γ_k such that X(t) as given by Equation A.11 best fits the given prime data.

Method A. The most direct method of curve-fitting is accomplished by visual inspection of plots of the prime data itself. A discussion of this method and the results of its use in the present application are presented in Section 5.1.2.

Method B. A second method consists of rather standard technique from the theory contained in the calculus of finite differences (see The Calculus of Observations, Whittaker, E., and Robinson, A.). It is assumed now that the prime data are given in equal interval tabular form.

Let the interval of tabulation of the function X(t) be Δ, and designate X(t) at the time when

$$t = n\Delta \qquad n = 0, 1, \ldots P$$

as X_n. The assumed form of $X(t)$ (Equation A.11) may then be written as

$$X_n = \sum_{k=1}^{M} c_k \lambda_k^n \qquad (A.12)$$

where

$$\lambda_k = e^{\gamma_k \Delta} \qquad (A.12a)$$

This method of curve-fitting rests upon the observation that Equation A.12 is the solution to a linear finite difference equation with constant coefficients. This finite difference equation may be written for each consecutive group of $(L + 1)$ tabulated values of X_n as

$$\sum_{l=0}^{L} D_l X_{n+l} = 0 \qquad (A.13)$$

where $D_L = 1$ and the remaining D's are to be determined. If $(P + 1)$ is the total number of tabulated values of X_n, Equation A.13 may be written $(P - L + 1)$ times, each equation corresponding to each of the values of n in the range

$$n = 0, 1, 2, \ldots (P - L)$$

Consider the resulting set of simultaneous equations

$$\left.\begin{aligned} D_o X_o + D_1 X_1 + \ldots + D_{L-1} X_{L-1} &= -X_L \\ D_o X_1 + D_1 X_2 + \ldots &= -X_{L+1} \\ D_o X_{P-L} + D_1 X_{P-L} + &= -X_P \end{aligned}\right\} \qquad (A.14)$$

where the X_n's are known from the tabulated function $X(t)$. This set of simultaneous equations consists of $(P - L + 1)$ equations in the $(L + 1)$ unknown D's. A solution to the system of equations is possible if $P > 2L$. When L, the number of exponential terms used to approximate $X(t)$, is chosen equal to $P/2$, the system has a unique solution if the determinant of the coefficients of X_n is non-zero. Normally, this condition exists and the unknown D's are determined by ordinary methods (see The Calculus of Observations, by Whittaker, E., and Robinson, A.) and are used to form the characteristic equation which is the polynomial

$$0 = D_o + D_1 \lambda + D_2 \lambda^2 + \ldots + D_{L-1} \lambda^{L-1} + \lambda^L \qquad (A.15)$$

The roots of Equation A.15 are the λ_k's referred to in Equation A.12 and, hence, may be used to determine the γ_k's which, in turn, are used to form the approximate representation of $X(t)$.

The actual determination of the γ_k's is considered now, since the roots of Equation A.15 may be positive, negative, or complex. Regardless of the type of root, λ_k can be written as

$$\lambda_k = \left|\lambda_k\right| e^{-i\Theta} \qquad (i = \sqrt{-1})$$

where Θ is equal to zero or pi (π) if λ_k is positive or negative, respectively. If λ_k is a complex root, Θ is the Cauchy principal angle and lies between $-\pi$ and π. If λ_k is positive,

$$\gamma_k = \frac{1}{\Delta} \log \lambda_k \tag{A.16a}$$

If λ_k is negative,

$$\gamma_k = \frac{1}{\Delta} \log (-\lambda_k) + \frac{i\pi}{\Delta} \tag{A.16b}$$

In the latter case the imaginary part of γ_k is dropped, since it introduces an extraneous frequency whose period is 2Δ. The conclusion that this frequency is extraneous is based upon the observation that it is dependent only upon the choice of the tabulation interval, and, therefore may be changed to any value by a suitable choice of interval.[2/] Thus, for all real values of λ_k

$$\gamma_k = \frac{1}{\Delta} \log \left|\lambda_k\right| \tag{A.17a}$$

2/ An alternate method of dropping the frequency introduced by the negative roots is to consider only the even terms in Equation A.12. Equation A.12 becomes

$$X_{2n} = \sum_{k=1}^{M} c_k (\lambda_k^2)^n$$

And Equation A.12a becomes

$$(\lambda_k^2) = e^{\gamma_k(2\Delta)}$$

from which

$$\gamma_k = \frac{1}{2\Delta} \log (\lambda_k^2)$$

and $X(t)$ again has the form of Equation A.12 where the extraneous frequency corresponding to π/Δ is not present.

If λ_k is complex, it must be one of a conjugate pair and both pairs are contained in

$$\gamma_k = \frac{1}{\Delta} \log \left|\lambda_k\right| \quad \pm \frac{i\theta}{\Delta} \tag{A.17b}$$

Having obtained the γ_k's from Equations A.17a and A.17b, the c_k's may be obtained from Equation A.12 in combination with the initial conditions. These conditions are satisfied if

$$\sum_{k=1}^{M} c_k = 0 \tag{A.18}$$

and

$$\sum_{k=1}^{M} \gamma_k c_k = 0 \tag{A.19}$$

Since Equation A.12 is to be satisfied for each tabulated value of $X(t)$, there results the following P equations in $(L - 2)$ unknowns,

$$\left.\begin{aligned} c_1\lambda_1 + c_2\lambda_2 + \ldots + c_L\lambda_L &= X_1 \\ c_1\lambda_1^2 + c_2\lambda_2^2 + \ldots + c_L\lambda_L^2 &= X_2 \\ c_1\lambda_1^P + c_2\lambda_2^P + \ldots \quad c_L\lambda_L^P &= X_P \end{aligned}\right\} \tag{A.20}$$

where Equations A.18 and A.19 are to be used to eliminate two of the c_k's. The above system of equations is overdeterminate and usually inconsistant, since a finite number of terms is used to approximate $X(t)$. The method of least squares is used to determine the most probable set of $(L - 2)$ equations in the $(L - 2)$ unknowns, (see The Calculus of Observations, Whittaker,E., and Robinson, A.) and then this set of equations is solved for the c_k's.[3]

Method C. A third method of curve-fitting utilizes an analog computer, and represents a rapid trial-and-error process. A discussion of this method is presented in Section 5.1.4.

A.5 DISCUSSION OF APPLICATION OF TRANSIENT ANALYSIS (Method B)

The application of transient analysis as described in Method B consists of the following steps:

a. The frequencies and exponents occurring in the expansion of the response curves (prime data) are determined by analogy with

3/ If $L < P/2$, the method of least squares is used to reduce the equations to a determinate number.

finite difference equations. The prime data are interpreted as representing the solution of a system of linear finite difference equations. The characteristic equation (polynomial) for this system of difference equations is constructed using the prime data and solved to obtain the characteristic roots. These roots, in turn, are taken as the desired frequencies and exponents of the response curve expansion.

b. Having obtained the frequencies and exponents of the response curve expansion, the amplitudes associated with each of the exponential terms are then determined by a straightforward least squares fit to the prime data.

c. With the expansion of the response curve determined, the forcing function is then associated with the real exponential terms and is obtained through Equation A.10.

The success of the application of transient analysis to the predicting of actual forcing functions hinges upon several reasonable but crucial assumptions. First, and of utmost importance, is the assumption that the dynamic system producing the response curves be essentially linear. Just what magnitude of non-linear effects such as stochastic errors, or baseline shifts are tolerable is not known at present, and, indeed, represents a major area of required investigation before any net force measurement technique of the present type can be evaluated. The effect of errors (known or unknown) in the prime data affect the analysis most critically in step a above. In fact, if the frequencies and exponents determined in step a are realistic, the success of the entire analysis appears to rest only upon the identification made in step c, which will be discussed presently. One criticism of the procedure in step a for determining the all-important frequencies and exponents appears immediately as the result of using the prime data itself. Since these data in the present application are known to contain various types of errors, it would be desirable to incorporate some data-smoothing process prior to the application of transient analysis. There are several types of data-smoothing techniques available with various degrees of reliability and meaningfulness to the present application, but the most promising appears to be the use of the autocorrelation function. For the latter application step a would use the autocorrelation function defined as

$$\bar{X}(t) = \frac{1}{T} \int_0^T X(\tau)\, X(t+\tau)\, d\tau \qquad (A.21)$$

instead of the prime data $X(t)$, itself.[4/]

4/ The fixed interval T is taken approximately as representing the extent of the data available.

The autocorrelation function $\bar{X}(t)$ contains the same frequencies and exponentials as do the prime data $X(t)$ and smooths the data by eliminating stochastic and/or bias errors. This smoothing technique is being tried and tested at present in other and similar applications (see Operation TEAPOT Project 3.2, Study of Drag Loading on Structures in and out of the Precursor Zone, WT-1124).

Of course, the analogy technique applied in step a does itself perform some sort of averaging on the data fed in. Just what the nature of this averaging is, is not known at present. A perturbation study of the effect on the exponents and frequencies as determined by step a is necessary before a realistic evaluation of transient analysis can be made. Because of the complications involved, such a study would, no doubt, have to be carried on in the sphere of numerical experimentation.

Step b determines a "best fit" of the prime data. The fit obtained itself is, in many respects, a measure of the reliability of transient analysis in the present application. However, a realistic criteria for "goodness" of fit has not yet been established; at least, not in terms of the reliability or meaningfulness of the forcing function so obtained. A point-by-point check on the fit may not be too meaningful, since the analysis, to be successful, must, of necessity, ignore "errors" in the prime data and pick out only pertinent information. However, the method of least squares as applied in step b appears, at present, to have the most reliable characteristics for curve-fitting as applied in this application.

The procedure of step c is based on the assumption that the forcing function is represented, or "sufficiently well" represented, by a sum of real exponentials. Just what is "sufficiently well" to assure success of transient analysis has not yet been determined. The limits of reliability could most likely (and probably of necessity) be determined by numerical experimentation, also.

Finally, the assumption that all forcing functions are timewise proportional needs to be considered. The first question to be answered is whether the forcing functions considered are essentially proportional or not. The second question to be answered is what is "sufficiently proportional" in terms of success of the application of transient analysis. Thirdly (since the first two questions have not as yet been answered), what happens to transient analysis if the forcing functions are not essentially timewise proportional. In particular, does the forcing function obtained by applying transient analysis in this latter case have any significance or yield any real information. Of these three questions, only the third can be answered (to some degree at least) at the present time.

In answer to the question of what happens if the forcing functions are not timewise proportional, the analysis of the preceding section, is repeated in brief as follows:

Equation A.6 is written in the form

$$X(t) = \sum_{k=1}^{N} \int_{o}^{t} f_k(\tau) \sum_{n=-N}^{N} a_n^k e^{\lambda_n (t-\tau)} d\tau \qquad (A.22)$$

where the index j has been dropped, since the only concern is the response in a single degree of freedom. The forcing function $f_k(t)$ is written in the form

$$f_k(t) = \sum_{i=1}^{K} F_i^k e^{\alpha_i t} \tag{A.23}$$

where the α_i range over all exponentials appearing in any of the degrees of freedom, so that some of the F_i^k may be zero. With Equation A.23 substituted in Equation A.22 and the integration performed, there results the equation:

$$X(t) = \sum_{i=1}^{K} \left[\sum_{k=1}^{N} \sum_{n=-N}^{N} \frac{F_i^k \alpha_n^k}{\alpha_i - \lambda_n} \right] e^{\alpha_i t} - \sum_{n=-N}^{N} \left[\sum_{k=1}^{N} \sum_{i=1}^{K} \frac{F_i \alpha_n^k}{\alpha_i - \lambda_n} \right] e^{\lambda_n t}$$

$$= \sum_{i=1}^{K} a_i e^{\alpha_i t} - \sum_{n=-N}^{N} B_n e^{\lambda_n t} \tag{A.24}$$

which is precisely the same form as Equation A.9. However, the a_i and B_n are related to the forcing coefficients F_i^k and the transfer function coefficients α_n^k by

$$\left.\begin{aligned} a_i &= \sum_{k=1}^{N} \sum_{n=-N}^{N} \frac{F_i^k \alpha_n^k}{\alpha_i - \lambda_n} \\ B_n &= \sum_{k=1}^{N} \sum_{i=1}^{K} \frac{F_i^k \alpha_n^k}{\alpha_i - \lambda_n} \end{aligned}\right\} \tag{A.25}$$

which are the counterparts of Equation A.10. The relationships between Equation A.10 and A.25 results in (dropping the index j)

$$\sum_{k=1}^{N} F_i^k \alpha_n^k = \beta_n F_i \tag{A.26}$$

$$n = \pm 1, \pm 2, \ldots \pm N$$

$$i = 1, 2, \ldots K$$

Hence, the curve-fitting of step b may be applied to Equation A.24 resulting in the a_i, α_i, B_n and λ_n which, in turn, are used in Equation A.10 to determine the β_n and F_i. However, step c is not, in general, valid since the F_i are not the actual forcing function coefficients. In fact, there is no longer a single forcing function in

question, but one for each degree of freedom. The actual forcing function coefficients F_i^k are related to the β_n and F_i by Equation A.26. However, in Equation A.26 only the β_n and F_i are known, while both sets of F_i^k and α_n^k are unknown. Since there are (2N) x K equations in Equation A.26 and (2N) x K x N unknowns, Equation A.26 does not, in general, determine the actual forcing function coefficients F_i^k uniquely and an infinitude of solutions may be constructed. It should be mentioned, however, that some information about the forcing functions has already been determined in step b.; namely, all the exponents α_i appearing in any of forcing functions $f_k(t)$ have been determined, and Equation A.26 represents a number (even though, in general, not enough) of necessary conditions on the coefficients F_i^k. Certain auxiliary information about either or both the dynamic system or forcing functions obtained analytically or experimentally together with Equation A.26 can, in certain instances, determine a unique set of coefficients F_i^k. For example, if curve-fitting results in but one real exponential, transient analysis yields a unique forcing function (in a trial way, of course).

It is interesting to see how the assumption of timewise proportionality of forcing functions, together with Equation A.26 yields a unique solution (as it must, by previous considerations).

The assumption of proportionality is equivalent to Equations A.24, A.6a, and A.8:

$$F_i^k = c_k F_i \text{ for each } i \text{ and } k \tag{A.27}$$

so that Equation A.26 may be written

$$\sum_{k=1}^{N} c_k F_i \alpha_n^k = \left[\sum_{k=1}^{N} c_k \alpha_n^k \right] F_i = \beta_n F_i \tag{A.28}$$

$$n = \pm 1, \pm 2, \ldots \pm N$$

$$i = 1, 2, \ldots K$$

which identifies the F_i, as well as the

$$\beta_n = \sum_{k=1}^{N} c_k \alpha_n^k$$

of Equation A.7a[5/] uniquely, since the right members of Equation A.28 are known. In effect the assumption of proportionality uncouples Equation A.26 (which is generally coupled in the independent indices i and n) into two independent sets of equations

$$F_i = F_i, \qquad i = 1, 2, \ldots K$$

5/ Dropping the index j.

and

$$\sum_{k=1}^{N} c_k \alpha_n^k = \beta_n \quad : \qquad n = \pm 1, \pm 2, \ldots \pm N$$

Less drastic assumptions regarding the forcing functions or transfer functions could be expected to yield additional information about the forcing functions. For example, if Equation A.26 is summed with respect to i, there results

$$\sum_{k=1}^{N} \left[\sum_{i=1}^{K} F_i^k \right] \alpha_n^k = \beta_n \left[\sum_{i=1}^{K} F_i \right] \tag{A.29}$$

The inner sum

$$\left(\sum_{i=1}^{K} F_i^k \right)$$

is clearly (see Equation A.23) the quantity $f_k(0)$ which is the magnitude of the forcing function in the kth component at time $t = 0$. Hence, Equation A.29 may be written:

$$\sum_{k=1}^{N} f_k(0) \alpha_n^k = \beta_n \sum_{i=1}^{N} F_i \tag{A.30}$$

$$n = \pm 1, \pm 2, \ldots \pm N$$

It is possible that at least the relative magnitudes (if not the absolute magnitudes) of the $f_k(0)$ can be estimated from theory, etc., so that Equation A.30 could be used to yield additional independent conditions on the unknowns of Equation A.26. If the absolute magnitudes of the $F_i^k(0)$ are known, Equation A.30 yields 2N additional equations. If only their relative magnitudes are known, 2N-1 additional equations result.

Another possibility is that some of the F_i^k may be known from other considerations, in effect, reducing the number of unknowns in Equation A.26. For example, some degrees of freedom may not admit a forcing function and are known to be excited only through coupling with other degrees. Hence, the corresponding F_i^k are zero. Certain time-wise proportionality conditions may also exist between certain degrees of freedom, such as the set of all bending modes, further reducing the number of unknowns.

BIBLIOGRAPHY

Operation UPSHOT-KNOTHOLE, Project 1.1d, Dynamic Pressure Versus Time and Supporting Air Blast Measurements, WT-714. SECRET RESTRICTED DATA

Operation UPSHOT-KNOTHOLE, Project 3.1, Tests on the Loading of Building and Equipment Shapes, by T. Schiffman and E. Gallagher, WT-721. SECRET RESTRICTED DATA

Operation GREENHOUSE, Annex 3.3, Appendix I, Section 1, U. S. Air Force Structures: Blast Loading and Response of Structures, WT-87. SECRET RESTRICTED DATA

Operation UPSHOT-KNOTHOLE, Project 3.28.1, Structures Instrumentation, Ballistic Research Laboratories, WT-738. SECRET-RESTRICTED DATA

Operation UPSHOT-KNOTHOLE Project 3.3, Tests on the Loading of Horizontal Cylindrical Shapes, Contract No. AF33(038)-30029, WT-722. SECRET-RESTRICTED DATA

Armour Research Foundation, Planning Program For Air Force Structures Tests, Final Pretest Report, Part V, Regular Reflection on Cubical Structures, Contract No. AF33(038)-30029, June, 1953. SECRET

Armour Research Foundation, Planning Program for Air Force Structures Test. Final Report, Part VIII, Tests on Open-Grid Structures, Contract No. AF33(038)-30029, June, 1953. SECRET

Bleakney, W., The Diffraction of Shock Waves Around Obstacles and the Resulting Transient Loading of Structures, Physics Department, Princeton University, Technical Report II-3, March, 1950.

Bleakney, W., Weimer, D. K., and White, D. R., The Diffraction of Shock Waves Around Obstacles and the Resulting Transient Loading of Structures, Physics Department, Princeton University, Technical Report II-6, August, 1950.

Bleakney, W., et al., Shock Loading of Rectangular Structures, Physics Department, Princeton University, Technical Report II-11, January, 1952.

Brooks, N. B., and Newmark, N. M., Development of Procedures For Rapid Computation of Dynamic Structural Response, Contract No. AF33(600)-24994, University of Illinois. CONFIDENTIAL

Chien, Feng, Wang, Siao, Wind Tunnel Studies of Pressure Distribution on Elementary Building Forms, Institute of Hydraulic Research, State University of Iowa, Report No. ONR N8-onr-500, 1951.

Eiffel, G., Nouvelles Recherches sur la Resistance de l'air, 1919.

Timoshenko, S., Vibration Problems in Engineering, D. Van Nostrand Co., Inc., New York, 1937.

Whittaker, E. and Robinson, A., The Calculus of Observations, Fourth Edition, Blockie and Son Ltd., London, 1944.

DISTRIBUTION

Military Distribution Categories 5-21 and 5-60

ARMY ACTIVITIES

1 Asst. Chief of Staff, G-3, D/A, Washington 25, D.C. ATTN: Dep. CofS, G-3 (RR&SW)
2 Chief of Research and Development, D/A, Washington 25, D.C. ATTN: Special Weapons and Air Defense Division
3 Chief of Ordnance, D/A, Washington 25, D.C. ATTN: ORDTX-AR
4- 6 Chief Signal Officer, D/A, P&O Division, Washington 25, D.C. ATTN: SIGOP
7 The Surgeon General, D/A, Washington 25, D.C. ATTN: Chief, R&D Division
8- 9 Chief Chemical Officer, D/A, Washington 25, D.C.
10 The Quartermaster General, D/A, Washington 25, D.C. ATTN: Research and Development Div.
11- 15 Chief of Engineers, D/A, Washington 25, D.C. ATTN: ENGNB
16 Chief of Transportation, Military Planning and Intelligence Div., Washington 25, D.C.
17- 19 Commanding General, Continental Army Command, Ft. Monroe, Va.
20 President, Board #1, Headquarters, Continental Army Command, Ft. Sill, Okla.
21 President, Board #2, Headquarters, Continental Army Command, Ft. Knox, Ky.
22 President, Board #3, Headquarters, Continental Army Command, Ft. Benning, Ga.
23 President, Board #4, Headquarters, Continental Army Command, Ft. Bliss, Tex.
24 Commanding General, U.S. Army Caribbean, Ft. Amador, C.Z. ATTN: Cml. Off.
25 Commander-in-Chief, European Command, APO 128, c/o PM, New York, N.Y.
26- 27 Commander-in-Chief, Far East Command, APO 500, c/o PM, San Francisco, Calif. ATTN: ACofS, J-3
28- 29 Commanding General, U.S. Army Europe, APO 403, c/o PM, New York, N.Y. ATTN: OPOT Div., Combat Dev. Br.
30- 31 Commandant, Command and General Staff College, Ft. Leavenworth, Kan. ATTN: ALLLS(AS)
32 Commandant, The Artillery and Guided Missile School, Ft. Sill, Okla.
33 Secretary, The Antiaircraft Artillery and Guided Missile School, Ft. Bliss, Texas. ATTN: Maj. George L. Alexander, Dept. of Tactics and Combined Arms
34 Commanding General, Medical Field Service School, Brooke Army Medical Center, Ft. Sam Houston, Tex.
35 Director, Special Weapons Development Office, Headquarters, CONARC, Ft. Bliss, Tex. ATTN: Lt. Arthur Jaskierny
36 Commandant, Army Medical Service Graduate School, Walter Reed Army Medical Center, Washington 25, D.C.
37 Superintendent, U.S. Military Academy, West Point, N.Y. ATTN: Prof. of Ordnance
38 Commandant, Chemical Corps School, Chemical Corps Training Command, Ft. McClellan, Ala.
39 Commanding General, Research and Engineering Command, Army Chemical Center, Md. ATTN: Deputy for RW and Non-Toxic Material
40- 41 Commanding General, Aberdeen Proving Grounds, Md. (inner envelope) ATTN: RD Control Officer (for Director, Ballistics Research Laboratory)
42- 44 Commanding General, The Engineer Center, Ft. Belvoir, Va. ATTN: Asst. Commandant, Engineer School
45 Commanding Officer, Engineer Research and Development Laboratory, Ft. Belvoir, Va. ATTN: Chief, Technical Intelligence Branch
46 Commanding Officer, Picatinny Arsenal, Dover, N.J. ATTN: ORDBB-TK
47 Commanding Officer, Army Medical Research Laboratory, Ft. Knox, Ky.
48- 49 Commanding Officer, Chemical Corps Chemical and Radiological Laboratory, Army Chemical Center, Md. ATTN: Tech. Library
50 Commanding Officer, Transportation R&D Station, Ft. Eustis, Va.
51 Director, Technical Documents Center, Evans Signal Laboratory, Belmar, N.J.
52 Director, Waterways Experiment Station, PO Box 631, Vicksburg, Miss. ATTN: Library
53 Director, Armed Forces Institute of Pathology, 7th and Independence Avenue, S.W., Washington 25, D.C.
54 Director, Operations Research Office, Johns Hopkins University, 7100 Connecticut Ave., Chevy Chase, Md. Washington 15, D.C.
55- 56 Commanding General, Quartermaster Research and Development Command, Quartermaster Research and Development Center Natick, Mass. ATTN: CBR Liaison Officer
57- 63 Technical Information Service, Oak Ridge, Tenn. (Surplus)

NAVY ACTIVITIES

64- 65 Chief of Naval Operations, D/N, Washington 25, D.C. ATTN: OP-36
66 Chief of Naval Operations, D/N, Washington 25, D.C. ATTN: OP-03EG
67 Director of Naval Intelligence, D/N, Washington 25, D.C. ATTN: OP-922V
68 Chief, Bureau of Medicine and Surgery, D/N, Washington 25, D.C. ATTN: Special Weapons Defense Div.
69 Chief, Bureau of Ordnance, D/N, Washington 25, D.C.
70 Chief, Bureau of Ships, D/N, Washington 25, D.C. ATTN: Code 348
71 Chief, Bureau of Yards and Docks, D/N, Washington 25, D.C. ATTN: D-440
72 Chief, Bureau of Supplies and Accounts, D/N, Washington 25, D.C.
73- 74 Chief, Bureau of Aeronautics, D/N, Washington 25, D.C.
75 Chief of Naval Research, Department of the Navy Washington 25, D.C. ATTN: Code 811
76 Commander-in-Chief, U.S. Pacific Fleet, Fleet Post Office, San Francisco, Calif.
77 Commander-in-Chief, U.S. Atlantic Fleet, U.S. Naval Base, Norfolk 11, Va.
78- 81 Commandant, U.S. Marine Corps, Washington 25, D.C. ATTN: Code A03H
82 President, U.S. Naval War College, Newport, R.I.
83 Superintendent, U.S. Naval Postgraduate School, Monterey, Calif.
84 Commanding Officer, U.S. Naval Schools Command, U.S. Naval Station, Treasure Island, San Francisco, Calif.
85 Commanding Officer, U.S. Fleet Training Center, Naval Base, Norfolk 11, Va. ATTN: Special Weapons School
86- 87 Commanding Officer, U.S. Fleet Training Center, Naval Station, San Diego 36, Calif. ATTN: (SPWP School)
88 Commanding Officer, Air Development Squadron 5, VX-5, U.S. Naval Air Station, Moffett Field, Calif.
89 Commanding Officer, U.S. Naval Damage Control Training Center, Naval Base, Philadelphia 12, Pa. ATTN: ABC Defense Course
90 Commanding Officer, U.S. Naval Unit, Chemical Corps School, Army Chemical Training Center, Ft. McClellan, Ala.
91 Commander, U.S. Naval Ordnance Laboratory, Silver Spring 19, Md. ATTN: EE

[redacted]

92 Commander, U.S. Naval Ordnance Laboratory, Silver Spring 19, Md. ATTN: EH
93 Commander, U.S. Naval Ordnance Laboratory, Silver Spring 19, Md. ATTN: R
94 Commander, U.S. Naval Ordnance Test Station, Inyokern, China Lake, Calif.
95 Officer-in-Charge, U.S. Naval Civil Engineering Res. and Evaluation Lab., U.S. Naval Construction Battalion Center, Port Hueneme, Calif. ATTN: Code 753
96 Commanding Officer, U.S. Naval Medical Research Inst., National Naval Medical Center, Bethesda 14, Md.
97 Director, Naval Air Experimental Station, Air Material Center, U.S. Naval Base, Philadelphia, Penn.
98 Director, U.S. Naval Research Laboratory, Washington 25, D.C. ATTN: Code 2029
99 Commanding Officer and Director, U.S. Navy Electronics Laboratory, San Diego 52, Calif. ATTN: Code 4223
100-101 Commanding Officer, U.S. Naval Radiological Defense Laboratory, San Francisco 24, Calif. ATTN: Technical Information Division
102-103 Commanding Officer and Director, David W. Taylor Model Basin, Washington 7, D.C. ATTN: Library
104 Commander, U.S. Naval Air Development Center, Johnsville, Pa.
105 Director, Office of Naval Research Branch Office, 1000 Geary St., San Francisco, Calif.
106-111 Technical Information Service, Oak Ridge, Tenn. (Surplus)

AIR FORCE ACTIVITIES

112 Asst. for Atomic Energy, Headquarters, USAF, Washington 25, D.C. ATTN: DCS/O
113 Director of Operations, Headquarters, USAF, Washington 25, D.C. ATTN: Operations Analysis
114 Director of Plans, Headquarters, USAF, Washington 25, D.C. ATTN: War Plans Div.
115 Director of Research and Development, Headquarters, USAF, Washington 25, D.C. ATTN: Combat Components Div.
116-117 Director of Intelligence, Headquarters, USAF, Washington 25, D.C. ATTN: AFOIN-IB2
118 The Surgeon General, Headquarters, USAF, Washington 25, D.C. ATTN: Bio. Def. Br., Pre. Med. Div.
119 Deputy Chief of Staff, Intelligence, Headquarters, U.S. Air Forces Europe, APO 633, c/o PM, New York, N.Y. ATTN: Directorate of Air Targets
120 Commander, 497th Reconnaissance Technical Squadron (Augmented), APO 633, c/o PM, New York, N.Y.
121 Commander, Far East Air Forces, APO 925, c/o PM, San Francisco, Calif.
122 Commander-in-Chief, Strategic Air Command, Offutt Air Force Base, Omaha, Nebraska. ATTN: Special Weapons Branch, Inspector Div., Inspector General
123 Commander, Tactical Air Command, Langley AFB, Va. ATTN: Documents Security Branch
124 Commander, Air Defense Command, Ent AFB, Colo.
125-126 Commander, Wright Air Development Center, Wright-Patterson AFB, Dayton, O. ATTN: WCRRN, Blast Effects Research
127 Commander, Air Training Command, Scott AFB, Belleville, Ill. ATTN: DCS/O GTP
128 Assistant Chief of Staff, Installations, Headquarters, USAF, Washington 25, D.C. ATTN: AFCIE-E
129 Commander, Air Research and Development Command, PO Box 1395, Baltimore, Md. ATTN: RDDN
130 Commander, Air Proving Ground Command, Eglin AFB, Fla. ATTN: AG/TRB
131-132 Director, Air University Library, Maxwell AFB, Ala.
133-140 Commander, Flying Training Air Force, Waco, Tex. ATTN: Director of Observer Training
141 Commander, Crew Training Air Force, Randolph Field, Tex. ATTN: 2GTS, DCS/O
142 Commander, Headquarters, Technical Training Air Force, Gulfport, Miss. ATTN: TA&D
143-144 Commandant, Air Force School of Aviation Medicine, Randolph AFB, Tex.
145-150 Commander, Wright Air Development Center, Wright-Patterson AFB, Dayton, O. ATTN: WCOSI
151-152 Commander, Air Force Cambridge Research Center, LG Hanscom Field, Bedford, Mass. Attn: CRQST-2
153-155 Commander, Air Force Special Weapons Center, Kirtland AFB, N. Mex. ATTN: Library
156 Commandant, USAF Institute of Technology, Wright-Patterson AFB, Dayton, O. ATTN: Resident College
157 Commander, Lowry AFB, Denver, Colo. ATTN: Department of Armament Training
158 Commander, 1009th Special Weapons Squadron, Headquarters, USAF, Washington 25, D.C.
159-160 The RAND Corporation, 1700 Main Street, Santa Monica, Calif. ATTN: Nuclear Energy Division
161 Commander, Second Air Force, Barksdale AFB, Louisiana. ATTN: Operations Analysis Office
162 Commander, Eighth Air Force, Westover AFB, Mass. ATTN: Operations Analysis Office
163 Commander, Fifteenth Air Force, March AFB, Calif. ATTN: Operations Analysis Office
164-170 Technical Information Service, Oak Ridge, Tenn. (Surplus)

OTHER DEPARTMENT OF DEFENSE ACTIVITIES

171 Asst. Secretary of Defense, Research and Development, D/D, Washington 25, D.C. ATTN: Tech. Library
172 U.S. Documents Officer, Office of the U.S. National Military Representative, SHAPE, APO 55, New York, N.Y.
173 Director, Weapons Systems Evaluation Group, OSD, Rm 2E1006, Pentagon, Washington 25, D.C.
174 Armed Services Explosives Safety Board, D/D, Building T-7, Gravelly Point, Washington 25, D.C.
175 Commandant, Armed Forces Staff College, Norfolk 11, Va. ATTN: Secretary
176-181 Commanding General, Field Command, Armed Forces Special Weapons Project, PO Box 5100, Albuquerque, N. Mex.
182-183 Commanding General, Field Command, Armed Forces, Special Weapons Project, PO Box 5100, Albuquerque, N. Mex. ATTN: Technical Training Group
184-192 Chief, Armed Forces Special Weapons Project, Washington 25, D.C. ATTN: Documents Library Branch
193 Office of the Technical Director, Directorate of Effects Tests, Field Command, AFSWP, PO Box 577, Menlo Park, Calif. ATTN: Dr. E. B. Doll
194-200 Technical Information Service, Oak Ridge, Tenn. (Surplus)

ATOMIC ENERGY COMMISSION ACTIVITIES

201-203 U.S. Atomic Energy Commission, Classified Technical Library, 1901 Constitution Ave., Washington 25, D.C. ATTN: Mrs. J. M. O'Leary (For DMA)
204-205 Los Alamos Scientific Laboratory, Report Library, PO Box 1663, Los Alamos, N. Mex. ATTN: Helen Redman
206-210 Sandia Corporation, Classified Document Division, Sandia Base, Albuquerque, N. Mex. ATTN: Martin Lucero
211-213 University of California Radiation Laboratory, PO Box 808, Livermore, Calif. ATTN: Margaret Edlund
214 Weapon Data Section, Technical Information Service, Oak Ridge, Tenn.
Technical Information Service, Oak Ridge, Tenn. (Surplus)

AEC, Oak Ridge, Tenn.